ABSTRACT

MANOGHARAN, GUHAPRASANNA. Hybrid Manufacturing: Analysis of Integrating Additive and Subtractive Methods. (Under the directions of Dr. Richard A. Wysk and Dr. Ola L.A. Harrysson)

Additive Manufacturing (AM) has enabled the fabrication of complex, tough-to-process alloys using a layer based approach but often produces parts with less desirable surface roughness and tolerance. Subtractive methods, e.g., machining, typically produce parts with more desirable feature accuracy and surface roughness but require special tooling and fixtures for each part design. In this work, a novel ‘Hybrid’ approach called AIMS (Additive Methods Integrated with Subtractive Methods) based on discrete integration of a recent development in CNC-RP (Rapid Prototyping) with AM methods is presented, which is particularly well suited for low volume batch production. The hypothesis of this research is that if properly configured, the best engineering aspects of additive processes (near-net shape parts) and subtractive processes (better geometric accuracy and surface finish) can be obtained for most part geometries using direct digital manufacturing methods.

In this research, salient features associated with critical geometrical tolerances and stacking in transforming the part design from CAD through AM, fixture design and finish machining in a 4-axis set-up are presented. An overall architecture comprising the computational and physical attributes of AIMS is developed. The effects of work-holding a near-net AM part for hybrid manufacturing are modeled to analyze the interactions between initial net-shape part geometric error and final part accuracy as a function of part geometry. This information is used to determine overgrowth requirements needed to accommodate finish-machining allowance. Specifically, the influence of fixture form accuracy and surface characteristics are analyzed to determine the maximum part manufacturing deviation. The

sacrificial fixture design and location with respect to CNC-RP visibility analysis is also developed. Based on the fixture deviation, a model for the part deviation (machining allowance) is developed based on part geometry and tolerance requirement along with validation. Further, an economic study of AIMS and CNC-RP is presented to identify and analyze the major cost variables associated with them, thereby providing an economic justification for the introduced AIMS hybrid process for low volume batch production of tough to machine alloys.

© Copyright 2014 by Guha Prasanna Manogharan

All Rights Reserved

Hybrid Manufacturing: Analysis of Integrating Additive and Subtractive Methods

by
Guhaprasanna Manogharan

A dissertation submitted to the Graduate Faculty of
North Carolina State University
in partial fulfillment of the
requirements for the Degree of
Doctor of Philosophy

Industrial Engineering

Raleigh, North Carolina

2014

APPROVED BY:

Dr. Richard A. Wysk Committee Chair	Dr. Ola L.A. Harrysson Committee Co- Chair
Dr. Jingyan Dong	Dr. Thomas A. Dow

DEDICATION

To my parents, Lalitha Manogharan and Manogharan Krishnamoorthy

BIOGRAPHY

Guha Prasanna Manogharan was born in Vellore, India to Mr. Manogharan Krishnamoorthy and Mrs. Lalitha Manogharan with a sister Srividya Iyer. He grew up in the industrial town of Neyveli, India which houses one of the biggest lignite-based thermal power stations in the country.

In August 2003, he began attending Shanmugha Arts Science Technology and Research Academy (SASTRA University), Thanjavur, India and obtained his Bachelors of Engineering in Mechanical Engineering in May 2007. In August 2007, he began pursuing a Master of Science in Industrial Engineering degree at North Carolina State University, Raleigh with a major in Manufacturing. He began pursuing research in rapid prototyping under the guidance of Dr. Denis R. Cormier and Dr. Ola Harrysson. Upon graduating in December 2009, he continued his research with Dr. Richard A. Wysk and Dr. Ola Harrysson as a doctoral student in the Department of Industrial and Systems Engineering. His research interests include direct metal additive manufacturing, hybrid manufacturing, CNC-RP and applications of advanced manufacturing for inter-disciplinary applications.

ACKNOWLEDGEMENTS

I would firstly like to thank my advisors, Dr. Richard Wysk and Dr. Ola Harrysson for their constant guidance, patience and support. This dissertation would not have been possible without their encouragement and insights. I would also like to thank my committee members Dr. Jingyan Dong and Dr. Thomas Dow for their suggestions and contributions during the course of this work. Many thanks also to Dr. Steven Jackson and Dr. Edward Grant for serving as the graduate school representatives on the committee.

I express my sincere gratitude to Dr. Denis Cormier for his advice and for providing me a platform to become a researcher. I would like to thank Dr. Paul Cohen for his encouragement and valuable advice throughout the course of my graduate school. Many thanks to Jason Low, Dr. Harvey West and Dr. Ron Aman for all their help over and beyond this dissertation. I sincerely acknowledge the help of Dr. Richard Leemaster with the surface characterization studies. I am grateful to Mike Garvey, Jeff Cunningham and Jason Adamowicz of M7 Technologies for helping me with the experimental set-up and data collection. I would also like to thank my colleagues Harshad Srinivasan, Chuang Wei, Tim Horn and Martin Samayoa for their support and friendship.

In no way would this have been possible without the unwavering support of my parents Manogharan and Lalitha Krishnamoorthy and sister Srividya. I thank them for their infinite reinforcement in my abilities. Finally, I would like to thank Sudha for being the constant source of inspiration, support and motivation during good and bad times and for always believing that I can.

TABLE OF CONTENTS

LIST OF FIGURES ix

LIST OF TABLES xiii

CHAPTER 1: INTRODUCTION 1

- Summary 5
- References 7

CHAPTER 2: LITERATURE REVIEW 9

- Introduction 9
- 2.1 Additive Manufacturing 9
  - 2.1.1 Binder Jetting 14
  - 2.1.2 Directed Energy Deposition 15
  - 2.1.3 Powder Bed-Fusion 16
  - 2.1.4 Attributes of Metal Additive Manufacturing 19
- 2.2 Subtractive Manufacturing 21
  - 2.2.1 CNC-RP 21
  - 2.2.2 Attributes of CNC-RP 24
- 2.3 Hybrid Manufacturing 25
  - 2.3.1 ECLIPSE-RP 27
  - 2.3.2 SLC 28
  - 2.3.3 LAMP process 30
  - 2.3.4 Ultrasonic Consolidation 31
  - 2.3.5 3D Deposition-Milling 32
  - 2.3.5 Attributes of Current Hybrid Processes 33

2.4 Desired Attributes in a Hybrid Method 34

2.5 Economic Analyses 35

Summary 38

References 38

CHAPTER 3: HYBIRD MANUFACTURING- AIMS SYSTEM ARCHITECTURE 46

Introduction 46

3.1 AIMS: Additive processing Integrated with Subtractive Methods..48

3.2 Hybrid Manufacturing Coordinate Systems..50

3.2 Feasibility Study..56

3.3 Location System and Errors 59

3.3.1 Transformation Models 63

3.4 Causes of Fixture Deviations..64

3.4.1 Surface Roughness 65

3.4.2 Non-Uniform Shrinkage..67

3.5 Broader Scope of Research 68

3.6 AIMS: Process Flow 70

3.6.1 Physical Components 72

3.6.2 Software Components 74

3.7 AIMS Performance Metrics 75

3.7.1 Metric (0.1): Minimize {Material Consumption, V_{total}} 76

3.7.2 Metric (0.2): Minimize {Production time, T_{total}}..79

3.7.3 Metric (0.3): Minimize {Production cost, T_{cost} } 81

Summary 84

CHAPTER 4: METHODOLOGY..85

Introduction 85

4.1. Fixture Deviations 86
  4.1.1 Form Accuracy 90
  4.1.2 Surface Characteristics 93
4.2. Fixture Design Principles 98
4.3. Part Deviation and Overgrowth 102
4.4. 2D Part Deviation CMM Analysis 106
4.3. 3D Between-Centers Fixture Deviation 109
Summary 114
References 115

CHAPTER 5: RESULTS AND ANALYSIS 116
Introduction 116
5.1. Fixture Deviation Analysis 116
  5.1.1 Fixture Inaccuracy 116
  5.1.2 Surface Characteristics 122
5.2. Part Deviation Analysis 124
5.3. Estimation of Fixture Deviation 131
5.4. Estimation of Part Datum Deviation 133
5.5. Analysis 134
Summary 136

CHAPTER 6: AIMS PERFORMANCE METRICS 139
Introduction 139
6.1. Metrics Model 140
6.2. Additive Manufacturing Model 142
6.3 CNC-RP Cost Model 142
6.4 AIMS Cost Model 143

6.5. Case Study 145
6.6 Results 148
6.7 Sensitivity Analysis- Influence of Cost Components 152
6.7 Discussion 164
Summary 168
CHAPTER 7: CONCLUSIONS AND FUTURE WORK 169
Introduction 169
7.1. Research Summary 169
7.2. Research Contributions 172
7.3. Future Research 173
APPENDICES Appendix 1: Machining Parameters 175
Appendix 1: Machining Parameters 176
Appendix 2: Circular Fixture- Calculation 177
Appendix 3: Tri-Planar Fixture- Calculation 181

LIST OF FIGURES

Figure 1: Principle of Additive Manufacturing 10

Figure 2: Part Volume and Sacrificial Support Volume 10

Figure 3: Functional Classification of Thermal Energy based AM Methods 11

Figure 4: Principle of Binder Jetting 14

Figure 5: Principle of LENS 15

Figure 6: Principle of EBF^3 16

Figure 7: Principle of EBM 18

Figure 8: Principle of SLM 19

Figure 9: Metal-AM Part Design Complexities 20

Figure 10: CNC-RP Process; (a) Setup (b) Example 22

Figure 11: CNC-RP Process- Setup and after Hogging 24

Figure 12: ECLIPSE-RP Hybrid process 27

Figure 13: Hybrid SLC process 29

Figure 14: LAMP process 30

Figure 15: Ultrasonic Consolidation 32

Figure 16: The AIMS process 49

Figure 17: AM-Coordinate System C_{AM} 51

Figure 18: CNC-Machine Tool and CNC-RP Coordinate System 52

Figure 19: Fixture and Part Coordinate System 53

Figure 20: Desired Part Specifications 54

Figure 21 Tolerance Stacking Chain 55

Figure 22: Addition of Machining Allowance 56

Figure 23: Flat Surfaces-used to align the Part with the Machine Axis 57

Figure 24: Desired Part and Near-net AIMS part 58

Figure 25: Near-net AIMS part in CNC-RP setup 59

Figure 26: Initial observations from AIMS 60

Figure 27: Effect of Integrating Lattice Structures 61

Figure 28: Deviation of Fixture Coordinate System 62

Figure 29: Part Coordinate System 62

Figure 30: Ideal Set-up vs. Actual Set-up 65

Figure 31: Co-axial Ideal Set-up 66

Figure 32: Non Co-axial Set-up 66

Figure 33: Effect of Non-uniform Shrinkage 67

Figure 34: Effect of Build Orientation and Part Geometry 68

Figure 35: Overview of Process Factors and Research Scope in AIMS 69

Figure 36: AIMS Process Flow 70

Figure 37: Physical Architecture of AIMS 73

Figure 38: AIMS Software Components 74

Figure 39: Machining All vs. Critical Part Features 76

Figure 40: Material Consumption 78

Figure 41: Machining Allowance for CNC-RP 79

Figure 42: List of Major and Local Objectives. 83

Figure 43: 2D Vector Model-Distance between Fixtures 86

Figure 44: Fixture Geometries 88

Figure 45: 2D Interaction of Feature Form Inaccuracy and Surface characteristics 89

Figure 46: 2D Contact Surfaces across the 3-jaw Chuck with respect to the Machine Axis 90

Figure 47: Maximum-Minimum Deviation 91

Figure 48: Cylindrical Fixture – Form Measurement 92

Figure 49: Tri-planar Fixture – Form Measurement 93

Figure 50: Contact between Smooth and Rough Surface 94

Figure 51: Surface Profile Measurement 96

Figure 52: Raw Data of a Surface Scan #1 97

Figure 53: Filtered Data of all the Scans of the surface 97

Figure 54: Influence of Critical Features on Fixture Design 99

Figure 55: Fixture Design Principles 100

Figure 56: Interactions between Fixture Error and Part Geometry 103

Figure 57: Evaluation of Fixture Inaccuracies 108

Figure 58: Impact of referencing from near-net metal additive parts 110

Figure 59: 3D Fixturing Deviation parts 111

Figure 60: Part Coordinate System w.r.to Fixturing Deviation parts 112

Figure 61: Maximum-Minimum Deviation 118

Figure 62: Maximum-Minimum Deviations- Plane# 3 and Plane#1 120

Figure 63: Total Absolute Deviation of the Planes 120

Figure 64: Reorientation of Tri-planes 121

Figure 65: Total Deviation of the Fixture designs for average diameters of 15-18 mm. 124

Figure 66: Downward Tri-plane Fixture Defects- DMLS 125

Figure 67: Part Design for Validation 125

Figure 68: Non-Contact Scanner in CNC Machine 127

Figure 69: AIMS Part Fixtured between Centers 128

Figure 70: Toolpath superimposed on the CAD part 129

Figure 71: Raw Cloud Point from a Scan 129

Figure 72: Location of the Datum w.r.to Fixtures 131

Figure 73: Unit and batch production of sample part in EBM 145

Figure 74: (a) EBM build slices and (b) Individual layers 147

Figure 75: Unit cost through batch production in CNC-RP and Hybrid process- AIMS 151

Figure 76: Time Components in the AIMS production based on batch size 152

Figure 77: Total Unit Cost for Hybrid Manufacturing 156

Figure 78: Influence of cost factors on Single-unit CNC-RP 157

Figure 79: Influence of CNC-RP-related variables: operating cost, material and MRR 159

Figure 80: Interaction between production cost and MRR 160

Figure 81: Influence of EBM cool time and EBM operating cost 161

Figure 82: AIMS Unit Cost for different Batch Sizes 162

Figure 83: Unit Cost for different Aspect Ratios 163

LIST OF TABLES

Table 1: Intercepts for the Jaw contact lines 107

Table 2: Expected vs. Measured Fixture Inaccuracies 109

Table 3: Cylinder Form Inaccuracy 117

Table 4: Fixture characterization of Tri-planar faces 119

Table 5: Plane Positive and Negative Deviation 119

Table 6: Separation Distance of Tri-planar surfaces 122

Table 7: Separation Distance of Cylindrical fixture 122

Table 8: Total Deviation including Surface Roughness and Form Inaccuracy 123

Table 9: Location of the centers for the nominal part 130

Table 10: Measured diameters of the features 130

Table 11: Deviation of Fixture at Center#2 132

Table 12: Deviation of Fixture at Center#1 133

Table 13: Estimation Part Datum Location Deviation 134

Table 14: Measured Datum Location (10000-1) 135

Table 15: Estimation Error 136

Table 16: Actual Error 136

Table 17: Nomenclature for cost models for additive, subtractive and hybrid processes 141

Table 18: Breakdown of CNC-RP operation and tooling cost 149

Table 19: EBM cost-component in unit and batch production 150

Table 20: Hybrid process unit and batch production 150

Table 21: Variable Conditions 154

CHAPTER 1: INTRODUCTION

Ever since its development in the 1980s, Additive Manufacturing (AM) (Rapid Prototyping as it was originally called), has emerged as a powerful facet of advanced manufacturing [1]. Additive manufacturing is defined by the American Society of Testing and Materials (ASTM) as “The process of joining materials to make objects from 3D model data, usually layer upon layer, as opposed to subtractive manufacturing methodologies; Synonyms: 3D printing, additive fabrication, additive process, additive techniques, additive layer manufacturing, layer manufacturing, and freeform fabrication” [2]. This chapter provides an introduction to AM processes, their advantages, limitations and a novel hybrid process to combine the capabilities of both AM and subtractive methods.

In about the same period, the digital revolution has contributed to the ever-growing computing and communication capabilities [3]. This culmination of cloud-based technology and reverse engineering of complex part designs (such as implants through CT/MRI) along with AM capabilities has revolutionized advanced manufacturing. The Society of Manufacturing Engineers (SME) defines this Direct Digital Manufacturing as “The process of going directly from an electronic, digital representation of a part to the final product via additive manufacturing” [4]. The processing capabilities of AM methods of this decade have gradually evolved from their early application for ‘Rapid Prototyping-RP’, where the principle of 3D printing was used only in the product development stage in manufacturing. This was primarily due to the limited mechanical strength of the materials that could be processed through 3D printers, e.g. plastics and sand.

Since then, the range of materials that can be processed has grown steadily and now includes elastomers, biomaterials, alloys ranging from Aluminum to high-temperature Nickel, Chromium based superalloys such as Inconel, and ceramics. Some of these expensive alloys are often difficult to process through conventional manufacturing methods such as casting, forging, and machining. AM offers a unique advantage for processing such materials through the layer-based approach as opposed to the traditional 'bulk' manufacturing and material removal methods. In some materials, traditionally cast ingots suffer from inhomogeneity in the grain and phase distributions [5 and 6].

Another distinctive contribution of AM to the field of manufacturing is 'freeform fabrication', i.e. the ability to fabricate complicated part designs without the need for stock material and custom fixtures for every part design. This layer-based approach furthers the design-driven application of manufacturing ranging from conformal cooling channels [7] to life-saving custom biocompatible implants [8].

In summary, AM provides the capabilities to process an ever-growing range of materials and produce parts with complex geometries without the additional cost and time associated with making fixtures, dies and tools (as in conventional manufacturing). However, when compared to conventional methods (Subtractive Methods-SM such as machining), current AM methods produce parts with poorer surface finish and part accuracy. These aspects are not critical factors in certain applications such as biomedical implants where rougher surfaces are preferred to accelerate bone ingrowth [9]. However, for most mechanical and aerospace applications, superior surface finish and part accuracies are desired. Hence, there is a tremendous need to solve two major challenges in AM: (1) Increasing part accuracy and (2) Improving surface finish.

The fundamental approaches in addressing these challenges are to: (1) Improve the performance of each AM processes and/or (2) Develop a hybrid process that incorporates AM methods as a pre-cursor where ‘near-net’ AM-made parts can be coupled with conventional material removal processes such as machining. The former is relatively challenging and time-consuming since there are multiple AM processes with unique processing techniques and characteristics such as energy source (laser, electron beam), processing nature (binder jetting, material powder bed fusion), etc. In order to improve the process performance of each AM method, discrete research efforts targeted at specific AM technologies are required.

The second approach employs AM to produce near-net parts and incorporate a ‘hybrid strategy’ where SM is the secondary operation to improve part accuracy and surface finish. Several investigators have identified the need for secondary operations and the advantages in coupling AM and SM methods [10 and 11]. Hybrid strategies have been developed for specific AM methods where additive and subtractive operations are repeated in a cycle until the final part is created [11 and 12] but limited to the nature of each individual AM process. For instance, in AM processes categorized as powder bed fusion processes where the material is spread across in each layer, such hybrid strategies are not feasible. Hence, it is more efficient and rational to develop a hybrid strategy which is versatile and independent of any AM process characteristics.

Such a hybrid process needs to be consolidated yet adaptable to combine any near-net AM process with conventional SM process. Successful development and implementation of such a hybrid process can accelerate the applications of AM-made parts and efficiently incorporate functionality such as part accuracy and surface finish (e.g. assembly sub-parts). This thesis presents a novel hybrid process called **A**dditive methods **I**ntegrated with Subtractive **M**ethod**s** called **AIMS** which can be implemented with any near-net AM process to successfully produce AM-made parts with desirable surface finish and required part accuracy.

AIMS can integrate any AM method with a recently developed SM method called CNC-RP [13 and 14]. Similar to AM methods, the part is fabricated in layers in CNC-RP. However, rather than adding materials in each layers, CNC-RP removes materials through island-milling and automatic tool path planning via a CAD/CAM system. The part is machined from a symmetrical bar stock supported between the centers of a rotary indexer. Sacrificial fixtures are added to the part design to support the part throughout the process of machining. Due to the use of rotary indexer, manual refixturing of the stock is eliminated. However, both traditional SM and CNC-RP processes can result in inefficient material utilization due to loss through chips and scraps. AIMS combines the advantages of AM processes (elimination of fixtures, processing of tough-to-machine alloys, etc.) with those of CNC-RP (better surface finish and process accuracy, automatic re-configurability using an indexer) while collectively eliminating the disadvantages of AM (need for secondary machining) and CNC-RP (material utilization).

However, as previously mentioned, near-net metal AM parts have feature inaccuracies and as-cast like surface roughness. There are significant deviations associated with work-holding a near-net part/fixture when compared to using a conventional bar-stock (as in CNC-RP). Hence, an analytical model that captures the effects of tolerance stacking associated with the CNC machine set-up, fixtures' location and part design is required. This research aims to model the maximum part-feature deviations as a function of errors associated with the fixtures in a 4-axis set-up (CNC-RP). This information can then be used to compensate for machining allowance in order to produce the final part. Findings from this study will further efforts to completely automate this hybrid process. Additional efforts to adapt this hybrid approach to a variety of part geometries, sacrificial fixture designs, materials and tolerances are required. This research is the primary step in characterizing the fixture error and part deviation. This information can be used to optimize machining allowance and better predict fixturing inaccuracies.

Summary

In this chapter, an overview of two different manufacturing approaches i.e. AM and SM is presented along with the motivation for the development of a generic hybrid process in AIMS. The fundamental difference between work-holding a conventional bar stock and a near-net shaped part is noted. The remainder of this dissertation is organized as: Chapter 2 describes direct digital manufacturing methods including AM, SM and current hybrid processes. This chapter also outlines the advantages and limitations of existing hybrid processes.

Chapter 3 describes the objectives of this study and a framework for the development and implementation of the AIMS process including the physical and software architecture required to develop an automated AIMS system. Chapter 4 presents the methodology associated with developing models to address the objectives. Chapter 5 presents the results and analysis based on this study. Chapter 6 details an economic model to evaluate the economic justification for this hybrid process. A summary of research and future directions are presented in Chapter 7.

References

1) Kruth, J.-P., Leu, M. C. and Nakagawa, T., 1998, “Progress in additive manufacturing and rapid prototyping”, CIRP Annals- Manufacturing Technology, vol. 47(2), pp. 525-540.

2) ASTM Designation: F2792-12a, “Standard Terminology for Additive Manufacturing Technologies”, pp.1-3.

3) Pereira, C.E. and Carro, L., 2007, “Distributed real-time embedded systems: Recent advances, future trends and their impact on manufacturing plant control”, Annual Reviews in Control, vol. 31(1), pp. 81-92.

4) Manufacturing Engineering-SME Speaks: SME Forms, accessed as of July 18, 2013, url< http://www.sme.org/MEMagazine/Article.aspx?id=21720&taxid=1427>

5) Auburtin, P., Wang, T., Cockcroft, S.L., and Mitchell, A., 2000, “Freckle formation and freckle criterion in superalloy castings”, Metallurgical and Materials Transaction B, vol. 31, pp. 801-11.

6) Felicelli, S.D., Poirier, D.R. and Heinrich, J.C., 1998, “Modeling freckle formation in three dimensions during solidification of multicomponent alloys”, Metallurgical and Materials Transaction B, vol. 29, pp. 847-855.

7) Xu, X., Sachs, E. and Allen, S., 2001, “The design of conformal cooling channels in injection molding tooling”, Polymer Engineering and Science, vol. 41(7), pp.1265–1279.

8) Murr, L. E. and et al., 2010, “Next-generation biomedical implants using additive manufacturing of complex, cellular and functional mesh arrays”, Philosophical Transactions of The Royal Society A, vol. 368(1917), pp.1999–2032.

9) Bartolo, P., Kruth, J.P., Silva, J. and et al., 2012, “Biomedical production of implants by additive electro-chemical and physical processes”, CIRP Annals- Manufacturing Technology, vol. 61(2), pp. 635-655.

10) Hur, J. and Lee, K., 2002, “Hybrid rapid prototyping system using machining and deposition”, Computer-Aided Design, vol. 34(10) pp.741–754.

11) Xiong, X., Zhang, H. and Wang, H., 2009, “Metal direct prototyping by using hybrid plasma deposition and milling”, Journal of Materials Processing Technology, vol. 209, pp. 124-130.

12) Karunakaran, K.P., Suryakumar, S., Pushpa, V., and Akula, S., 2010, “Low cost integration of additive and subtractive processes for hybrid layered manufacturing”, Robotics and Computer-Integrated Manufacturing, vol. 26, pp. 490–499.

13) Manogharan, G.P., Wysk, R.A., Harrysson, O.L.A and Cohen, P.H., "Hybrid manufacturing: Unique approach to integrating additive and subtractive rapid prototyping process", Proceedings of the 22nd FAIM Conference, June 10-12 2012, Helsinki, Finland.

14) Manogharan, G.P., Soundarajan, D.K and Wysk, “Study of energy efficiencies in rapid prototyping”, ISERC Conference, May 21- 25, 2011, Reno, Nevada.

CHAPTER 2: LITERATURE REVIEW

Introduction

In order to address the requirement of a hybrid process applicable to all AM methods, it is important to understand the principles of different AM methods. Learning about existing hybrid approaches enables us to identify the requirements and constraints that need to be considered. This chapter aids in the development of a new system by reviewing some of the prior research corresponding to additive manufacturing, subtractive manufacturing and current hybrid methods. Since this research is targeted at metal-based AM processes, they are reviewed in detail. Section 2.1 identifies the major types of AM and details some of the current metal-based AM processes. Advantages and limitations of current metal-AM processes are outlined. Section 2.2 outlines a specific subtractive manufacturing method namely, CNC-RP. Section 2.3 overviews the current hybrid manufacturing method in the context of metal additive methods. Subsequently, based on the review of current methods, the motivation for a new hybrid manufacturing method and the desired hybrid process capabilities are stated. Finally, Section 2.4 presents a review of cost models developed for AM processes and identifies the need for a hybrid cost model for metal AM.

2.1 Additive Manufacturing

The principle of additive manufacturing lies in fabricating a part layer-by-layer through a bottom-to-top approach by combining materials. The CAD file of the required part is sliced across each layer along the direction of fabrication as shown in Figure 1 below [1].

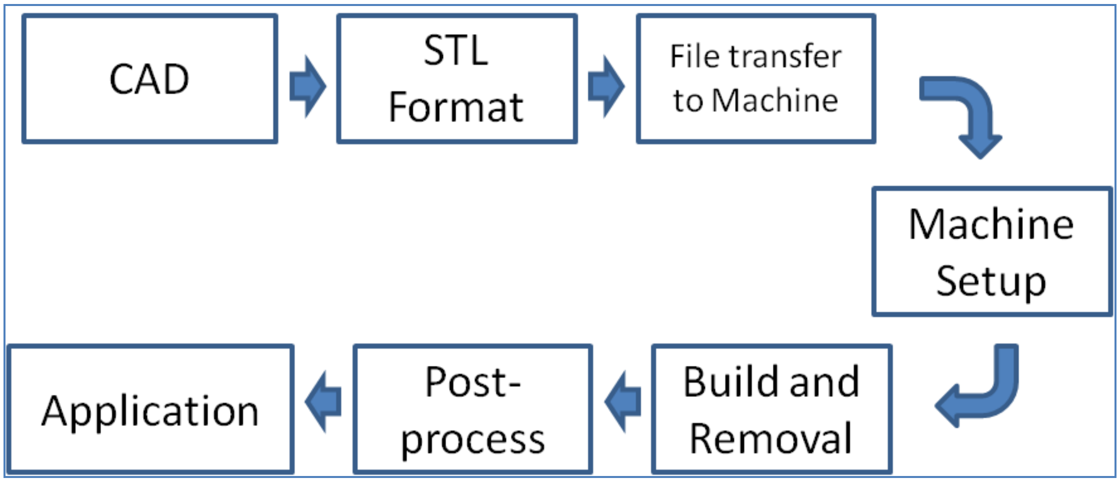
CAD
STL Format
File transfer to Machine
Machine Setup
Build and Removal
Post-process
Application

Figure 1: Principle of Additive Manufacturing

Upon generating process files for the machine, the file is transferred to the machine and built layer-by-layer. The part is then removed from the AM machine for post-processing such as removal of sacrificial supports for any overhanging edges. Figure 2 below shows an example of such sacrificial support structures.

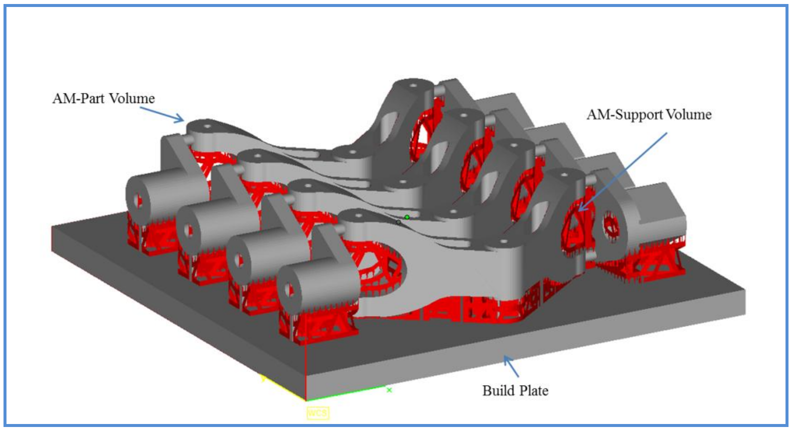
AM-Part Volume
AM-Support Volume
Build Plate

Figure 2: Part Volume and Sacrificial Support Volume

Based on this layered approach, AM has evolved over the past few decades to process a variety of materials such as polymers, metals, ceramics, etc. Also, the techniques for combining those materials in layers vary from using laser for selectively solidifying photo-curable polymers to using electron-beam for selectively melting superalloys. There are several approaches to categorize all AM methods based on the nature of raw material [2], aggregation geometry during deposition [3] and energy or process source [4]. Another study classified AM techniques based on functional framework such as material, patterning energy, phenomena of creating primitive geometry, nature of adding materials and support mechanism [5]. Figure 3 [5] shows the functional classification of Electron Beam Melting (EBM), Direct Metal Laser Sintering (DMLS), Laser Sintering (LS) and Laser Engineered Net Shaping (LENS) based on the framework.

	Store Material	**Pattern Material**	**Pattern Energy**	**Create Primitive**	**Provide New Material**	**Support Material**
EBM	Single Phase Powder	No Material Patterning	1D Heat Energy	Solidify Melt	Recoat by spreading	Bed of Build Material
DMLS						
LS	Coated Powder			Fusion		
LENS	Single Phase Powder	1D Powder Deposition		Solidify Melt	Direct Material Addition	5 Axis Deposition

Figure 3: Functional Classification of Thermal Energy based AM Methods

AM process categories developed by ASTM International, ASTM F2792-12a for existing AM methodologies are a recent development and are being adopted by the ISO TC 261 committee [6]:

- **Binder Jetting:** "An additive manufacturing process in which a liquid bonding agent is selectively deposited to join powder materials". They are often used to bind a range of materials including plastic, metals, ceramics and sand to produce molds and parts; e.g. Exone® systems
- **Directed Energy Deposition:** "An additive manufacturing process in which focused thermal energy is used to fuse materials by melting as they are being deposited". They are often used for both wire and powder based materials using laser, electron beam or plasma arc as the energy source. They are preferred for repair applications; e.g. LENS from Optomec® and EBF^3 developed by NASA Langley Research Center which uses a wire feed along with an electron beam gun to deposit material.
- **Material Extrusion:** "An additive manufacturing process in which material is selectively dispensed through a nozzle or orifice". They are mostly used to process polymers and are often used for prototyping during the product development stage; e.g. Dimension® from Stratasys® and Cube® series from 3D systems®.

- **Material Jetting:** “An additive manufacturing process in which droplets of build material are selectively deposited”. They are mostly used to process wax and photopolymers; e.g. Objet® from Stratasys®.
- **Powder Bed Fusion:** “An additive manufacturing process in which thermal energy selectively fuses regions of a powder bed”; e.g. DMLS® from EOS® using laser and EBM S12® and A2® from Arcam®.
- **Sheet Lamination:** “An additive manufacturing process in which sheets of material are bonded to form an object”; e.g. SonicLayer® series from Fabrisonic® using ultrasonic transducer to merge layers of metals.
- **Vat Polymerization:** “An additive manufacturing process in which liquid photopolymer in a vat is selectively cured by light-activated polymerization”. They are only used to process photo-curable polymers; e.g. iPro™ SLA® (StereoLithography Apparatus) from 3Dsystems®.

Sub-sections 2.1.1-2.1.3 provide examples from specific **metal**-based AM processes from the categories of binder jetting, directed energy deposition and powder-bed fusion. Since this research focuses on part accuracy and surface finish of metal-AMs, the difference in the metallurgical and mechanical properties across these methods are not identified (although they are important factors to be considered for load-bearing applications).

2.1.1 Binder Jetting

In the process of binder jetting, a layer of material (metal, polymers, sand and ceramics) is spread with selective deposition of binders. Figure 4 outlines the binder jetting principle [7].

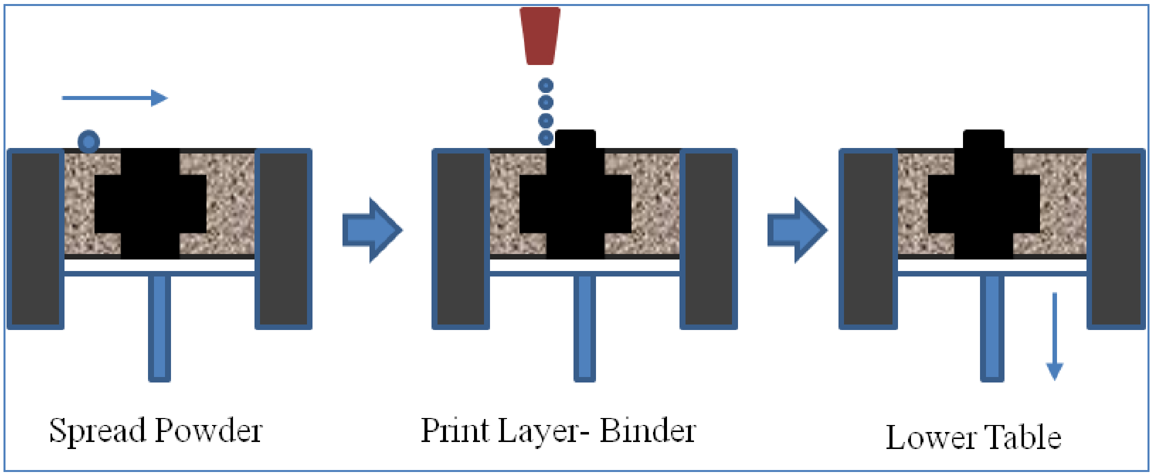

Figure 4: Principle of Binder Jetting

Depending on the slices from the CAD file, binders are selectively applied using inkjet-printing technology. Subsequently, the next layer is spread across the platform and this process is continued until the final layer is finished. After the dispensing of binder for the final layer, the bound metal part (called the 'green part') is metallurgically bonded through sintering in a furnace to produce the final part, often through infiltration of other materials (e.g. bronze) to achieve full density.

2.1.2 Directed Energy Deposition

In the case of directed energy deposition, an energy source (laser or electron beam) is targeted at a flow of material (powder or wire) and deposits material based on information from each layer of the CAD file through precisely coordinated motion control between the energy source and material supply. An illustration of directed energy principle based on LENS process using laser and directed powder supply is presented in Figure 5 [8 and 9]. In some cases, the substrate/build plate and/or laser-powder supply are mounted on a 5-axis platform in order to create parts with overhanging edges without creating sacrificial supports [8].

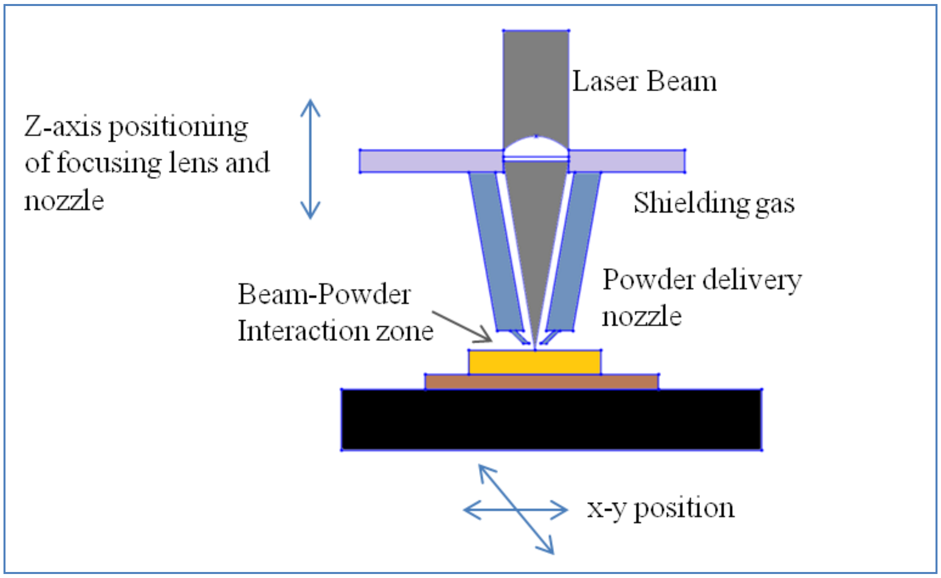
Laser Beam
Z-axis positioning of focusing lens and nozzle
Shielding gas
Powder delivery nozzle
Beam-Powder Interaction zone
x-y position

Figure 5: Principle of LENS

Another example of the directed energy deposition process is the Electron Beam Freeform fabrication- EBF^3 where the electron beam is the energy source and the material is supplied through a wire feeding system [10].

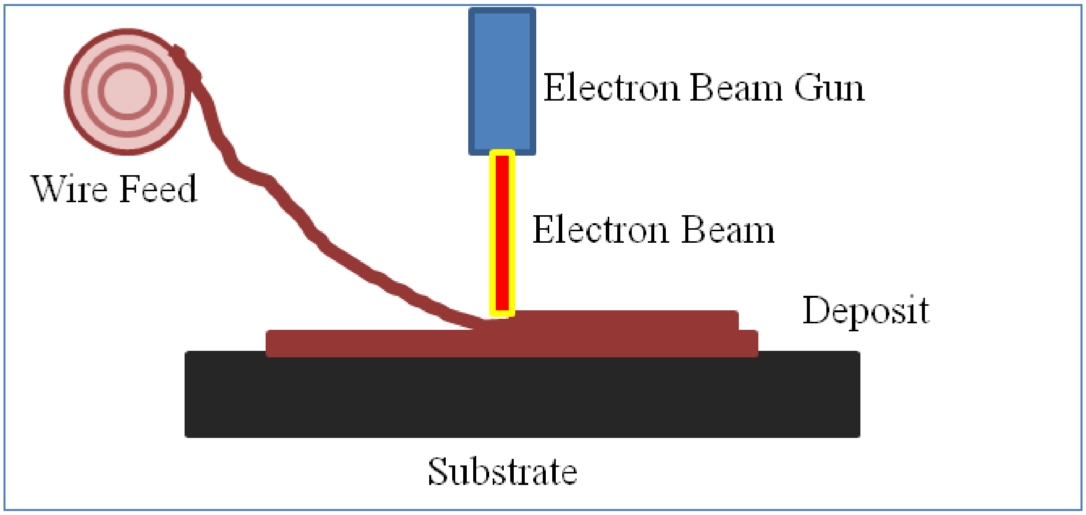

Figure 6: Principle of EBF^3

Figure 6 presents a directed energy deposition process using electron beam and wire-fed material [10]. Similar to the LENS process, studies have been conducted to optimize the EBF^3 process by varying the wire feed angle and the electron beam process parameters taking place in the vacuum environment [10].

2.1.3 Powder Bed-Fusion

In the case of powder bed-fusion methods, an energy source (laser or electron beam) is targeted at a spread layer of powder material (metal) to specifically melt segments of material based on information from each layer of the CAD file. Figure 7 outlines the powder bed-fusion principle in the case of the EBM process using an electron beam as the energy source with spread powder layers.

A unique aspect of such a metal based powder-bed fusion is the ability to vary the processing parameters (power, speed, energy distribution, etc.) to easily generate support structures for complex overhanging surfaces as shown in Figure 2 with relatively simple process planning. EBM is classified as a hot-bed AM process since the entire powder bed is maintained at an elevated temperature throughout the build process. When compared to other powder-bed laser (cold bed) processes, EBM functions in vacuum as opposed to inert gas and accelerated electron beam employs higher power to completely melt the powder particles. It should also be noted that currently, there is only one EBM based AM process in the market (Arcam, Sweden).

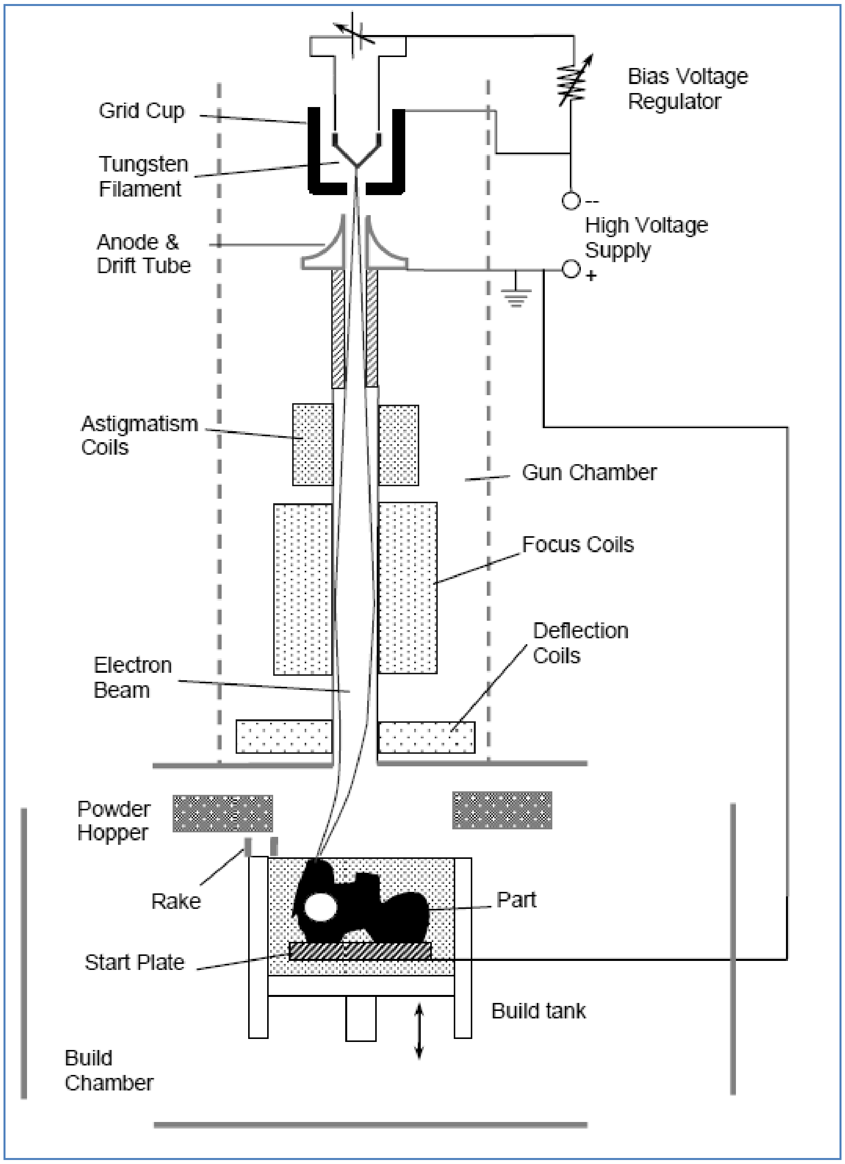
Bias Voltage
Regulator
Grid Cup
Tungsten
Filament
--
High Voltage
Supply
+
Anode &
Drift Tube
Astigmatism
Coils
Gun Chamber
Focus Coils
Deflection
Coils
Electron
Beam
Powder
Hopper
Rake
Part
Start Plate
Build tank
Build
Chamber

Figure 7: Principle of EBM

Another example of the powder bed-fusion process is the Selective Laser Melting (SLM) where the laser beam is the energy source and the powder material is spread across the build platform as shown in Figure 8 [12]. There are several laser based cold powder bed AM machines including DMLS and SLS that fully melt the powder.

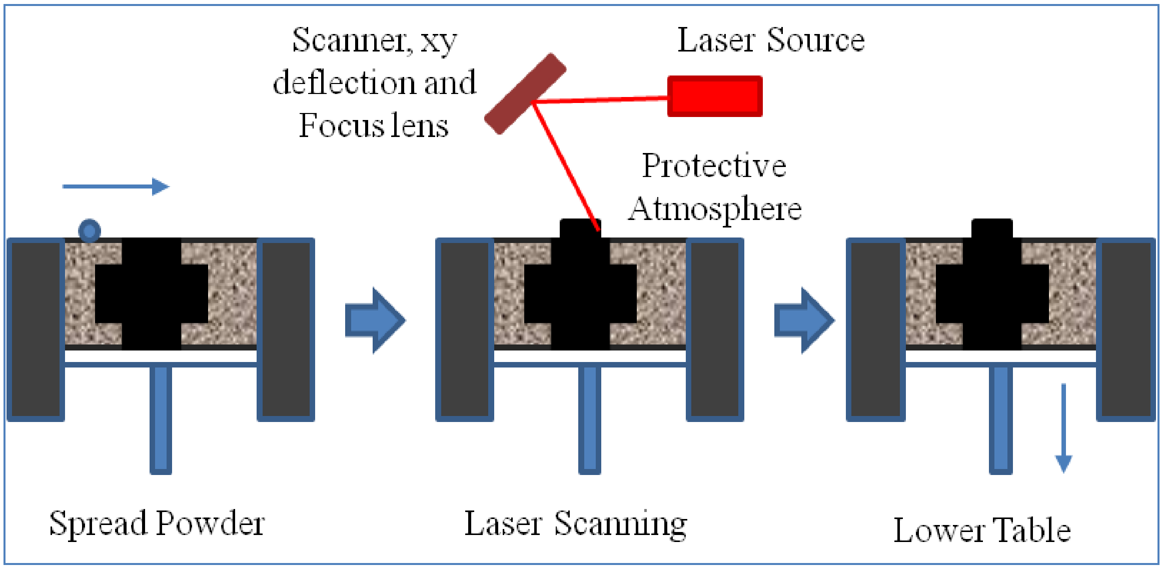
Scanner, xy deflection and Focus lens
Laser Source
Protective Atmosphere
Spread Powder
Laser Scanning
Lower Table

Figure 8: Principle of SLM

2.1.4 Attributes of Metal Additive Manufacturing

The ‘freeform’ fabrication principle of AM eliminates the need for expensive tooling that adds significant cost and production time, particularly for smaller batch sizes. When compared to conventional manufacturing methods (including subtractive methods), the material utilization rate is very high in the case of AM since often there is little wastage of expensive materials in the form of support materials when compared to machining scraps and chips from a stock material. In some metal AM processes, considerable process planning and secondary operations are required to remove the support material. From the material standpoint, metal-AM has an advantage over other methods since it can be used to easily process tough-to-process alloys (casting, machining). In some cases, conventional bulk formation methods such as casting of superalloys suffer from non-homogeneity across the cast ingots, hence compromising the mechanical and metallurgical properties [13].

Several studies have shown that metal-AM parts have similar or superior mechanical properties when compared to similarly wrought alloys [14 and 15]. Another major advantage of metal-AM is the limitless possibility of design complexity as shown in Figure 9 below (ranging from complex biomedical implants to engineered lattice structures).

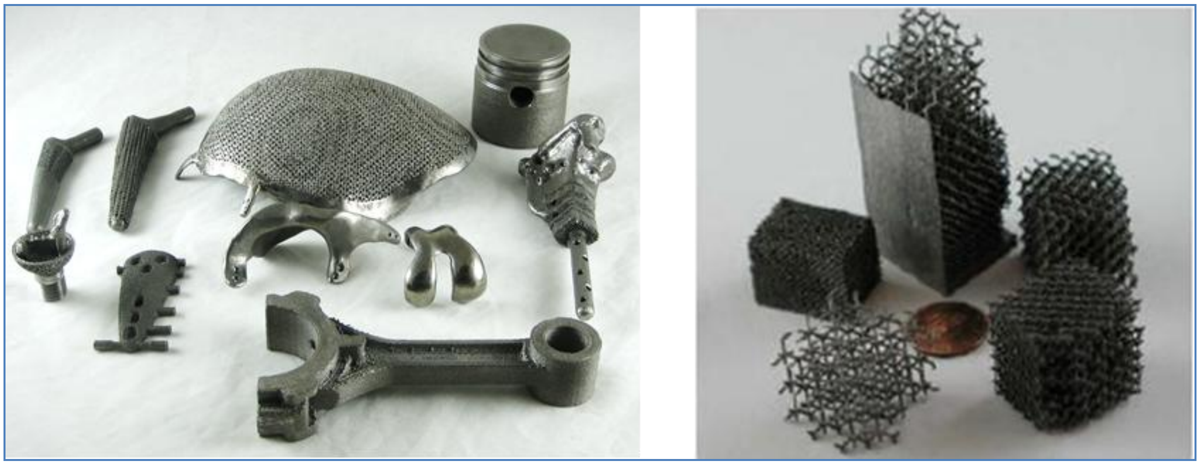

Figure 9: Metal-AM Part Design Complexities

The applications of metal-AM range from custom biomedical implants [16], complex aerospace parts [17] to the fabrication of injection molding tooling with conformal cooling channels [12]. However, current metal-AM methods suffer from poor surface finish and part inaccuracies when compared to subtractive methods [18]. In the case of powder-bed fusion processes (such as SLM and EBM), metallurgical (and often mechanical) bonding of unprocessed metal powders with processed surface occurs leading to surfaces similar to 'as-cast' parts. In the case of binder-jetting process, similar limitations are accompanied by warping and shrinkage during the sintering process in the furnace.

In the case of directed energy deposition methods such as EBF^3 (without any subtractive elements), the layer thickness is relatively high, leading to loss of finer part features. Also, there are issues such as bundling of material at corners and overflow of molten materials along edges. Hence it is apparent that while metal-AM has several unique advantages over other manufacturing approaches, they require significant secondary processing to generate parts within the tolerances of the required specification and surface finish (two critical aspects when the part is involved in assemblies).

2.2 Subtractive Manufacturing

In the case of subtractive manufacturing, as opposed to AM principle, material is removed from a stock using several techniques such as machining (using a machine tool), laser cutting, Electric Discharge Machining (EDM), etc. Contrary to the AM principle, subtractive manufacturing has a 'top-to-bottom' approach. While there are several such methods, this research focuses on a recently developed subtractive process called CNC-RP, since it is analogous to the 'layer approach' found in AM processes [19]. Further, as in the 'freeform' aspect of AM, CNC-RP provides a comparable yet unique aspect of generating a part directly from a CAD file without any custom fixtures or tooling through machining. Similarly, a single-setup approach of CNC-RP has been extended to 'subtract' material through EDM [12].

2.2.1 CNC-RP

The recently developed CNC-RP produces accurate functional parts directly from a CAD model and available tool library (of the machine tool) without any human intervention or specialized fixtures (similar to AM) by using a 4-axis CNC setup and sacrificial fixturing techniques (similar to AM) as shown in Figure 10 [19].

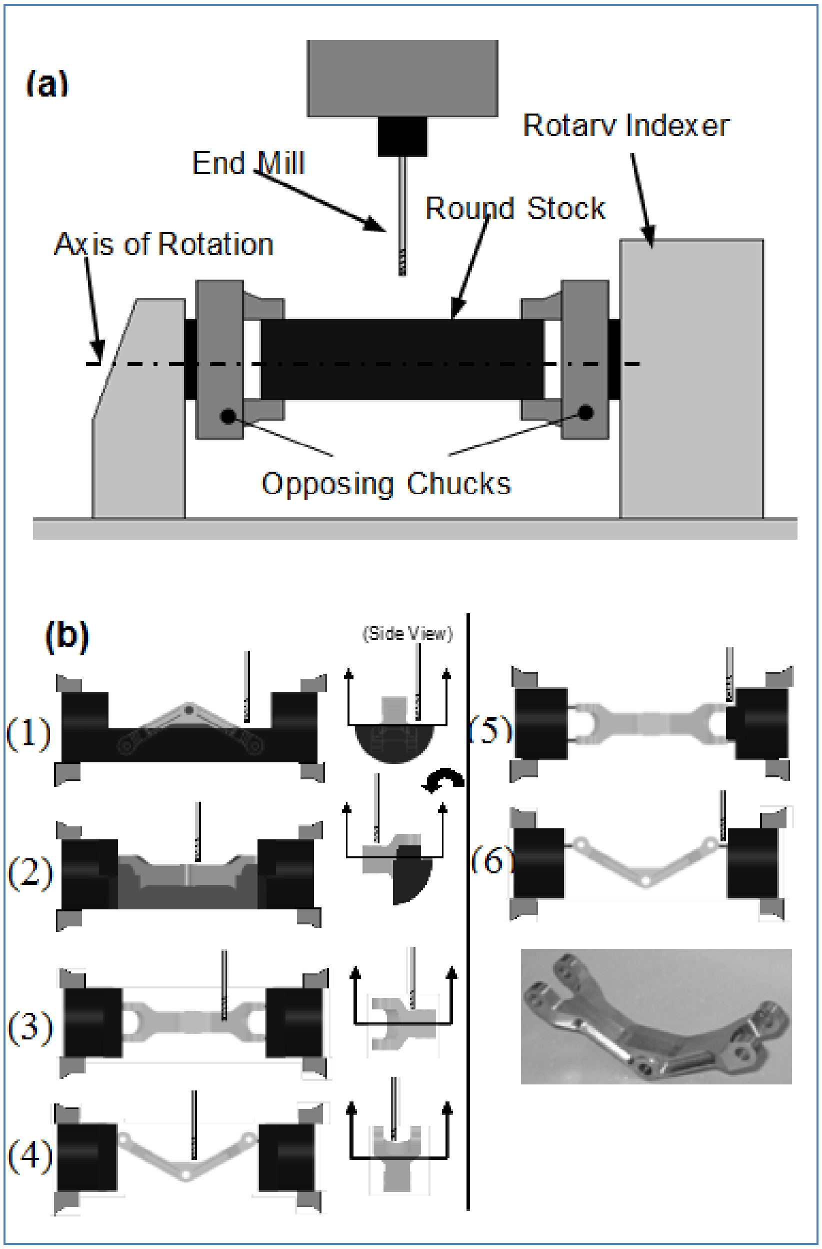
(a)
Rotarv Indexer
End Mill
Round Stock
Axis of Rotation
Opposing Chucks
(b)
(Side View)
(1)
(2)
(3)
(4)
(5)
(6)

Figure 10: CNC-RP Process; (a) Setup (b) Example

A CAD file of the desired part is analyzed by the CNC-RP software using visibility analysis to identify the sequence and minimal orientations required to produce the part from a round bar stock [19, 21 and 22]. Sacrificial fixtures or struts are added to the original STL model to support the finished part within the stock and for it to remain in place for the duration of the manufacturing process. The size of the sacrificial fixturing is a function of the material properties of the stock and is determined based on an allowable deflection during milling. Upon determining the sequence and machining orientations from the visibility analysis, the sacrificial fixtures are integrated into the STL model automatically.

From the standpoint of selection of machining parameters and tooling, CNC-RP operations can be distinguished into the following stages: (1) Hogging, where feature-independent *z*-planar roughing operation with larger depth of cut is used to reduce the cylinder into a roughing stock, (2) Roughing, where feature-dependent island milling is pursued based on visibility analysis to reduce the part to 'near-net' dimensions and finally, (3) Finishing, where feature-dependent island milling with a smaller cutting tool at finish machining conditions is pursued to produce the part to required dimensions. The grouping of CNC-RP stages is based on the material removal rate and individual purpose of the stages. This grouping enables the identification of the 'finishing' CNC-RP stage that can be integrated with 'near-net' additive processes in a hybrid process. Figure 11 outlines the purpose of hogging, which is for 'material clearance' in order to machine based on the required part geometry at each layer.

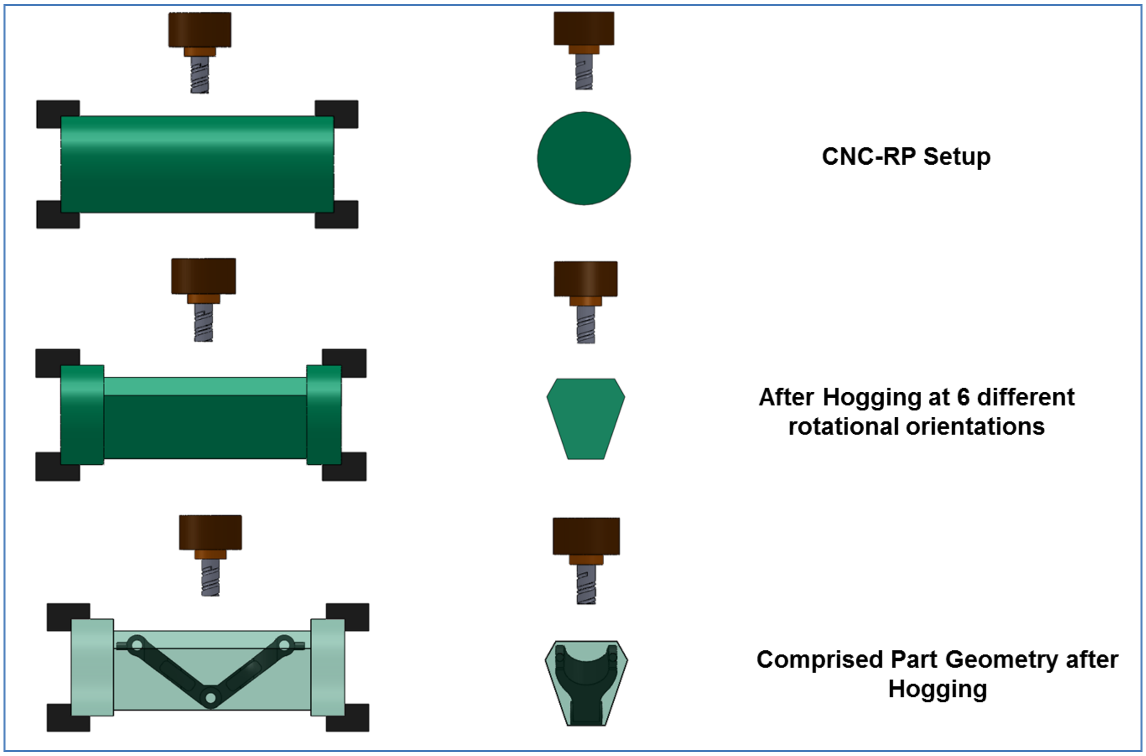
CNC-RP Setup
After Hogging at 6 different rotational orientations
Comprised Part Geometry after Hogging

Figure 11: CNC-RP Process- Setup and after Hogging

2.2.2 Attributes of CNC-RP

When compared to AM methods, CNC-RP provides superior part accuracy and surface finish (similar to conventional machining methods). In most cases, the part accuracy is that of the machine tool tolerance in the order of a few microns. Further, the automated aspect of CNC-RP requires minimal expertise to execute the ‘click-to-machine’ program, similar to the commonly used AM methods. However, due to geometric limitations similar to traditional manufacturing, CNC-RP is limited to the part design complexities that can be created.

For instance, part geometries like non-stochastic lattice structures and complex contours as shown in Figure 10 cannot be produced through CNC-RP (or traditional machining without multiple fixtures). From a sustainability standpoint, the raw material-part volume ratio is often very low for subtractive processes since the majority of the material can end up as scrap and chips. In the cases of machining expensive superalloys using CNC-RP, the low material efficiency is coupled with the low machinability and such alloys are often difficult to process through other conventional methods. As a result, the tooling cost is high, which increases the unit price, particularly in the case of low volume batch production.

2.3 Hybrid Manufacturing

In order to economically produce a part with required accuracy and specifications, often several manufacturing processes are combined. These are often referred to as 'hybrid processes'. Such an integrated approach eliminates the limitations of individual processes while aggregating their advantages. There have been several studies that have compared different definitions and classifications of hybrid processes [23, 24 and 25]. Researchers have extensively focused on 'hybrid machining' where more than one distinct machining process (e.g. milling, boring, drilling, etc.) has been employed to remove material and generate the required part [26, 27 and 28]. The definition of a 'hybrid process' has varied based on the material used (such as composite products) [29], the combination of more than one 'active principle' (such as laser assisted turning/ milling) [23 and 30], the combination of different energy forms [28], etc.

In the case of hybrid additive manufacturing, there is a comprehensive review of multiple techniques such as melting of deposited material at different heat conditions, mixing of different materials during deposition, deposition of discrete materials, etc. [23]. The International Academy for Production Engineering- CIRP has proposed the following definitions for hybrid processes [23]:

1) "Open definition: A hybrid manufacturing process combines two or more established manufacturing processes into a new combined set-up whereby the advantages of each discrete process can be exploited synergistically;"
2) "Narrow definition: Hybrid processes comprise a simultaneous acting of different (chemical, physical, controlled) processing principles on the same processing zone."

In the context of this research, a hybrid process refers to the combination of an additive and subtractive process. By combining the advantages of such different manufacturing approaches, the disadvantages associated with the individual techniques can be eliminated. Sub-section 2.3.1 details such hybrid processes. With respect to the major metal AM processes detailed in Section 2.1, much of the current hybrid methods are focused only on directed energy deposition and are not applicable for binder jetting and powder bed-fusion methods.

2.3.1 ECLIPSE-RP

Most AM and Hybrid processes uses STL (Stereolithography) file format, which is a triangulated mesh of the desired part and is feature and unit independent.

As opposed to the STL file format, this hybrid process uses STEP AP203 file format to identify three-dimensional part volumes that can be derived from machining segments (holes, slot, pocket and miscellaneous surfaces) in a thicker layer of sheet material (3-30mm) and are subsequently, glued to each other using a custom 6-axis set-up. The 6-axis set up enables machining of vertical walls in the part if required [31].

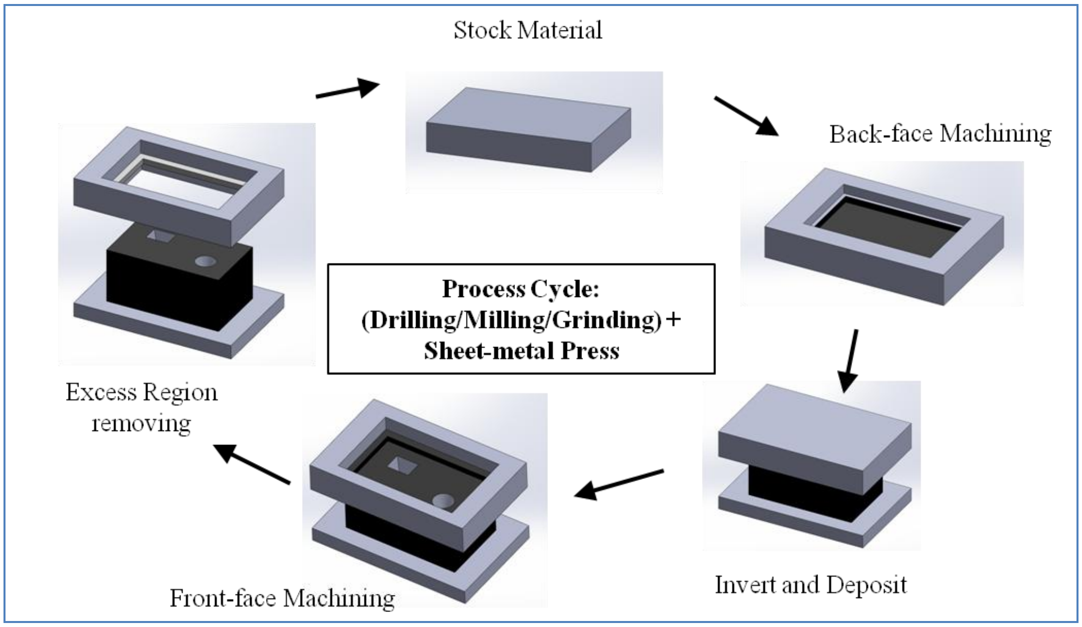
Stock Material
Back-face Machining
Process Cycle:
(Drilling/Milling/Grinding) +
Sheet-metal Press
Invert and Deposit
Front-face Machining
Excess Region
removing

Figure 12: ECLIPSE-RP Hybrid process

As shown in Figure 12 [31], after intensive process planning a sheet stock material is machined, reversed in a special fixture and additional sheet of stock material is glue-pressed on to its backside. Then, machining is conducted on the newly pressed sheet metal and this process continues until the final part is fabricated. The mechanical strength of parts produced via this method depends on the adhesive strength across layers.

2.3.2 SLC

The Selective Laser Cladding process shown in Figure 13 uses metal powder with a polymer binder along with Selective Laser Sintering (SLS) to apply laser energy onto the thermo-plastic coated metal powder bed, thereby vaporizing the thermoplastic coating.

The process planning considers the sequence of laser cladding and machining (i.e. layers at which machining is pursued and the corresponding toolpath) [32].

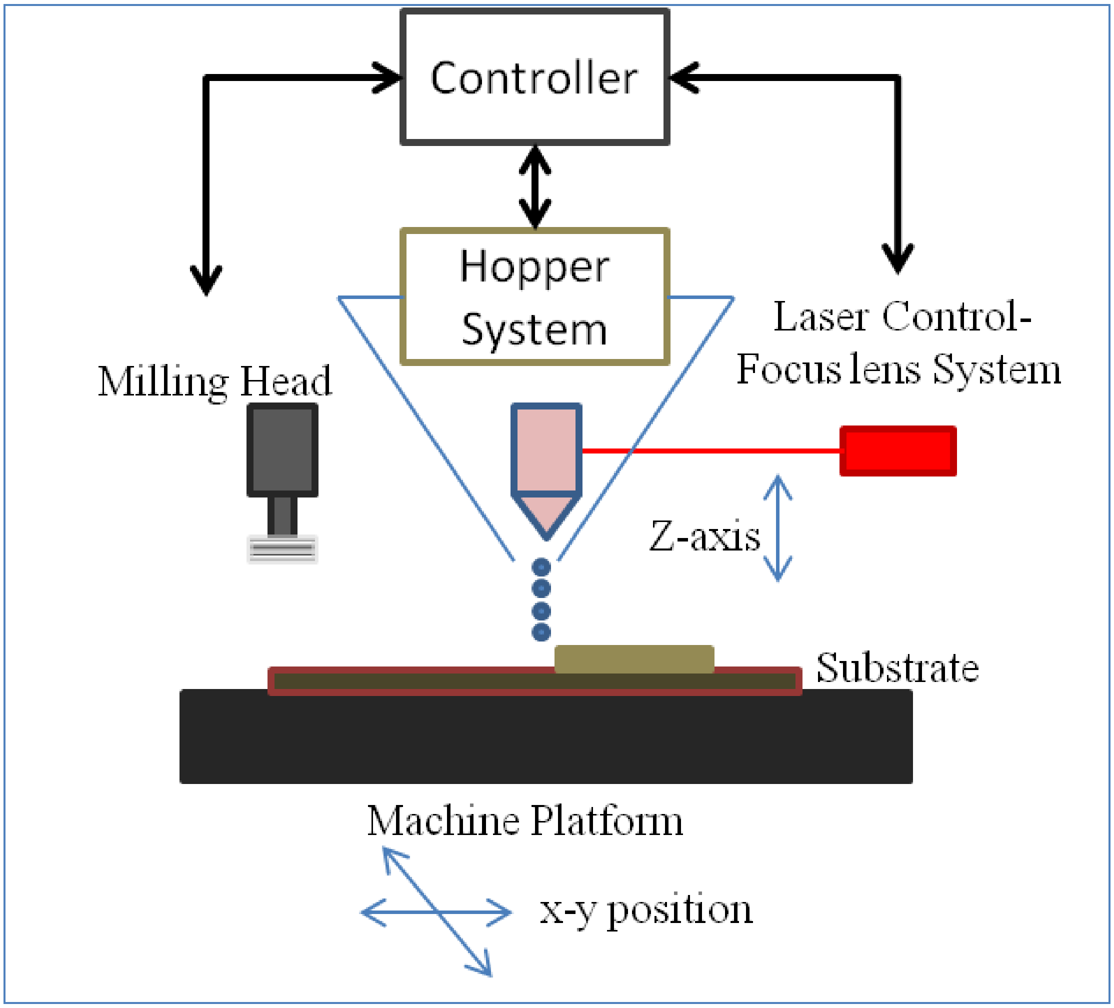
Controller
Hopper System
Milling Head
Laser Control-Focus lens System
Z-axis
Substrate
Machine Platform
x-y position

Figure 13: Hybrid SLC process

Finally, the part is infiltrated with copper to fill the voids caused by the vaporization of the photo-polymers. The process was validated through a fabrication of 3 mm tall square part. Further, as prevalent in most laser-cladding operations/applications, the process was successfully implemented to modify/repair a CNC-made injection mold.

2.3.3 LAMP process

Laser-aided Manufacturing Process (LAMP) process is a hybrid process comprising of powder-fed laser deposition process and a 5-axis CNC machining system [33 and 34]. Upon process planning (sequence of deposition and machining toolpath), a laser is used to selectively deposit material in the machine volume and a milling tool is used to finish machine the layers as shown in Figure 14 [34].

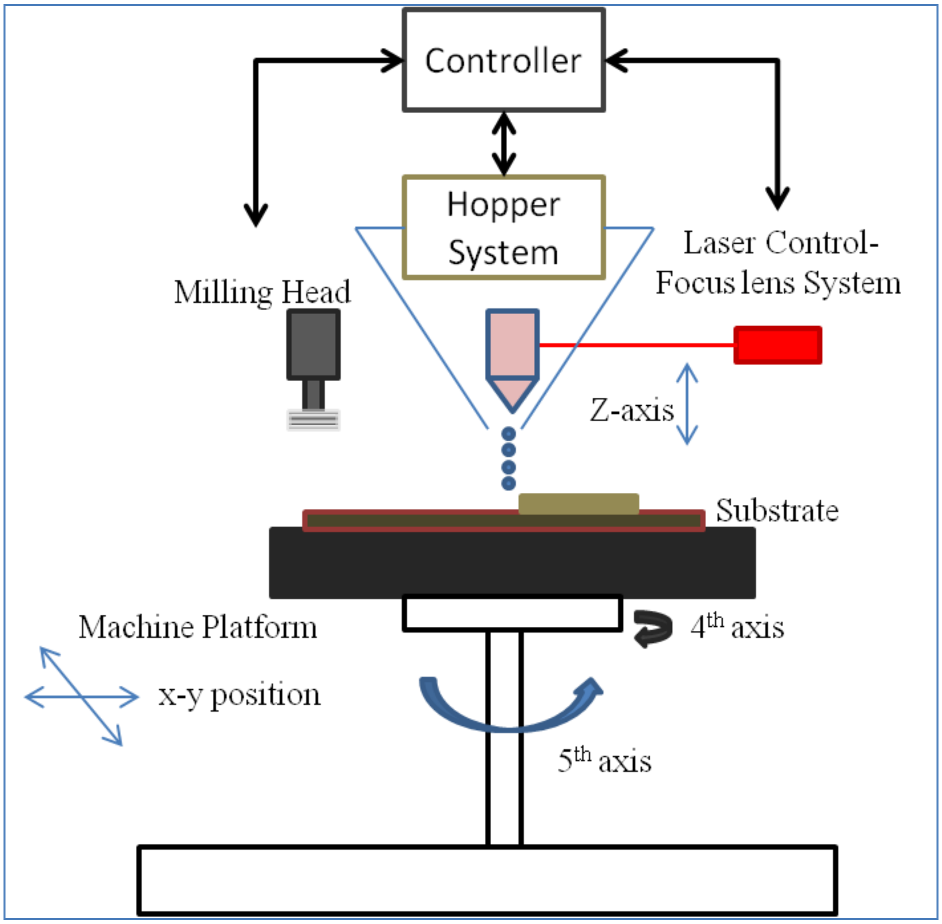
Controller
Hopper System
Laser Control-Focus lens System
Milling Head
Z-axis
Substrate
Machine Platform
4th axis
x-y position
5th axis

Figure 14: LAMP process

In order to fabricate parts with overhanging edges, the deposition plate is rotated about the machine axis by adding 5-axis capability. The process was demonstrated to generate parts with overhanging angle of 45º. It should be noted that the largest cross-section of the part should always be the first layer of the build in order to withstand machining forces.

Detailed process planning is required to produce complex parts by decomposing a solid model to identify the sequence of deposition and machining of each individual volume features in the model [33].

A study was conducted to evaluate the complexity of possible part designs for hybrid processes involving layered manufacturing and subtractive machining based on manufacturability indexes [35].

2.3.4 Ultrasonic Consolidation

Ultrasonic Consolidation (UC) is a hybrid technique where high-frequency ultrasonic energy applies combined static and oscillating shear forces to sheets of metal foils to cause metallurgical bonds as shown in Figure 15 [36]. UC is combined with CNC milling to produce part features on the adhered layers [36 and 37]. As with traditional material removal processes, there is lower material utilization (machining chips) and when compared to hot-bed and laser AM processes, the mechanical properties of the part highly depends on the strength of metallurgical adhesion between each layers. Further, as opposed to powder-bed processes, sacrificial support features cannot be included and thereby limiting the feasible part designs.

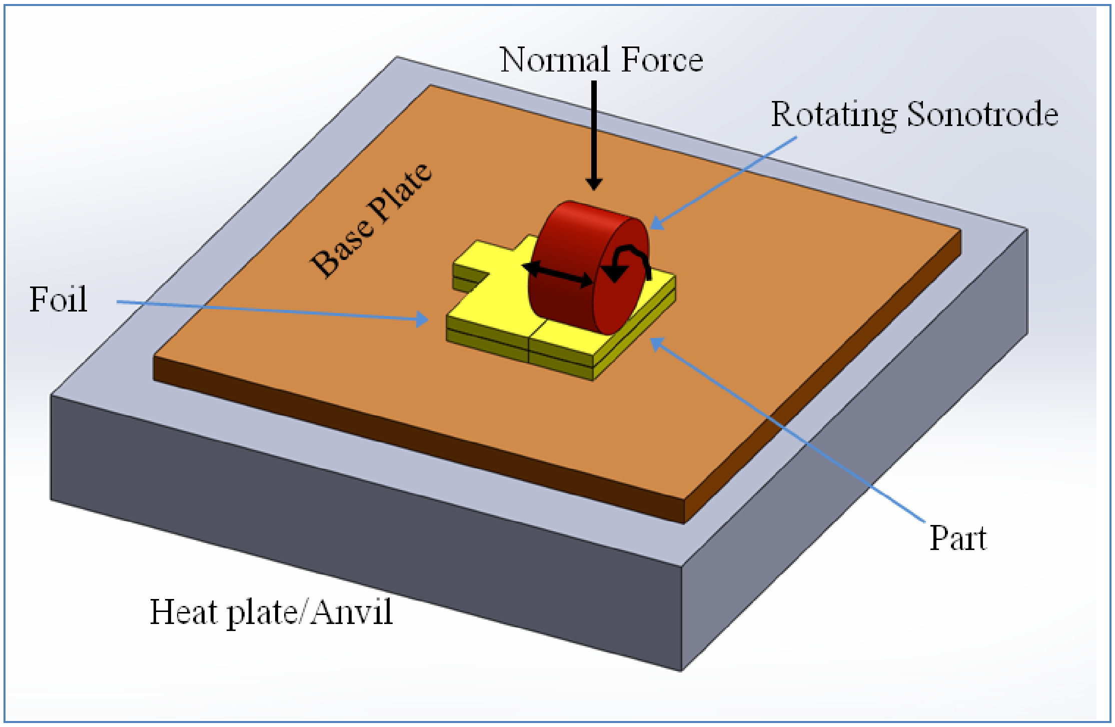

Figure 15: Ultrasonic Consolidation

2.3.5 3D Deposition-Milling

There are several studies focused on the development of hybrid processes via welding based deposition using laser arc welding [38] and metal inert gas welding [39] with wire-feed for deposition. Similar to aforementioned hybrid processes, the welding torches are retro-fitted into a CNC machine to enable the cycle of deposition and machining. The microstructures from such processes showed the non-uniform microstructure evolution (in size and phase distribution) at the base layer and across layers. Additionally, there were discontinuous grain structures due to gaps in the weld beads [38].

2.3.5 Attributes of Current Hybrid Processes

The following are some of the major collective attributes of the existing hybrid systems (within the realm of additive-subtractive hybrid processes):

- **Constant/Fixed Constant coordinate system** to seamlessly switch between additive and subtractive operations
- Because of the access to various CNC machine tools, several machining operations such as milling, drilling, grinding etc. can be pursued along with the additive approach.
- Significant process planning is required to identify the sequence of deposition and machining, since ‘inference/gauge check’ is indispensable to ensure that the deposition element (weld or laser heads, powder feed) and the machine tool do not collide with each other **or** with the part.
- The down-time associated with constant tool changes caused by switching between deposition and milling tool is a non-value adding step.
- There are concerns with the microstructure associated with the irregular heat distribution cycles (e.g. machining every 2 layers vs. machining after 10 layers of deposition); post-processing heat treatment would be required here.
- The use of coolant during machining is not feasible because of the use of laser (optics) and welding heads. This is particularly detrimental while processing tough-to-machine alloys and could significantly increase the tooling cost.

- The weldability of superalloys is inferior to that of other commonly used alloys [40]. This could limit such hybrid processes from successfully producing parts for aerospace and mechanical applications.
- Complex part designs with non-uniformly varying cross-sections are a challenge to produce using such processes due to the infeasibility of incorporating support structures for overhanging edges.

In addition to these attributes, it should be noted that the current hybrid processes are applicable **only** to direct energy deposition processes.

2.4 Desired Attributes in a Hybrid Method

Based on the discussion from Section 2.3, it is important to develop a ‘global’ hybrid approach that can be integrated with other types of metal additive manufacturing methods such as the binder jetting and powder-bed fusion processes. The processing capability (range of materials and applications) are ever-growing in AM processes such as EBM, SLM, SLS, etc. It is therefore necessary to develop a hybrid process that can be integrated to combine advantages from such methods. For instance, existing hybrid approaches of deposition-machining are not feasible for powder-bed fusion processes as they would damage the non-processed powders and any support, making it impossible to proceed with subsequent layers. Further, in some AM process such as EBM, it is not feasible to operate/possess the machine tool in the same build environment because the EBM operates under high vacuum conditions.

Because of the nature of such AM processes (hot-bed temperature with slow cooling in inert atmosphere), they are preferred to process superalloys and have better metallurgical conditions. In conclusion, a novel hybrid process is desired such that it is not linked to a specific category of AM techniques but can cater to any AM process.

This can be used to produce parts made of tough-to-process alloys with minimal machining so as to achieve precision tolerance and surface finish. Similar to the ‘click-to-print’ approach of AM, the hybrid process should not require custom fixtures and tools based on part design and should be able to operate with minimal human intervention and expertise. The hybrid process should be applicable without any modifications to existing AM methods.

2.5 Economic Analyses

The success and widespread implementation of any manufacturing process is based on its technical viability and economic feasibility. The advantages and challenges of AM processes is highlighted in Section 2.1. In this section, an overview of prior work in metal AM economics and listed major cost factors in AM is presented. According to latest Wohler’s report (2013), the market for AM, including all products and services, grew by 26 % (Compounded Annual Growth Rate) to a total of \$ 2.204 billion globally [41]. This estimate consists of revenue associated with primary AM market in AM products including AM systems, upgrades, materials, etc. and AM services through service providers, contracts, training, R&D etc. In particular, revenues associated with metal AM grew by 38.3% to a total of \$ 24.9 million which indicates tremendous interest and potential for further improving end-metal AM products.

The project, CoA^{2}MPLy (Cost Analysis for Additive Manufacturing during Product Lifestyle) is focused on estimating the benefits of metal AM through a lifecycle-based approach [42 and 43]. It was noted that material cost is one of the two largest contributors to the total cost of the part along with operation cost [43]. In metal-AM operation, the build time (speed) and personnel cost were identified as the major factors in the high cost, particularly in the case of parts with shorter product lifecycle [42 and 43]. Hence, it was highlighted that part design optimization should be verified to lower part renewal. The final cost driver noted by the project was that of data-preparation due to higher labor costs since skilled and experienced engineering is required to 'prepare' building plans, particularly in the case of higher units of smaller parts [43].

A recent study analyzed the AM supply chain in the production of spare parts and concluded that lower machine cost and distributed production system with decentralized production location is more economical for rapid manufacturing [44]. The study focused on spare parts supply chain and noted that such supply chains for capital-intensive technologies like AM will result in lower overall operation costs, down time and higher flexibility. Similar findings were listed in another study which conducted make or buy analysis for rapid manufacturing [45]. Prior studies have compared the cost of producing parts through traditional methods and AM and it was consistently noted that AM is suited for small batch production but the cost is impacted by AM machine and labor costs [46 and 47]. Advantage of AM capabilities was highlighted through a FEA-based case study on an aerospace part redesign and the AM cost (DMLS) was compared to high-pressure design casting [46].

The significant impact of AM machine cost was shown with respect to production volume (e.g. Inject molding) and cost of computational tools required in metal AM were detailed [47]. In the case of powder-bed processes, studies have shown that part size and packing ratio are the two critical features in lowering unit cost [48], particularly when simultaneously producing different part designs [49] and in some cases up to 41% [50] reduction has been realized.

The existing economic models assume a fixed amount of time for ‘post-processing’ which varies from removal of support-structures to heat-treatment (annealing) in laser powder-bed processes. The current literature lacks an economic model which takes into account the post-process planning, machining time, etc. based on the part geometry, machining allowance, machinability, etc. Such an economic model will better reflect the impact of ‘batch’ metal AM-production or mixed components production in powder-bed processes on overall unit cost. Secondary market associated with AM including tooling produced from AM products grew by 10% to $1.19 billion in 2012 [41]. This secondary market will further benefit from shorter lead-time in post-processing through modular finishing operation. Development of a hybrid AIMS cost model will be useful to evaluate the performance and critical cost factors in AIMS, similar to existing literature studies in identifying critical factors in pure AM processes.

Summary

This chapter provides an overview of different AM methods and their classifications. The metal-based AM processes are outlined in detail with their advantages and limitations. A 'layer-based' AM-like subtractive method, called CNC-RP is also detailed with its advantages and challenges. Further, existing hybrid processes are studied for their processing capabilities and limitations. Based on the review, attributes desired in a novel hybrid process that can be integrated with any AM process without considering constraints such as lack of support structures, limitations in part geometry, etc., are described. Finally, the need for an economic model that would include hybrid cost components is illustrated.

References

1) Gibson, I., Rosen, D.W. and Stucker, B., "Additive manufacturing technology: rapid prototyping to direct digital manufacturing", Springer Science + Business Media, Inc.; 2010, ch.1, pp. 3-5.
2) Pham, D.T. and Gault, R.S., 1998, "A comparison of rapid prototyping technologies", International Journal of Machine Tools and Manufacture, vol. 38(10-11), pp. 1257–1287.
3) Pegna, J., 1997, "Exploratory investigation of solid freeform construction", Automation in construction, vol. 5(5), pp. 427-437.
4) Kruth, J.P., Leu, M.C. and Nakagawa T, 1998, "Progress in additive manufacturing and rapid prototyping", CIRP Annals- Manufacturing Technology, vol. 47(2), pp. 525–540.
5) Williams, C. B., Mistree, F. and Rosen, D. W., 2011, "A functional classification framework for the conceptual design of additive manufacturing technologies," Journal of Mechanical Design, vol. 133, pp. 121002-1 – 121002-11.

6) ASTM Designation: F2792-12a, “Standard Terminology for Additive Manufacturing Technologies”, pp.1-3.

7) Ex-one Systems, accessed as of July 18, 2013, url< http://www.exone.com/sites/default/files/brochures/X1_Metal_sellSheets.pdf>

8) Ruan, J., Tang, L., Sparks, E.T. and et al., 2008, “Direct 3D layer metal deposition”, The Nineteenth Annual International Solid Freeform Fabrication Symposium, Austin,Texas, pp. 333–341.

9) Griffith, M.L., Ensz, M.T., Puskar, J.D. and et.al, 2000, “Understanding the microstructure and properties of components fabricated by Laser Engineered Net Shaping (LENS)”, Proceedings of MRS Spring meeting, San Francisco, California.

10) Taminger, K. M. B. and Hafley, R. A., “Electron beam freeform fabrication: a rapid metal deposition process”, Proceedings of 3rd Annual Automotive Composites Conference, Troy, Michigan.

11) Manogharan, G.P., Soundarajan, D.K and Wysk, “Study of energy efficiencies in rapid prototyping”, ISERC Conference, May 21- 25, 2011, Reno, Nevada.

12) National Instruments, “Developing a Quality Inspection Method for Selective Laser Melting of NI hardware and software”, accessed as of July 18, 2013, url< http://sine.ni.com/cs/app/doc/p/id/cs-13103>

13) Auburtin, P., Wang, T., Cockcroft, S.L., and Mitchell, A., 2000, “Freckle formation and freckle criterion in superalloy castings”, Metallurgical and Materials Transaction B, vol. 31, pp. 801-11.

14) Baufeld, B. and Biest, O.V., 2009, “Mechanical properties of Ti–6Al–4V specimens produced by Shaped Metal Deposition: Microstructure and mechanical properties”, Materials and Design, vol. 31(1), pp. S106-S111.

15) Santos, E.C., Shiomi, M., Osakada, K. and Laoui, T., 2006, “Rapid manufacturing of metal components by laser forming”, International Journal of Machine Tools and Manufacture, vol. 46(12-13), pp. 1459-1468.

16) Harrysson, O.L.A., Cansizoglu, O., Marcellin-Little, D.J., Cormier, D.R. and West, H.A., 2008, “Direct metal fabrication of titanium implants with tailored materials and mechanical properties using electron beam melting technology”, Material Science Engineering, Vol. 28 No.3, pp. 366-373.

17) Petrovic, V., Gonzalez, J.V.H. and et.al, 2011, “Additive layered manufacturing: Sectors of industrial application shown through case studies”, International Journal of Production Research, vol. 49 (4), pp. 1071–1079.

18) Manogharan, G.P., Wysk, R.A., Harrysson, O.L.A and Cohen, P.H., "Hybrid manufacturing: Unique approach to integrating additive and subtractive rapid prototyping process", Proceedings of the 22nd FAIM Conference, June 10-12 2012, Helsinki, Finland.

19) Frank, M. C., Wysk, R. A. and Joshi, S., 2004, “Rapid Planning for CNC Milling-A new Approach for Rapid Prototyping”, Journal of Manufacturing Systems, vol. 23 (3), pp. 242-255.

20) Yang, Z., Wysk, R. A., Joshi, S., Frank, M. C., and Petrzelka, J. E., 2009, “Conventional Machining Methods for Rapid Prototyping and Direct Manufacturing”, International Journal of Rapid Manufacturing, vol. 1(1), pp. 41–64.

21) Petrzelka, J.E and Frank, M., 2010, “Advanced process planning for subtractive rapid prototyping”, Rapid Prototyping Journal, vol. 16(3), pp. 216-224.

22) Yang, Z., Wysk, R.A. and Joshi, S., 2011, “Global Tangent Visibility Analysis for Polyhedral Computer Aided Design Models”, Journal of Manufacturing Science and Engineering, vol. 133, pp. 031012(1-9).

23) Zhu, Z., Dhokia, V., Nassehi, A. and Newman, S.T., 2013, “A review of hybrid manufacturing processes—state of the art and future perspectives”, International Journal of Computer Integrated Manufacturing, Taylor & Francis.

24) Klocke, F., Wegner, H., Roderburg, A. and Nau, B., 2010, “Ramp-up of hybrid manufacturing technologies”, Proceedings of 43rd CIRP Conference on Manufacturing Systems, Vienna, Austria, pp.407-415.

25) Nau, B., Roderburg, A. and Klocke, F., 2011, “Ramp-up of hybrid manufacturing technologies”, CIRP-Journal of Manufacturing Science and Technology, vol. 4, pp. 313 – 316.

26) Rajurkar, K.P., Zhu, D., McGeough, J.A., Kozak, J. and De Silva, A., 1999, “New developments in electro-chemical machining”, CIRP Annals- Manufacturing technology, vol. 48(2), pp. 567-579.

27) Aspinwall, D.K., Dewes, R.C., Burrows, J.M. and Paul, M.A., 2001, “Hybrid high speed machining (hsm): System design and experimental results for grinding/hsm and edm/hsm”, CIRP Annals- Manufacturing technology, vol. 50(1), pp. 145-148.

28) Menzies, I. and Koshy, P., 2008, “Assessment of abrasion-assisted material removal in wire edm”, CIRP Annals- Manufacturing technology, vol. 57(1), pp. 195-148.

29) Roderburg, A., Gerhardt, K., Hinke, C., Park, H.S., Buchholz, S. and Klocke, F., 2011, “Design methodology for innovative hybrid manufacturing technologies”, Proceedings of the 2011 17th International Conference on Concurrent Enterprising (ICE 2011), Aachen, Germany, pp.1-9.

30) Dandekar, C.R., Shin, Y.C. and Barnes, J., 2010, “Machinability improvement of titanium alloy (ti-6al-4v) via lam and hybrid machining”, International Journal of Machine Tools and Manufacture, vol. 50(2), pp.174-182.

31) Hur, J., Lee, K., Hu, Z. and Kim, J., 2002, “Hybrid rapid-prototyping system using machining and deposition”, Computer-Aided Design, vol. 34, pp. 741–754.

32) Jeng, J.Y. and Lin, M.C., 2001, “Mold fabrication and modification using hybrid processes of selective laser cladding and milling”, Journal of Materials Processing Technology, vol. 110 (1), pp. 98-103.

33) Liou, F., Slattery, K. and et.al, 2007, “Applications of a hybrid manufacturing process for fabrication of metallic structures”, Rapid Prototyping Journal, vol. 13(4), pp. 236-244.

34) Zhang, J. and Liou, F., 2004, “Adaptive slicing for a multi-axis laser aided manufacturing”, Journal of Mechanical Design, vol. 126 (2), pp. 254-261.

35) Kerbat, O., Mognol, P. and Hascoet, J.Y., 2010, “Manufacturing complexity evaluation at the design stage for both machining and layered manufacturing”, CIRP Journal of Manufacturing Science and Technology, vol. 2 (3), pp. 208-215.

36) Janki Ram, G.D., Yang, Y. and Stucker, B.E., 2006, “Effects of process parameters on bond formation during ultrasonic consolidation of Aluminum alloy 3003”, Journal of Manufacturing Systems, vol. 25 (3), pp. 221- 238.

37) Schick, D.E., Hahnlen, R.M., Dehoff, R. and et.al, 2010, “Microstructural characterization of bonding interfaces in Aluminum 3003 blocks fabricated by ultrasonic additive manufacturing”, Welding Journal, vol. 89, pp. 105-116.

38) Choi, D.S., Lee, S.H. and et.al, 2001, “Development of a direct metal freeform fabrication technique using CO_2 laser welding and milling technology”, Journal of Materials Processing Technology, vol. 113 (1-3), pp. 273-249.

39) Karunakaran, K.P., Suryakumar, S., Pushpa, V., and Akula, S., 2010, ‘Low cost integration of additive and subtractive processes for hybrid layered manufacturing’, Robotics and Computer-Integrated Manufacturing, vol. 26(5), pp. 490-499.

40) D.J. Tillack, 2007, “Welding superalloys for aerospace application”, Welding Journal, vol. 1, pp. 28-32.

41) Wohlers Report, 2013, Additive Manufacturing and 3D Printing State of the Industry: Annual Worldwide Progress Report.

42) Lindemann, C., Jahnke, U., Moi, M. and Koch, R., 2013, "Impact and Influence factors of additive manufacturing on Product Lifecycle costs", Proceedings of the twenty-fourth Annual International Solid Freeform Fabrication Symposium, Austin, Texas, pp. 998-1008.

43) Lindemann, C., Jahnke, U., Moi, M. and Koch, R., 2012, "Analyzing Product Lifecycle Costs for a Better Understanding of Cost Drivers in Additive Manufacturing", Proceedings of the twenty-third Annual International Solid Freeform Fabrication Symposium, Austin, Texas, pp. 177-188.

44) Khajavi, S.H., Partanen, J. and Holmstrom, J., 2014, "Additive manufacturing in the spare parts supply chain", Computers in Industry, vol. 65, pp. 50-63.

45) Ruffo, M., Tuck, C. and Hague, R., 2007, "Make or buy analysis for rapid manufacturing", Rapid Prototyping Journal, vol. 13 (1), pp. 23-29.

46) Atzeni, E. and Salmi, A., 2012, "Economics of additive manufacturing for end-usable metal parts", The International Journal of Advanced Manufacturing Technology, vol. 62, pp. 1147–1155.

47) Hopkinson, N. and Dickens, P., 2003, "Analysis of rapid manufacturing-using layer manufacturing processes for production", Proceedings of the Institution of Mechanical Engineers, Part C: Journal of Mechanical Engineering Science, vol. 217, pp. 31-39.

48) Ruffo, M., Tuck, C. and Hague, R., 2006, "Cost estimation for rapid manufacturing - laser sintering production for low to medium volumes", Proceedings of the Institution of Mechanical Engineers, Part B: Journal of Engineering Manufacture, vol. 220 (9), pp. 1417-1427.

49) Ruffo, M. and Hague, R.J.M, 2007, “Cost estimation for rapid manufacturing – simultaneous production of mixed components using laser sintering”, Proceedings of the Institution of Mechanical Engineers, Part B: Journal of Engineering Manufacture, 221 (B11), pp. 1585–1591.

50) Rickenbacher, L., Spierings, A. and Wegener, K., 2013, "An integrated cost-model for selective laser melting (SLM)", Rapid Prototyping Journal, vol. 19 (3), pp.208 – 214.

CHAPTER 3: HYBIRD MANUFACTURING- AIMS SYSTEM ARCHITECTURE

Introduction

This research is motivated by the need for integrating additive and subtractive processes to produce complex part geometries directly from a CAD model with minimal machining to achieve precision part-feature accuracy and fine surface finish. In the case of lots of ‘one-to-few’, it is extremely expensive to fabricate custom fixtures and special workholding devices that may be necessary to secure and locate complex part geometries. In many of these cases, the cost of the fixture can be significantly higher than that of the part being produced, especially since the fixture generally requires an accuracy of ten-times that of the part being produced. Further, there is a design and fabrication time associated with creating custom fixtures that will extend the time to actually make a final part. Therefore, the overall unit cost increases tremendously. Such approaches are preferable for mass production (e.g., sand casted engine blocks), where relatively large batch sizes of a single part design undergo secondary and/or finishing operation. In the proposed hybrid manufacturing process, sacrificial fixtures required to secure the part during the subtractive process are added to the desired part prior to ‘near-net’ manufacturing.

In order to characterize this process, it is important to define the hybrid approach and develop an architecture that details the flow of material (physical) and information (algorithmic) through the system. The objective of this chapter is to demonstrate the process flow and identify the variables and requirements during process planning at each stage of the process.

Such an approach will outline the overall requirements to further automate and develop this process. Section 3.1 details the fundamental approach of the proposed hybrid process using an AM system, or for presentation an Arcam EBM (Section 2.1.3) in the additive stage and CNC-RP (Section 2.2.1) in the subtractive stage. However, it should be noted that the concept of creating linkage through integrated sacrificial fixtures between these two discrete stages can be employed with any additive process (e.g., LENS, DMLS) and subtractive process (e.g., wire-EDM, CNC grinding, etc.) using a similar approach.

Section 3.2 presents the different coordinate systems and the corresponding modeling required to process a CAD part model through the AM system, CNC-RP set-up and intermediate fixture coordinate system. The rationale behind the preliminary concept to link an additive with a subtractive process, described in the preceding Section 3.3, is to 'over-grow' the final part geometry to accommodate for machining allowance. Based on preliminary results, this research is formulated with the basic hypothesis that **if properly configured, the best engineering aspects of additive processes (near-net shape parts) and subtractive processes (better geometric accuracy and surface finish) can be obtained for most part geometries using direct digital manufacturing methods.**

Sections 3.3 and 3.4 outline the observations from the feasibility study during preliminary experiments for the AIMS process. Subsequently, Section 3.5 details the broader scope of research associated with the proposed process and Section 3.6 overviews an overall architecture in terms of physical and software/computational components that are required to develop AIMS to its fullest potential. Section 3.7 provides the major performance metrics that are used to analyze the process effectiveness and the objectives for this study are also described.

3.1 AIMS: Additive processing Integrated with Subtractive Methods

A unique integration between direct metal additive manufacturing and subtractive-RP in CNC-RP is formulated through this novel AIMS technique. This system brings together process capabilities of two different state-of-the-art manufacturing approaches (e.g., EBM and rapid CNC machining). The concept is to use an ***additive*** direct metal process such as EBM or DMLS to create complex geometries to near net-shape geometries. Further, in a precisely controlled manner, it employs a secondary advanced ***subtractive*** rapid machining method to create critical surfaces and dimensions within the requirements. Integrating these two advanced technologies yields a hybrid system with capabilities to produce functional metal parts and prototypes with precision accuracy and good surface finish. More importantly, this hybrid technology will further the feasibility and cost-effectiveness for functional parts with complex geometries, which are desired to be made from expensive and high performance metal alloys that are often difficult to process through conventional methods such as casting. Figure 16 illustrates the basic concept behind the AIMS system, showing the creation of a metal linkage via AM (EBM) and SM (CNC-RP).

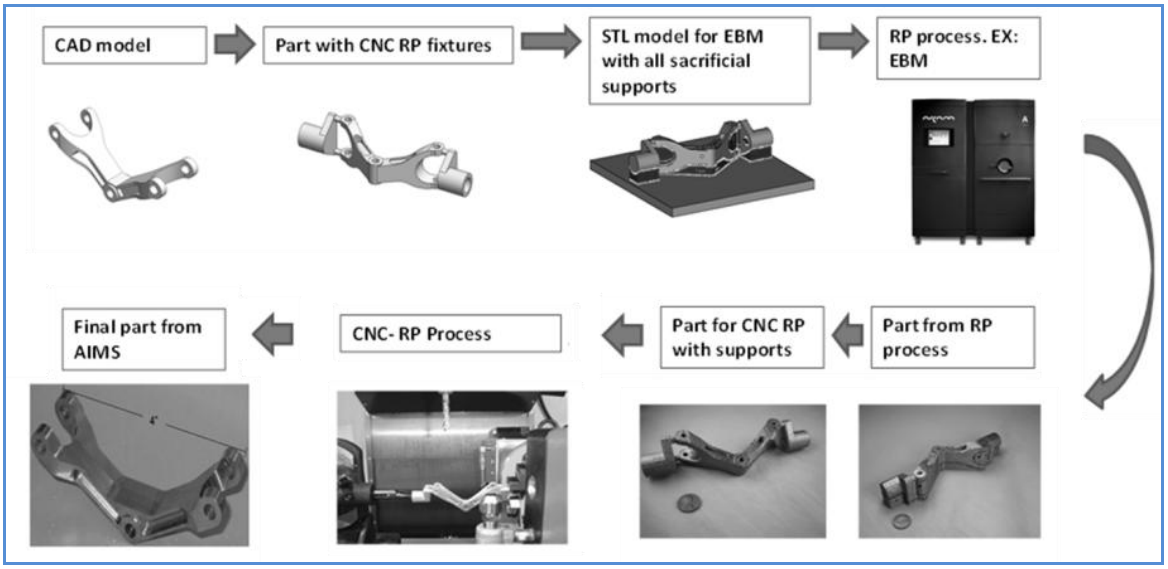
CAD model
Part with CNC RP fixtures
STL model for EBM with all sacrificial supports
RP process. EX: EBM
Part from RP process
Part for CNC RP with supports
CNC- RP Process
Final part from AIMS

Figure 16: The AIMS process

With a higher degree of integration and efficient process planning for AIMS, parts with complex features and accurate dimensions can be easily manufactured. In a limited sense, this research is analogous to the casting process, wherein a *formative* process creates a near-net shape geometry, and a machining process is used to satisfy tight tolerances on geometric and surface characteristics except without significant process planning and requirement for human expertise. However, no casting process has the capabilities to produce complex geometries of superalloys similar to direct metal systems. This emphasizes the broader extent of constraints that are addressed in the proposed objectives. A pioneering technology in rapid manufacturing could be attained upon achieving the objectives stated in this thesis. As shown in Figure 16, the process is hybrid in nature, utilizing a direct metal process like EBM to first manufacture a near-net shape of the desired part, with attached fixture elements designed for a subsequent rapid machining processing.

The AIMS process requires the use of two kinds of sacrificial supports; first to support overhangs in the layer based additive process and later, to support the part in a CNC machine fixture like a fixed structural beam. In addition to the planning of support location and geometry, it is important to identify the critical features of the part. The identified features (e.g. mating surfaces, a contour of a protruding feature, etc.) should be taken into account during process planning for both EBM or CNC-RP or a combination of the two. The ultimate goal is a push button process planning software interface that will process the CAD model of a desired part and then generate two *build* files/models; one for additive and one for subtractive.

3.2 Hybrid Manufacturing Coordinate Systems

In order to model the proposed AIMS system, we need to identify multiple physical production and part-based coordinate systems. Identification of the coordinate systems enables us to transform process accuracies across AM and CNC-RP activities with respect to the part specifications. This leads to the development of a method for estimating the tolerances stacked through AM-processing (such as shrinkage) and work-holding of AM-made fixtures in order to compensate for the errors arising from the successful production of the part. It is difficult to locate the near-net AM part properly in the position system used in CNC-RP. This is illustrated through a series of photographs of parts machined after AM builds, as well as CAD drawings that have been created to illustrate some of these concepts.

These figures will be used to define the displacement magnitudes and locations in: 1) the AM part coordinate system, 2) the part coordinate system, and 3) the

CNC-RP machine coordinate system and how each of these coordinate systems relates to the operations being performed.

There are multiple coordinate systems associated in the AIMS system, namely: 1) Global coordinate systems (AM-build and CNC machine tool), 2) CNC-RP coordinate system, 3) Fixture coordinate system and 4) Final part-coordinate system.

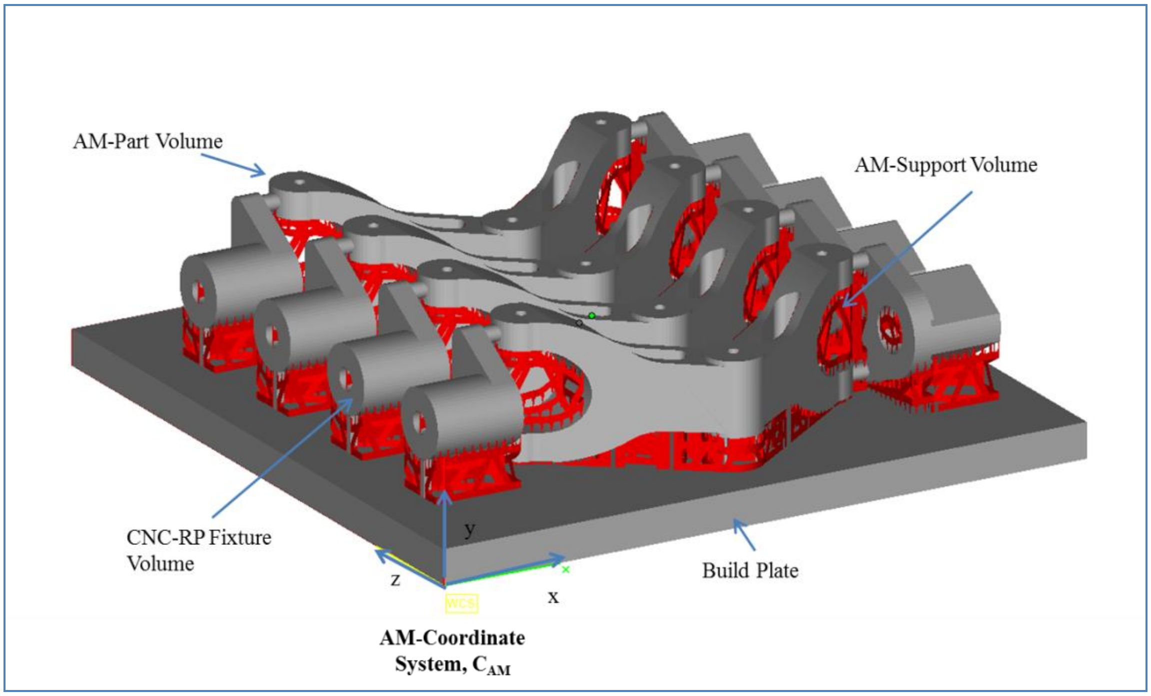
AM-Part Volume
AM-Support Volume
CNC-RP Fixture Volume
y
z
x
WCS
Build Plate
AM-Coordinate System, C_{AM}

Figure 17: AM-Coordinate System C_{AM}

Figure 17 shows the first physical coordinate system (C_{AM}), namely the AM-coordinate system. In most AM processes such as EBM and SLM, the bottom (or top) of the build plate with known dimensions is used to generate layer process parameters.

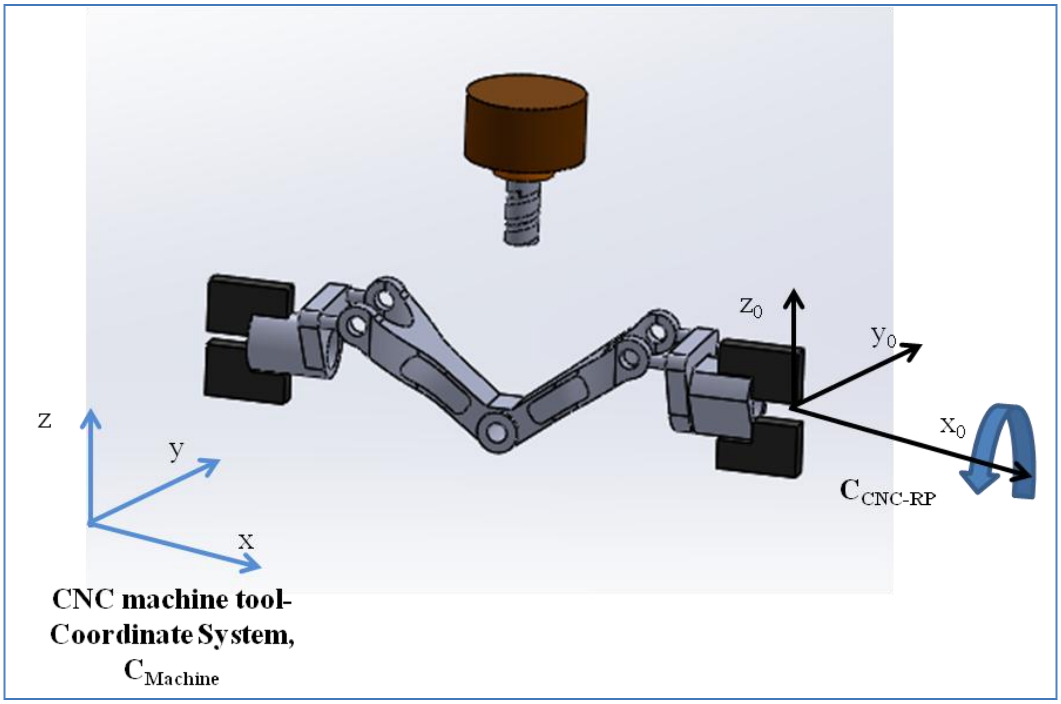
z
y
x
CNC machine tool-
Coordinate System,
C_Machine
z0
y0
x0
C_CNC-RP

Figure 18: CNC-Machine Tool and CNC-RP Coordinate System

We model this physical system such that the CNC-RP setup (4th-axis) (x_0,y_0,z_0,B) is aligned with the machine coordinate system as shown in Figure 18. The sacrificial machining fixture, which is used to hold the part and is removed after the finishing stage, is related to the part as shown in Figure 19 below. It should be noted that there are two different coordinate systems that interact in the secondary machining activity.

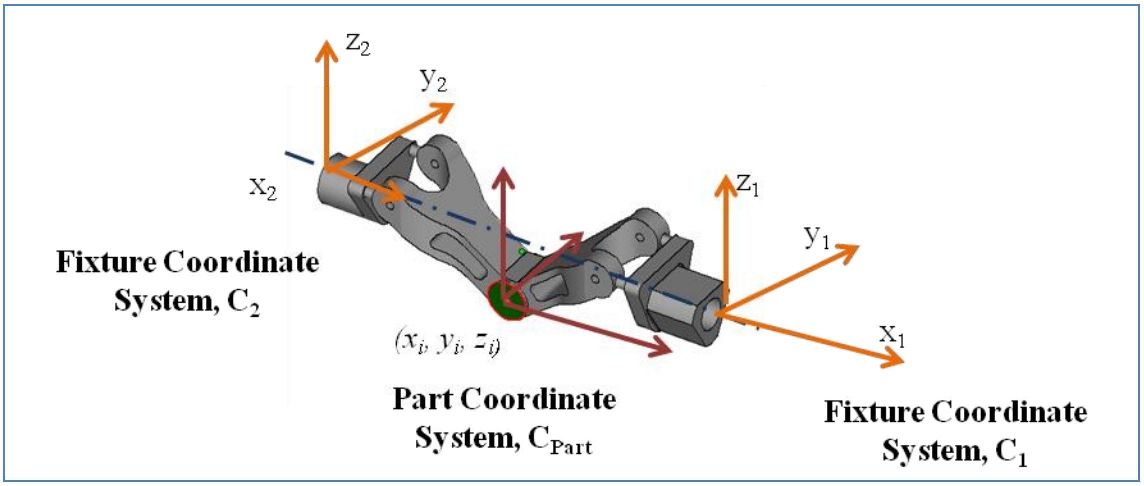
z2
y2
x2
Fixture Coordinate System, C2
(xi, yi, zi)
Part Coordinate System, CPart
z1
y1
x1
Fixture Coordinate System, C1

Figure 19: Fixture and Part Coordinate System

The part features are detailed with respect to the coordinate system as shown in Figure 20, where *i*, is the specification of the “final” part that will be produced through AIMS. Location of part features are linked to the part coordinate system C_{part} (x_i,y_i,z_i). Part coordinate system C_{part} (x_i,y_i,z_i) relates to the machine coordinate system C_{Machine} (x,y,z) through a series of part linkage transformation; Machine → CNC-RP → Fixtures → Part coordinate system → Part Features.

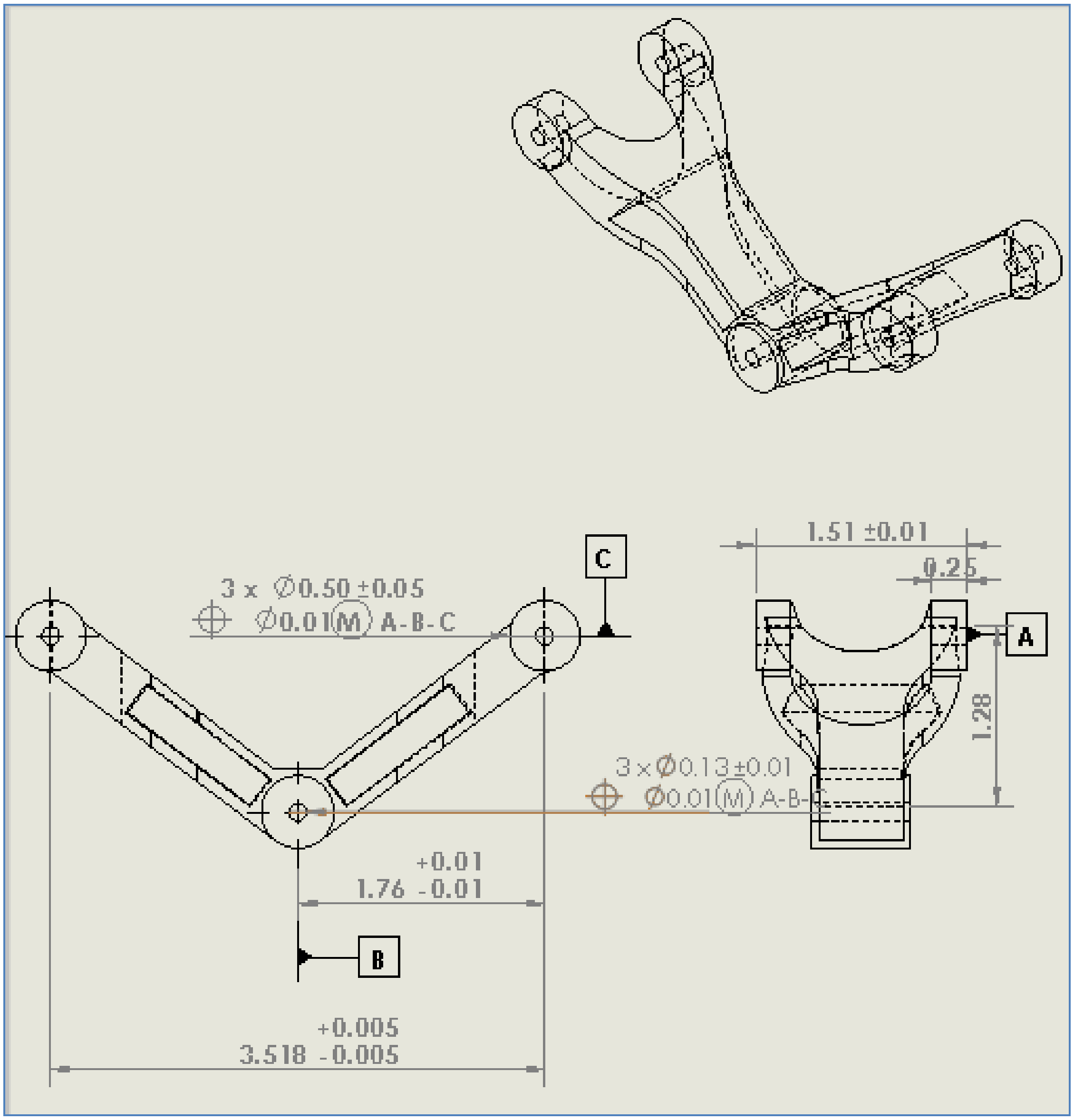
C
3 x Ø0.50 ±0.05
⌖ Ø0.01 Ⓜ A-B-C
1.51 ±0.01
0.25
A
1.28
3 x Ø0.13 ±0.01
⌖ Ø0.01 Ⓜ A-B-C
+0.01
1.76 -0.01
B
+0.005
3.518 -0.005

Figure 20: Desired Part Specifications

In this case, fixture coordinate systems C_1 (x_1, y_1, z_1) and C_2 (x_2, y_2, z_2) are translated through the attachment lugs that are used to clamp the fixtures in the $C_{CNC\text{-}RP}$ set-up. The toolpath used for machining in an orientation is aligned to the $C_{CNC\text{-}RP}$ coordinate system.

Any error in the alignment of the fixture coordinate systems to the CNC-RP coordinate system will be linked to the part coordinate system (and subsequently, to features within the part design). These inaccuracies in each link chain create a “tolerance stack” since the features that are created are dependent on the part coordinate system and this can be represented in 2-D as shown in Figure 21. Due to fixturing inaccuracies (e.g. t_1 and t_2), the location of the part coordinate system that is attached to the fixtures will have a tolerance associated with it (e.g. L ± t’). Since the part coordinate system has a tolerance stacked; any feature that will be created and referenced will have a tolerance, in this case l ± t_i’. Similar chains can be created for all the features in the part design. Finally, the total tolerance stacked on each individual features should satisfy the specifications of the part design (Figure 20).

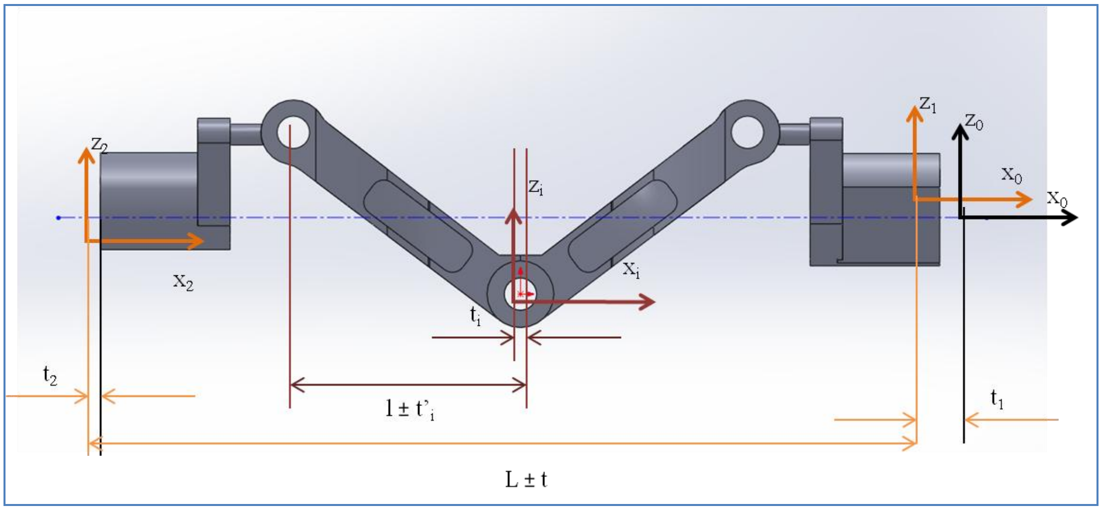

Figure 21 Tolerance Stacking Chain

Hence, based on the errors associated with the fixtures (t_1 and t_2) we could compensate for the error by adding more material to the original part design and machine the part with a toolpath corresponding to the original part design. In order to accommodate the subtractive finishing operation, the part is overgrown to include machining allowance (δ_v) similar to bulk operations such as casting as shown in Figure 22.

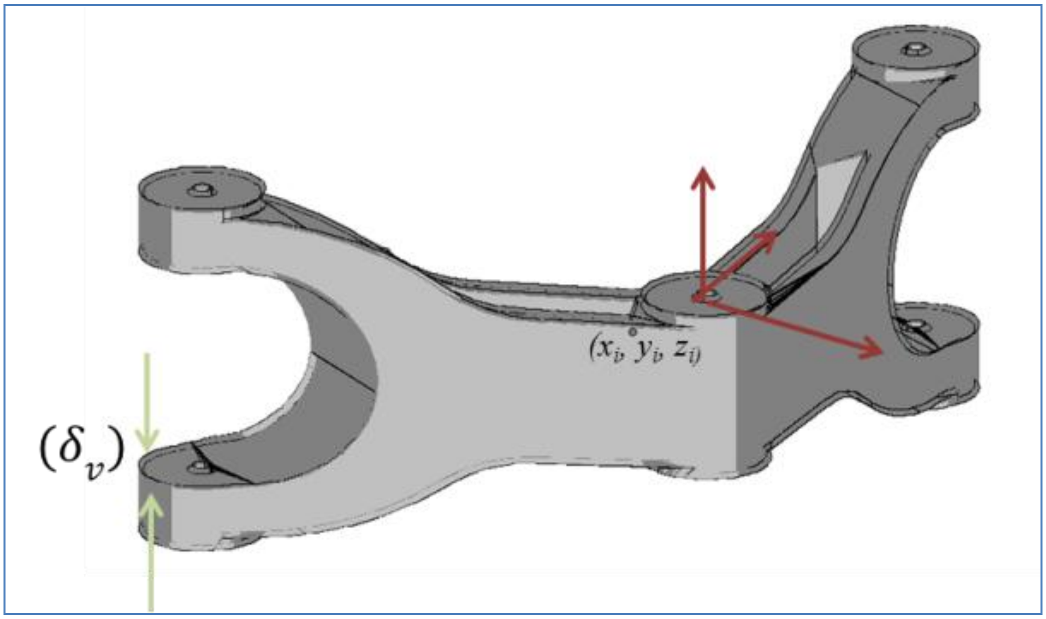

Figure 22: Addition of Machining Allowance

3.2 Feasibility Study

In order to verify the feasibility of the proposed method, the suspension part shown in Figure 22 was considered a candidate for the preliminary experiments. The part design is representative of a functional (load-bearing) part with assembly features that would require multiple re-fixturing when processed through conventional methods.

In order to accommodate the subtractive process, the part was overgrown - δ_v (in other words, the surfaces were uniformly offset) by 2.54 mm (0.1”) prior to process planning for AM (in this case, EBM). Since, the recommended depth of cut for finish machining Ti64 is about 1-2 mm (0.04-0.08”), the selected machining offset would accommodate about 2 finish passes.

As shown in Figure 24, fixturing features were added to the original CAD file. Currently, after clamping the near-net-shape AM part in the CNC-RP set-up, flat surfaces incorporated in the design of fixturing features are used to align the work coordinate system with the machine co-ordinate system, i.e. establish 0° for the rotational axis as shown in Figure 23.

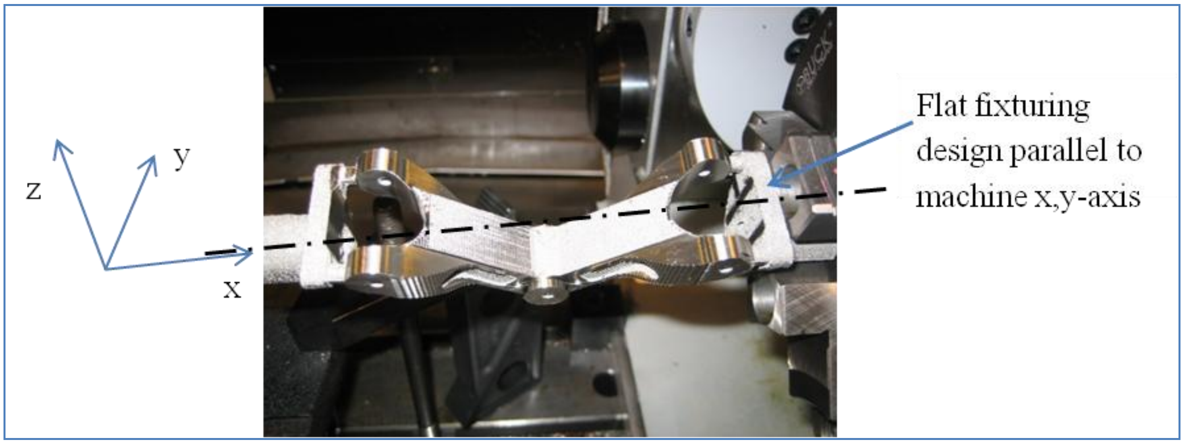

Figure 23: Flat Surfaces-used to align the Part with the Machine Axis

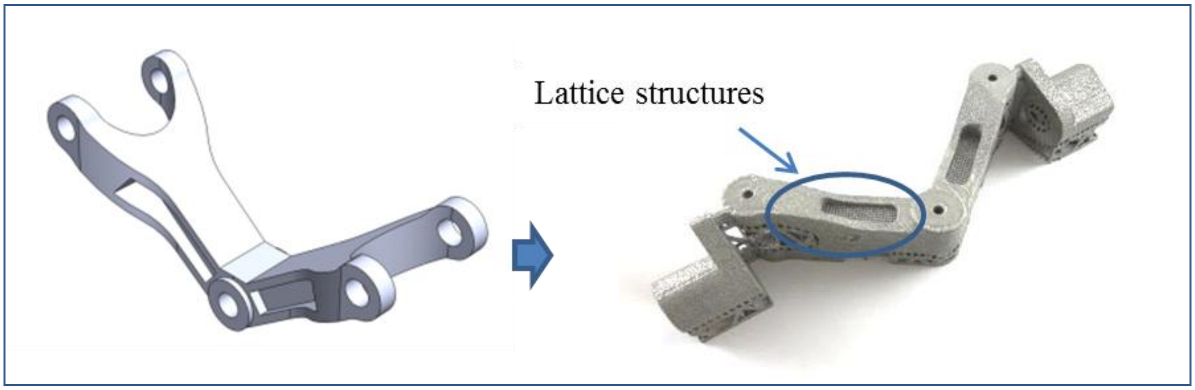

Figure 24: Desired Part and Near-net AIMS part

In order to harness the ‘freeform fabrication’ capability of additive methods, weight-reducing non-stochastic lattice structures were integrated into the design between external surfaces as shown in Figure 23. The near-net AIMS part shown in Figure 24 was made of Ti-6Al-4V (Ti64) using an Arcam® A2 EBM machine with manufacturer-recommended shrinkage compensation (x and y = 0.05 mm; z = 0.07 mm) and layer thickness of 0.07 mm. The sacrificial supports created in the EBM to support overhanging edges (known as wafer supports) were manually broken off the near-net part. Subsequently, the part was then located in a CNC machining center (HAAS VF3-SSYT) as shown in Figure 25 below.

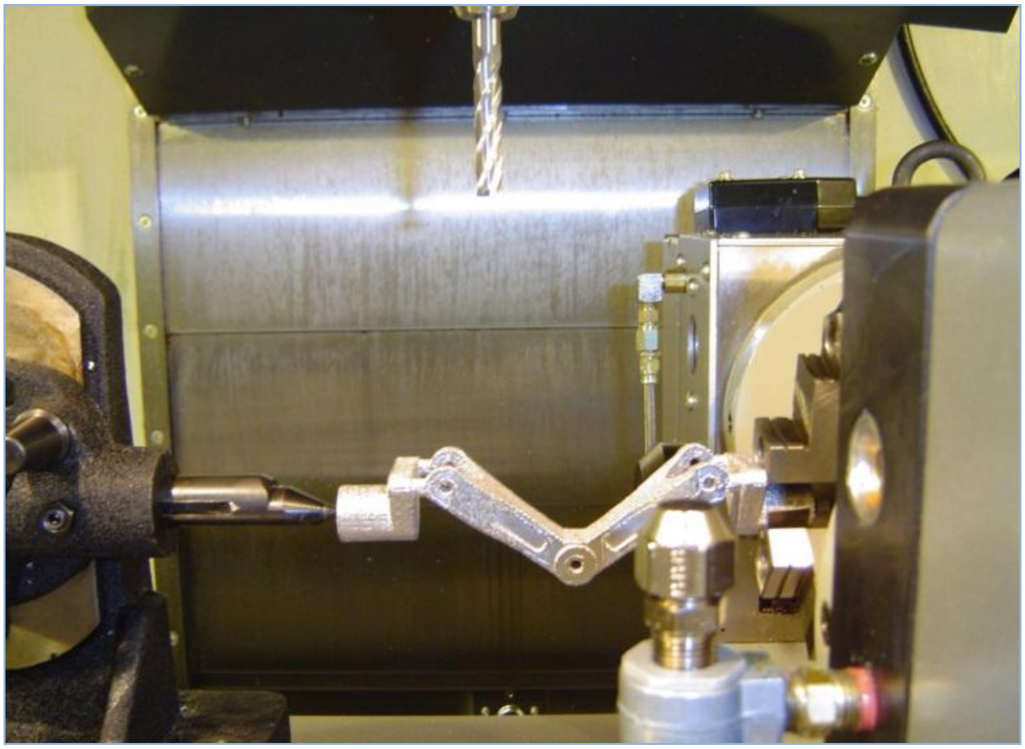

Figure 25: Near-net AIMS part in CNC-RP setup

The cutting tool and machining parameters are noted in Appendix-I.

3.3 Location System and Errors

In the feasibility study it was observed that the subtractive stage did not create the part within required dimensions, feature-dependencies and surface finish which is shown in Figure 26. This part was machined in two different orientations (0° and 180°). The holes shown in Figure 26 (a) where created in different orientations, and the feature locations are not collinear, which indicates that when the part was rotated about the *x*-axis, there were misalignment.

The surfaces that were machined in the same orientation- Figure 26 (b) were not uniform, which indicates that the fixture coordinate systems where not aligned with the CNC-RP coordinate system. This is attributed to the under-estimation of error in part location during fixturing of a near-net made AM surface. This did not meet the part requirements as shown in Figure 20.

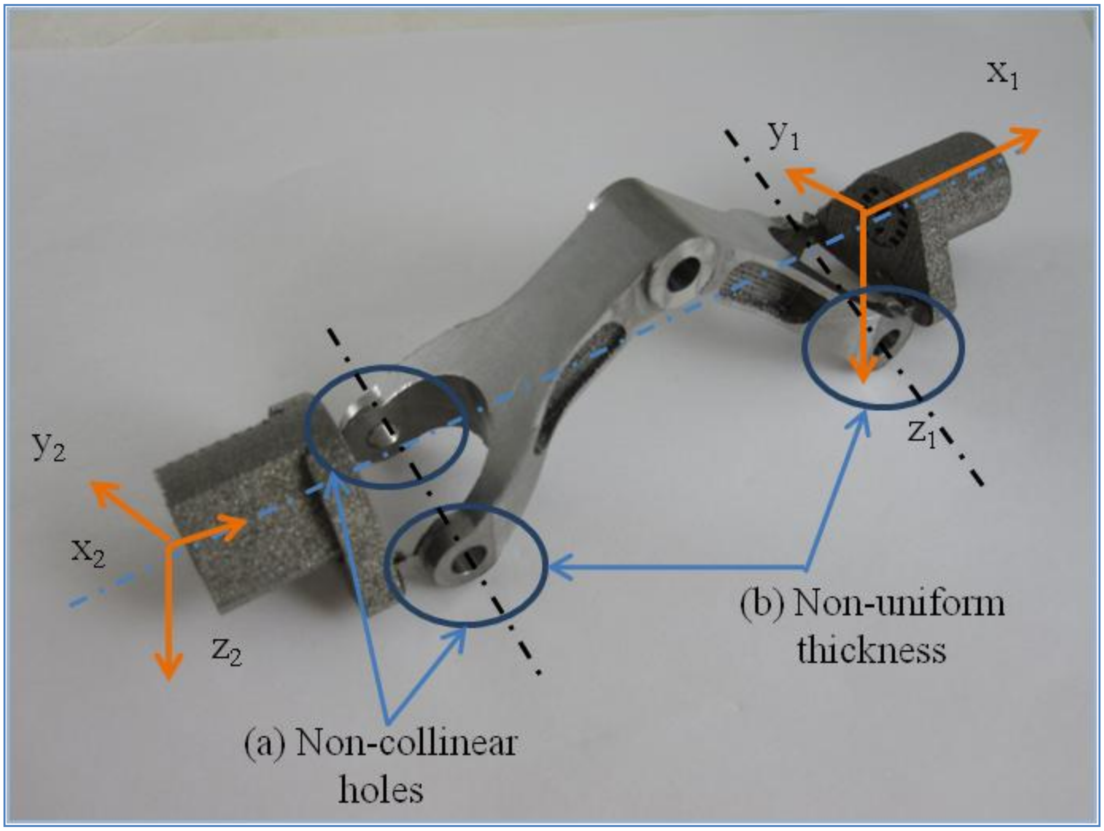
x_1
y_1
z_1
y_2
x_2
z_2
(b) Non-uniform thickness
(a) Non-collinear holes

Figure 26: Initial observations from AIMS

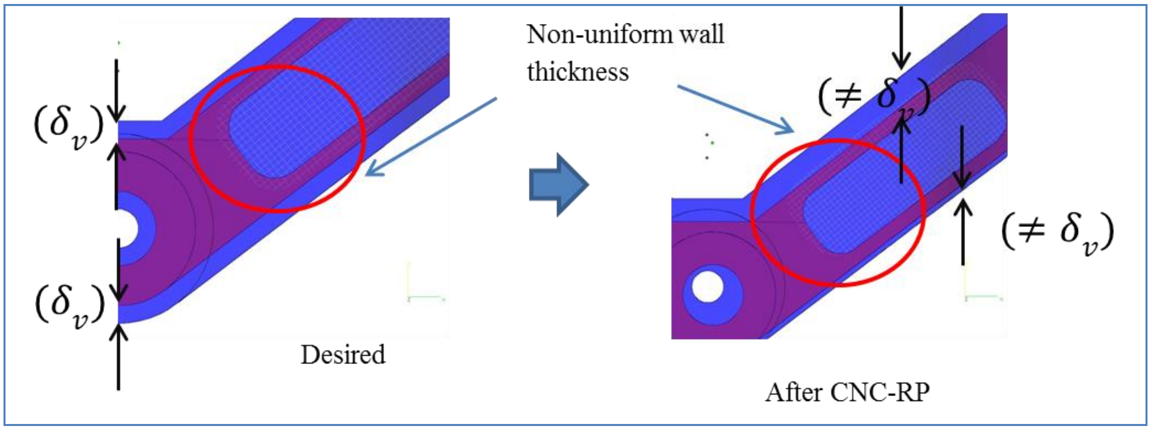

Figure 27: Effect of Integrating Lattice Structures

Figure 27 highlights another observation from the preliminary studies, where lattice structures where incorporated into the part design. Although, the required part geometry was created, the wall thicknesses (along the lattice structures) were not of uniform thickness. This indicates that the volume of material removed from both sides was not equal.

It can be observed that the toolpath, which was generated with the assumption that the fixture coordinate systems ($\mathbf{C_1}$and $\mathbf{C_2}$) and the CNC-RP coordinate system ($\mathbf{C_{CNC\text{-}RP}}$ → x_0, y_0, z_0), is not valid. Hence, we observed an error when the part was rotated about the machine axis, which is noted as fixturing deviation (ε_{yz-i}) as shown in Figure 28 below. As a result, the fixture coordinate system (x_1, $y1$, $z1$) is transformed with respect to the CNC-RP system as shown in Figure 28.

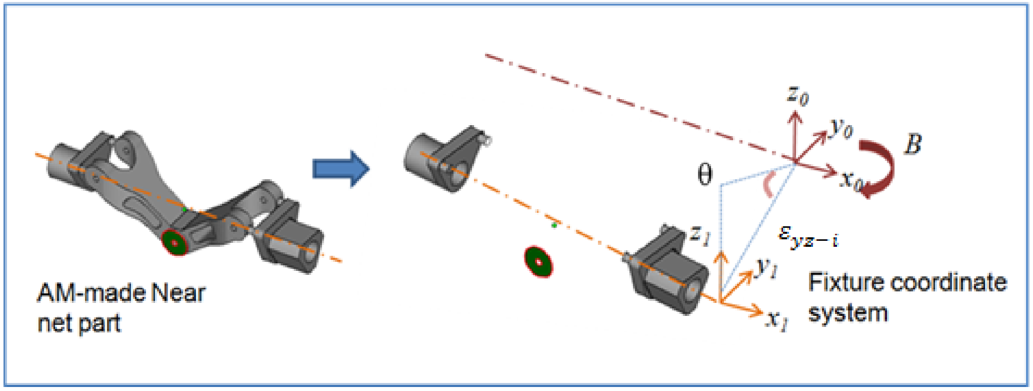
AM-made Near net part
z_0
y_0
x_0
B
θ
z_1
ε_{yz-i}
y_1
x_1
Fixture coordinate system

Figure 28: Deviation of Fixture Coordinate System

Due to fixture deviation, the toolpath generated (with respect to the CNC-RP setup) is no longer accurate. Any point in the part volume (x_i, y_i, z_i) is transformed as shown in Figure 29.

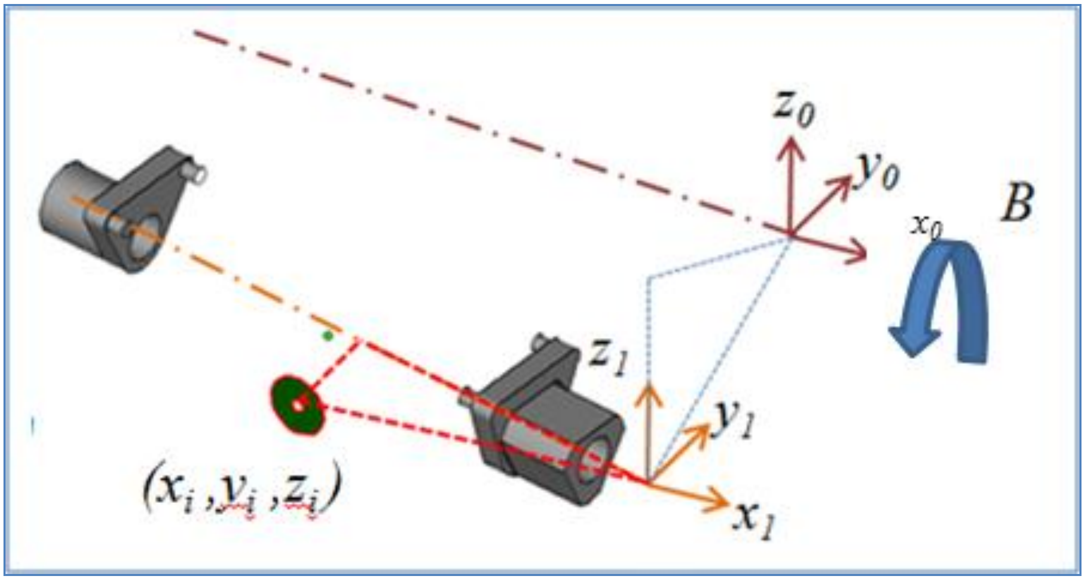
z_0
y_0
x_0
B
z_1
y_1
x_1
(x_i, y_i, z_i)

Figure 29: Part Coordinate System

The two approaches to create the appropriate cutting tool path with respect to the transformed part coordinate system are: 1) Modeling of the maximum deviation for the given part design and its orientations for the expected maximum deviation of the fixtures and 2) Modify the cutting tool path to the actual part location in the set-up. The latter approach could be pursued by re-generating the toolpath by recording and collecting data points of the actual part location with respect to the CNC-RP coordinate system using techniques such as laser scanning. In this study, the former approach is undertaken since it provides a model to estimate the amount of part overgrowth that is required to successfully produce the final desired part.

3.3.1 Transformation Models

In order to estimate the maximum part deviation, a series of coordinate transformations are required based on the part geometry and fixture deviation.

The fixture coordinate system (x_1, y_1, z_1) with respect to the CNC-RP coordinate system ((x_0, y_0, z_0) which is the work-offset) is given as:

$$\begin{bmatrix} x_1 \\ y_1 \\ z_1 \end{bmatrix} = \begin{bmatrix} 1 & 0 & 0 & 0 \\ 0 & 1 & 0 & (-\varepsilon_{yz-i}\ Sin\ \theta_i) \\ 0 & 0 & 0 & (-\varepsilon_{yz-i}\ Cos\ \theta_i) \\ 0 & 0 & 0 & 1 \end{bmatrix} \times \begin{bmatrix} x_0 \\ y_0 \\ z_0 \end{bmatrix} \tag{3.1}$$

And can be simplified into,

$$x_1 = x_0\,, \tag{3.2}$$

$$y_1 = y_0 \times (-\varepsilon_{yz-i}\ Sin\ \theta_i) \tag{3.3}$$

$$z_1 = z_0 \times (-\varepsilon_{yz-i}\ Cos\ \theta_i) \qquad (3.4)$$

The transformation represented in Eq. 3.1 considers the maximum deviation at each fixture-*i*, $(\varepsilon_{yz-i}, \Theta_i)$ with respect to the CNC-RP coordinate system. Referring to Figure 30, the location of any part coordinate system (x_i, y_i, z_i) based on the part specifications with respect to the deviated fixture coordinate system is given as,

$$\begin{bmatrix} x'_i \\ y'_i \\ z'_i \end{bmatrix} = \begin{bmatrix} 1 & 0 & 0 & (x_{1-}x_i) \\ 0 & 1 & 0 & (y_{1-}y_i) \\ 0 & 0 & 0 & (z_{1-}z_i) \\ 0 & 0 & 0 & 1 \end{bmatrix} \times \begin{bmatrix} x_0 \\ y_0 \\ z_0 \end{bmatrix} \qquad (3.5)$$

And based on values from Eq.3.1, the deviated part location can be expressed as,

$$x'_i = (x_{1-}x_0) \qquad (3.6)$$

$$y'_i = (y_{1-}(y_0 \times (-\varepsilon_{yz-i}\ Sin\ \theta_i)) \qquad (3.7)$$

$$z_1 = (z_{1-}(z_0 \times (-\varepsilon_{yz-i}\ Cos\ \theta_i)) \qquad (3.8)$$

Hence, modeling of the deviation associated with the fixture. The transformation represented in Eq. 3.6 considers the maximum deviation at each fixture-*i*, $(\varepsilon_{yz-i}, \Theta_i)$

3.4 Causes of Fixture Deviations

From the prior experiments, it was evident that there is a large disparity between the ideal setup (as in CNC-RP) desired as shown in Figure 10 and the results. Figure 30 below outlines the influence of using a near-net shaped part for finishing operations in a machining center.

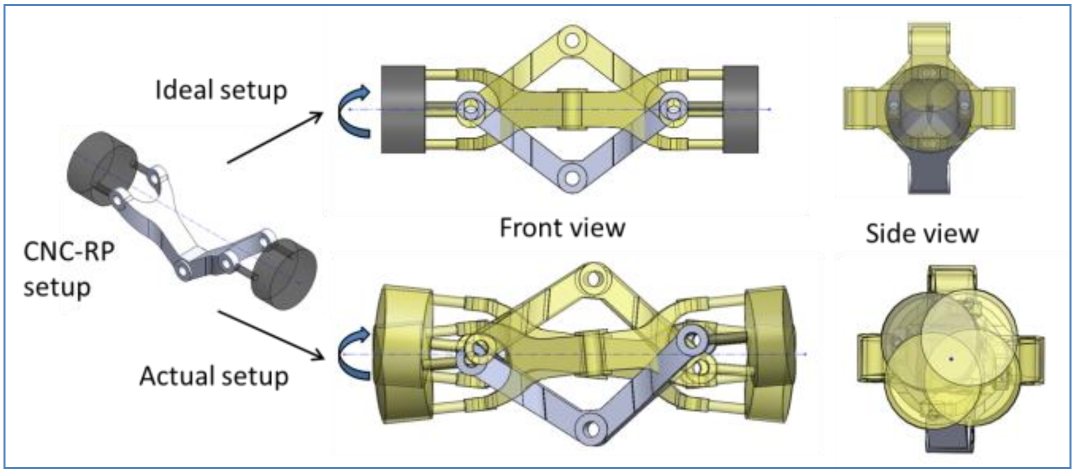

Figure 30: Ideal Set-up vs. Actual Set-up

As a result, the toolpath generated for the subtractive stage is not accurately related to the **actual** set-up observed. This can be attributed to two major factors: (1) Surface roughness of the fixturing features (R_a of 275-300 µm; although the part geometry is overgrown to accommodate machining allowance) which is more than ten times the machine tool tolerance (25.4 µm) and (2) Geometrical accuracy of the fixturing features, which is influenced by the shrinkage characteristics of metal additive processes such as EBM. The following sub-sections briefly detail these two factors and their influence on the success of the integrated subtractive stage.

3.4.1 Surface Roughness

In the case of an ideal setup (CNC-RP described in Section 2.2.1), both the centers of the cylindrical fixtures will be co-axial to the axis of rotation in the machining center as shown in Figure 31, where the physical work offset calibrated in the set-up is along the same x and z axis as that of both the fixtures.

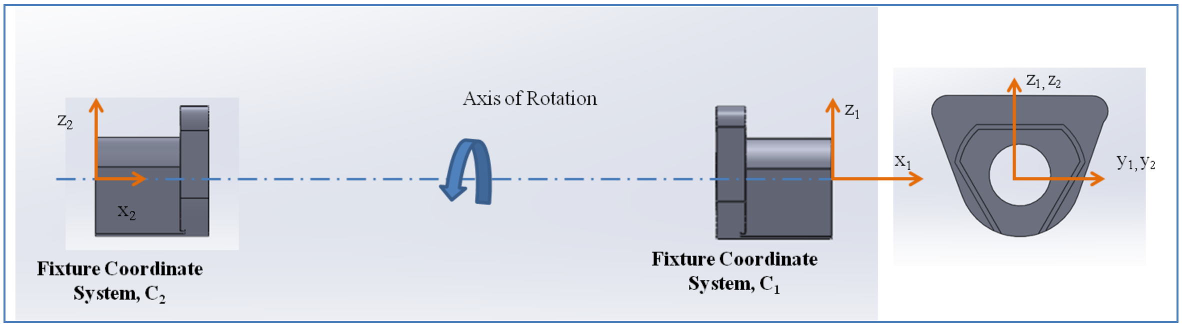
Axis of Rotation
z_2
x_2
Fixture Coordinate System, C_2
z_1
Fixture Coordinate System, C_1
x_1
z_1, z_2
y_1, y_2

Figure 31: Co-axial Ideal Set-up

As mentioned earlier, due to the inherent surface roughness resulting from the metal additive processes (such as EBM), while employing self-centering tandem 3-jaw chucks, the desired co-axial datum orientation is not achieved.

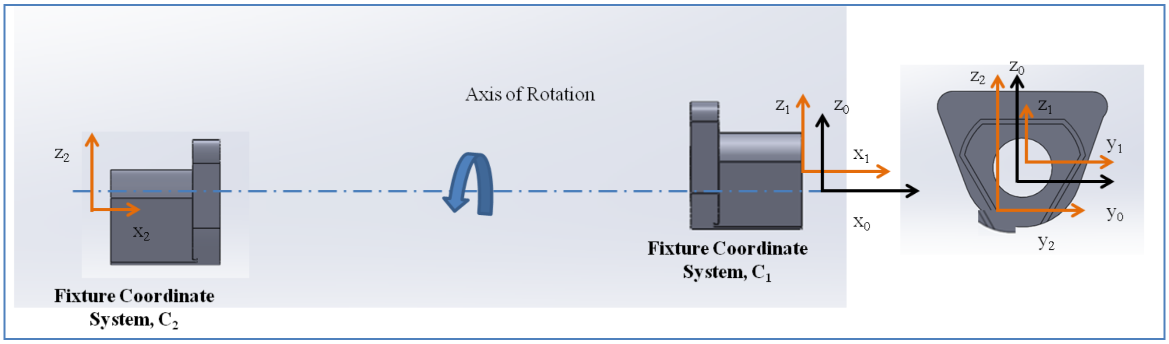
Axis of Rotation
z_2
x_2
Fixture Coordinate System, C_2
z_1
z_0
x_1
x_0
Fixture Coordinate System, C_1
z_2
z_0
z_1
y_1
y_0
y_2

Figure 32: Non Co-axial Set-up

Figure 32 shows the combined effects of AM-related surface roughness and self-centering chucks.

3.4.2 Non-Uniform Shrinkage

Due to the nature of most direct metal additive manufacturing processes, such as the EBM process, shrinkage during cooling of the melt is non-uniform.

This is attributed to the presence of a build tank around the powder bed. As a result, the shrinkage along the *x* and *y* directions (*xy* plane is perpendicular to the beam) are equal, but unequal to shrinkage along the *z* direction as shown in Figure 33. Similarly, in other AM processes such as DMLS and SLM, pronounced warping of the part occurs due to the cold-bed.

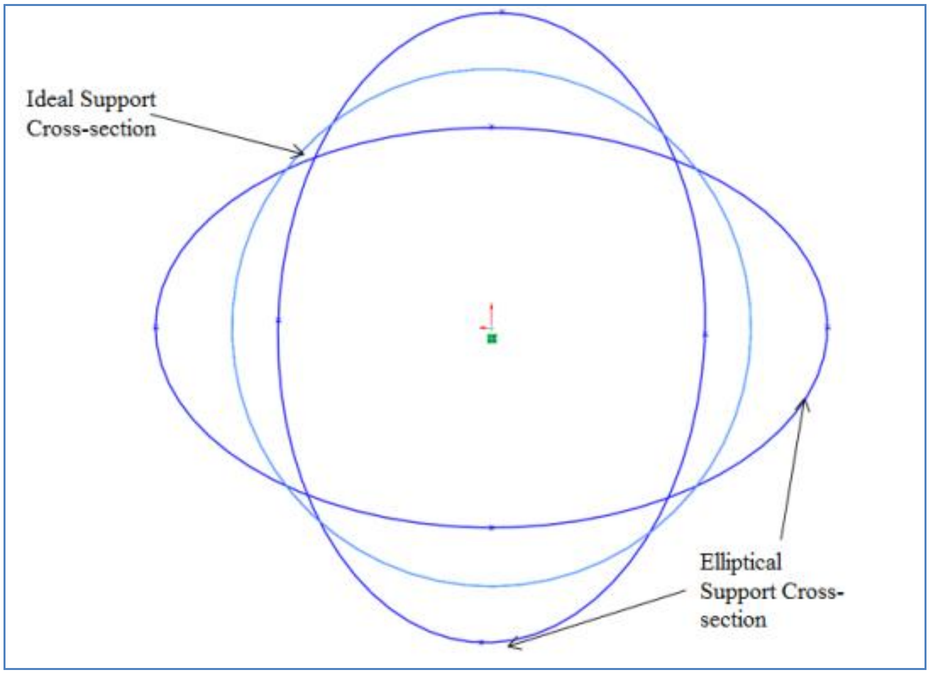
Ideal Support Cross-section
Elliptical Support Cross-section

Figure 33: Effect of Non-uniform Shrinkage

More importantly, this effect is observed in the part geometry as well (where the shrinkage of a thinner web is different from that of a thicker cross-section) as show in Figure 34.

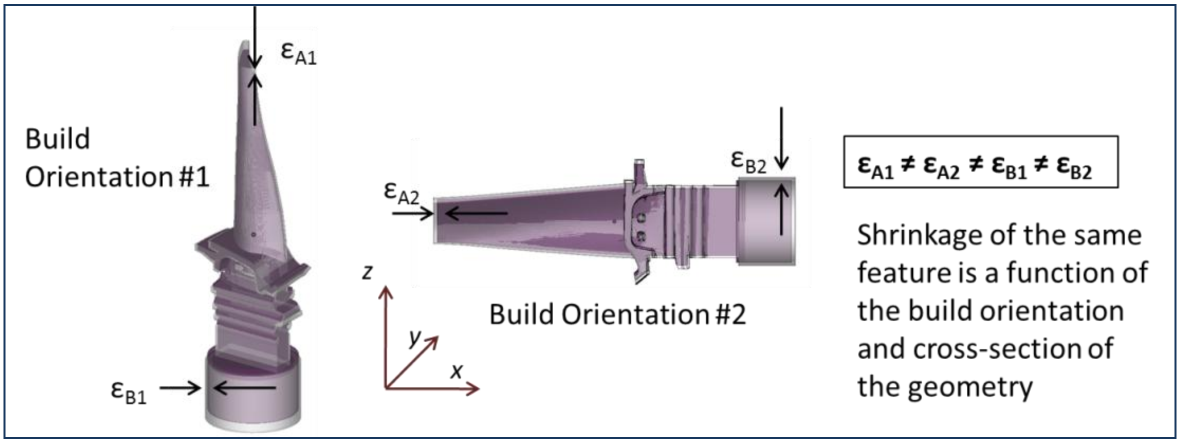
εA1
Build Orientation #1
εB1
εA2
z
y
x
εB2
Build Orientation #2
εA1 ≠ εA2 ≠ εB1 ≠ εB2
Shrinkage of the same feature is a function of the build orientation and cross-section of the geometry

Figure 34: Effect of Build Orientation and Part Geometry

The part overgrowth of 1 mm provided to accommodate the geometric deviations was not sufficient. Hence, with a higher part overgrowth, CNC codes for machining an ideal part with known material volume to be removed from the CAD file used in AM will generate accurate parts.

3.5 Broader Scope of Research

We have identified the major research components associated with the development of AIMS into an automated system based on AM processing characteristics, CNC-RP setup for AM, part-fixture designs and NC-programming. A set of activities required in AIMS is shown in Figure 35. This figure highlights some of the overall process factors that should be studied to improve and fully execute the AIMS process. Specific objectives and corresponding methodologies addressed in this study are detailed in Chapter 4.

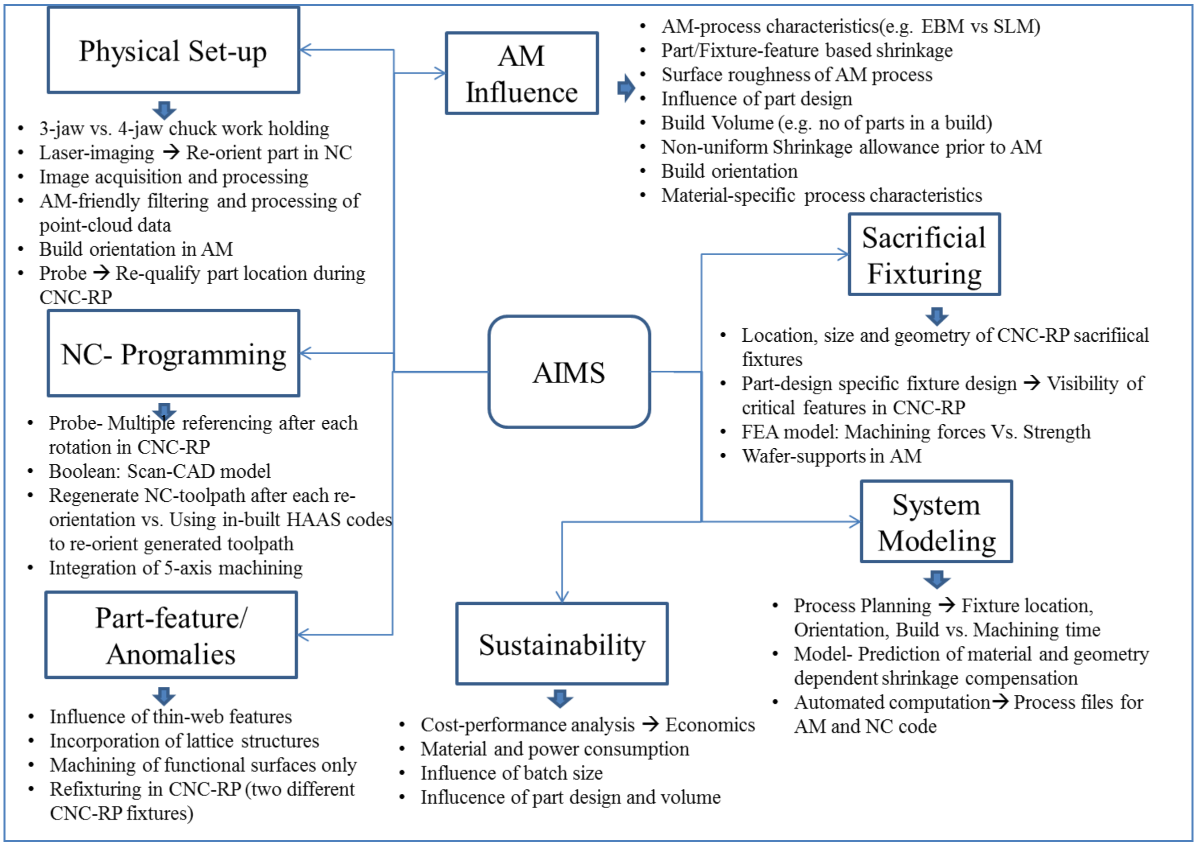
Physical Set-up
3-jaw vs. 4-jaw chuck work holding
Laser-imaging → Re-orient part in NC
Image acquisition and processing
AM-friendly filtering and processing of point-cloud data
Build orientation in AM
Probe → Re-qualify part location during CNC-RP
AM Influence
AM-process characteristics(e.g. EBM vs SLM)
Part/Fixture-feature based shrinkage
Surface roughness of AM process
Influence of part design
Build Volume (e.g. no of parts in a build)
Non-uniform Shrinkage allowance prior to AM
Build orientation
Material-specific process characteristics
Sacrificial Fixturing
Location, size and geometry of CNC-RP sacrifiical fixtures
Part-design specific fixture design → Visibility of critical features in CNC-RP
FEA model: Machining forces Vs. Strength
Wafer-supports in AM
NC- Programming
Probe- Multiple referencing after each rotation in CNC-RP
Boolean: Scan-CAD model
Regenerate NC-toolpath after each re-orientation vs. Using in-built HAAS codes to re-orient generated toolpath
Integration of 5-axis machining
AIMS
System Modeling
Process Planning → Fixture location, Orientation, Build vs. Machining time
Model- Prediction of material and geometry dependent shrinkage compensation
Automated computation→ Process files for AM and NC code
Part-feature/ Anomalies
Influence of thin-web features
Incorporation of lattice structures
Machining of functional surfaces only
Refixturing in CNC-RP (two different CNC-RP fixtures)
Sustainability
Cost-performance analysis → Economics
Material and power consumption
Influence of batch size
Inflcuence of part design and volume

Figure 35: Overview of Process Factors and Research Scope in AIMS

The major factors noted in Figure 35 are some of the integral components that need to be studied in order to develop a complete AIMS system. The preceding section 3.6 details the architecture associated with the AIMS system that can be built upon studies conducted for each of those factors.

3.6 AIMS: Process Flow

The overall process flow of the proposed AIMS system after development is detailed in Figure 36. It highlights the vital steps involved in the integration of AM and a subtractive process namely, CNC-RP.

Upon receiving the CAD file, the process planning should consider the information from the file and analyze the strategies for CNC-RP based on visibility analysis, tool library, etc. and also consider the limitations of that ‘specific’ AM machine such as maximum build volume, part accuracy, surface finish, etc.

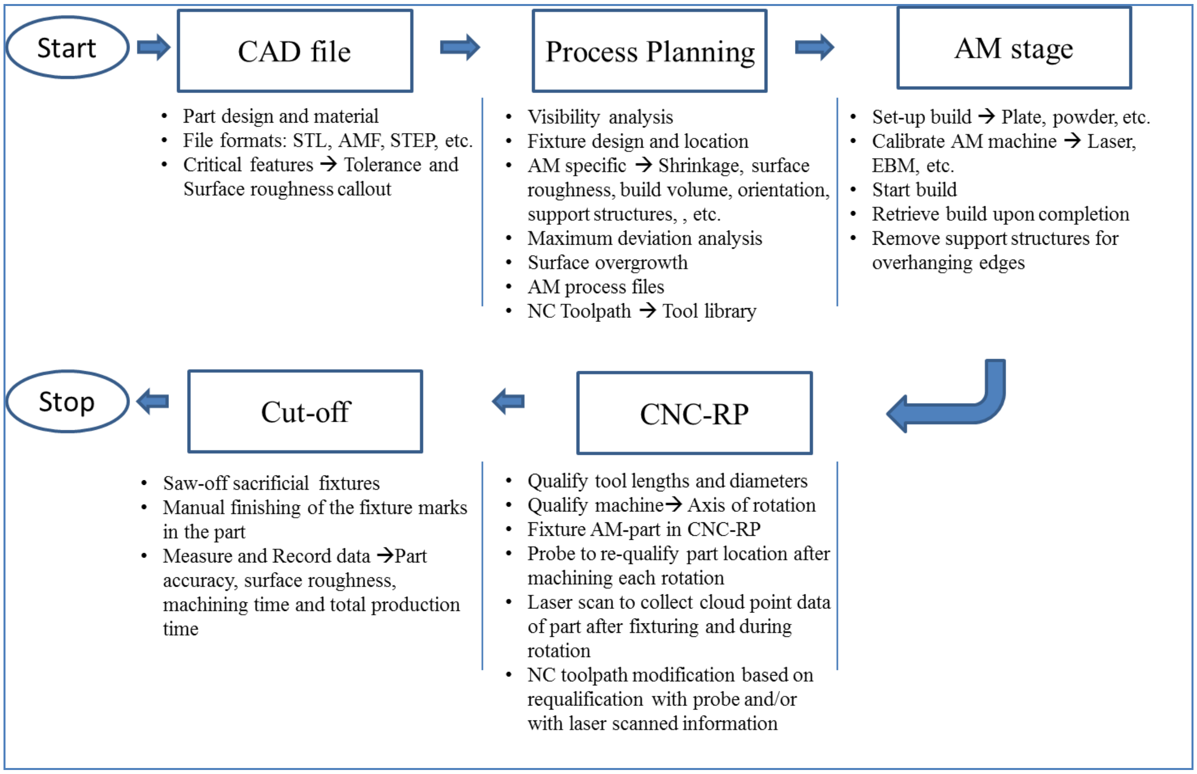
Start
CAD file
Process Planning
AM stage
• Part design and material
• File formats: STL, AMF, STEP, etc.
• Critical features → Tolerance and Surface roughness callout
• Visibility analysis
• Fixture design and location
• AM specific → Shrinkage, surface roughness, build volume, orientation, support structures, , etc.
• Maximum deviation analysis
• Surface overgrowth
• AM process files
• NC Toolpath → Tool library
• Set-up build → Plate, powder, etc.
• Calibrate AM machine → Laser, EBM, etc.
• Start build
• Retrieve build upon completion
• Remove support structures for overhanging edges
Stop
Cut-off
CNC-RP
• Saw-off sacrificial fixtures
• Manual finishing of the fixture marks in the part
• Measure and Record data →Part accuracy, surface roughness, machining time and total production time
• Qualify tool lengths and diameters
• Qualify machine→ Axis of rotation
• Fixture AM-part in CNC-RP
• Probe to re-qualify part location after machining each rotation
• Laser scan to collect cloud point data of part after fixturing and during rotation
• NC toolpath modification based on requalification with probe and/or with laser scanned information

Figure 36: AIMS Process Flow

After executing the process planning, the AM stage creates the part based on the build files generated. In CNC-RP, the AM-part is finish machined after qualifying the tools, part location using machine tool accessories such as touch-probe and/or laser scanner. Finally, the part is created by removing the sacrificial fixtures.

As can be identified from the process flow, there is a flow of information throughout the process based on the part design, the physical build, CNC-RP volume, tool path generation, etc. In order to more completely develop AIMS, there are two fundamentally different aspects associated: (1) Physical architecture defining material, AM process and CNC-RP, and (2) Software architecture which will define the individual components that need to be considered during process planning and operation of AIMS to achieve automation of all the steps involved in AIMS. It is important to identify these components to develop a seamless system because they are inter-related. For instance, processing a part design of a specific alloy through two varied AM processes such as DMLS and EBM will result in different part accuracy and surface roughness (which are physical components). As a result, part misalignment during CNC-RP will not be uniform and hence, toolpath generation using a CAD-CAM system (which is a computational component) has to account for the dissimilarities across AM technologies. Another example will be the influence of available build volume in the AM system. This will impact both the build orientation (which affects part accuracy and surface roughness) and the fixture design depending on the part volume. Hence, the computational component should consider this while determining the appropriate part offset and orientation in order to create the required final part.

3.6.1 Physical Components

The major physical components associated with AIMS are noted in Figure 37 below namely: material, AM process (equipment) and the CNC-RP setup.

At this stage of development of AIMS, specific part design attributes such as thin walls, and incorporation of lattice structures are not considered, thereby maintaining the generality associated with existing AM (CAD file → additive manufacturing). The influence of material is significant since the shrinkage characteristics of each material vary for individual AM processes, which affects part accuracies. Further, fixture design is dependent upon the material properties and part geometry such that the fixtures can withstand the cutting forces based on machining parameters.

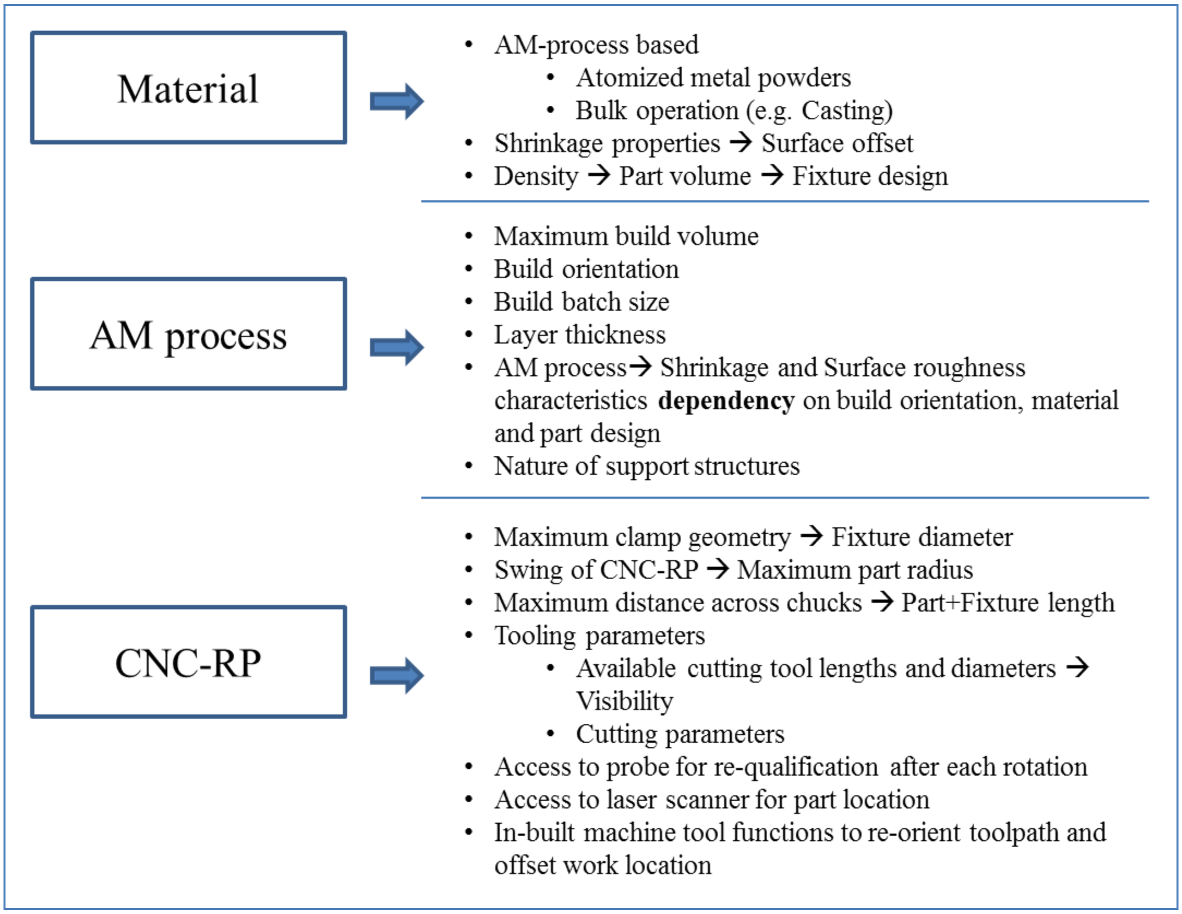
Material
AM process
CNC-RP
• AM-process based
• Atomized metal powders
• Bulk operation (e.g. Casting)
• Shrinkage properties → Surface offset
• Density → Part volume → Fixture design
• Maximum build volume
• Build orientation
• Build batch size
• Layer thickness
• AM process→ Shrinkage and Surface roughness characteristics **dependency** on build orientation, material and part design
• Nature of support structures
• Maximum clamp geometry → Fixture diameter
• Swing of CNC-RP → Maximum part radius
• Maximum distance across chucks → Part+Fixture length
• Tooling parameters
• Available cutting tool lengths and diameters → Visibility
• Cutting parameters
• Access to probe for re-qualification after each rotation
• Access to laser scanner for part location
• In-built machine tool functions to re-orient toolpath and offset work location

Figure 37: Physical Architecture of AIMS

Furthermore, depending on the specific AM process used, process planning has to consider the maximum build volume and orientation to appropriately design fixtures for the specific part volume. More importantly, the part accuracy and surface roughness characteristics of each unique AM technique need to be registered in order to gauge the maximum deviation that can be predicted correspondingly (at the software end). Regarding CNC-RP, in-addition to information on the maximum machining volume and accessibility, part and tool qualification methods need to be defined.

3.6.2 Software Components

The major software building blocks associated with AIMS are noted in Figure 38 below.

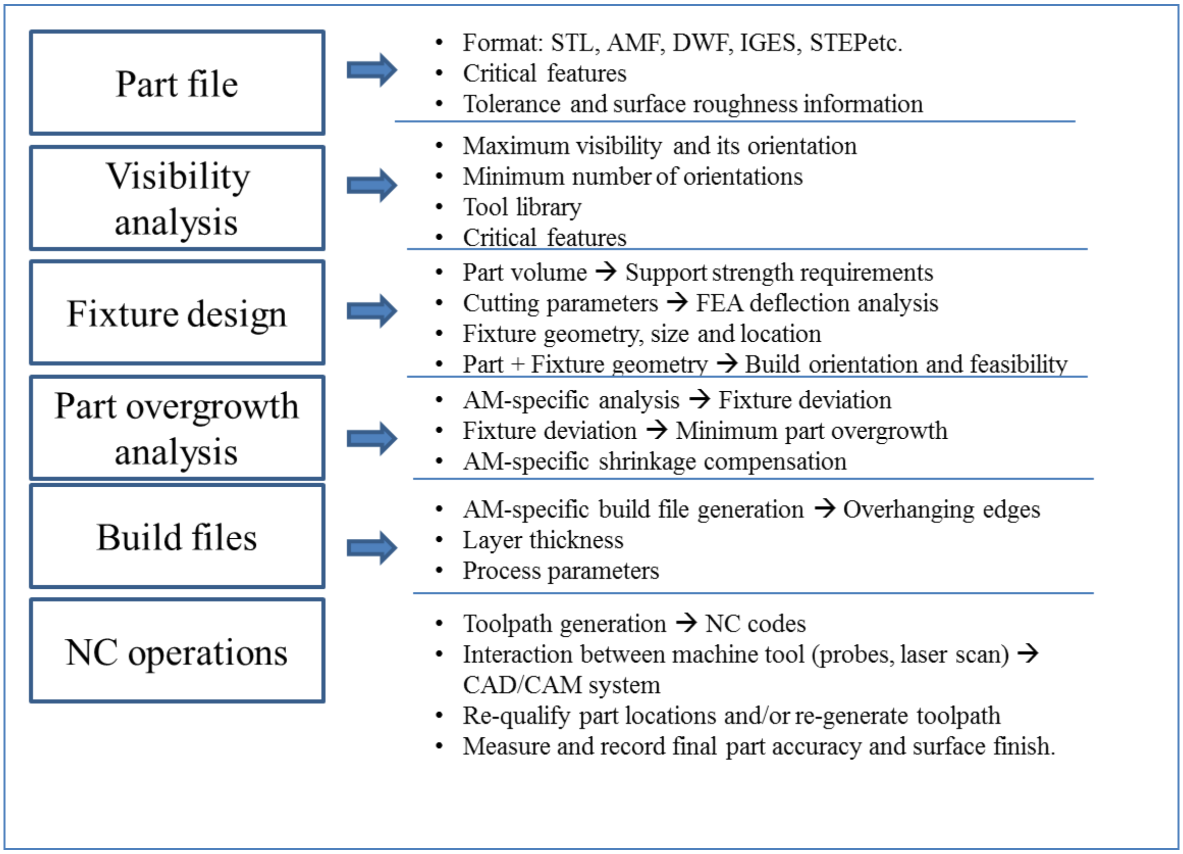
Part file
Format: STL, AMF, DWF, IGES, STEPetc.
Critical features
Tolerance and surface roughness information
Visibility analysis
Maximum visibility and its orientation
Minimum number of orientations
Tool library
Critical features
Fixture design
Part volume → Support strength requirements
Cutting parameters → FEA deflection analysis
Fixture geometry, size and location
Part + Fixture geometry → Build orientation and feasibility
Part overgrowth analysis
AM-specific analysis → Fixture deviation
Fixture deviation → Minimum part overgrowth
AM-specific shrinkage compensation
Build files
AM-specific build file generation → Overhanging edges
Layer thickness
Process parameters
NC operations
Toolpath generation → NC codes
Interaction between machine tool (probes, laser scan) → CAD/CAM system
Re-qualify part locations and/or re-generate toolpath
Measure and record final part accuracy and surface finish.

Figure 38: AIMS Software Components

The process flow in the computational aspect of AIMS is shown in Figure 38; fully developed software for AIMS should have the processing capabilities to: process the data available in the CAD file and correspondingly, analyze the visibility to identify the optimal orientations for machining in CNC-RP with consideration of critical features.

After visibility analysis in-conjunction with physical components (maximum build volume, orientation, etc.), analysis for sacrificial fixtures design should be conducted such that the fixtures can support machining forces in CNC-RP. Further, based on the specific AM process performance, fixture deviation analysis (in CNC-RP) should be predicted and corresponding part overgrowth should be compensated. Finally, process files for AM and CNC-RP should be generated and transferred to the machines through digital communication.

3.7 AIMS Performance Metrics

The major motivation to develop AIMS stems from the benefits of integrating two different manufacturing approaches namely, additive manufacturing and subtractive manufacturing. In the case of additive manufacturing, material consumption is very efficient since only the part volume (with sacrificial supports for AM) is consumed. This is of great significance since super-alloys such as Ti64 (which are favored for aerospace, mechanical and biomedical applications) are very expensive and tough-to-machine. On the other hand, subtractive manufacturing delivers desired precision accuracy and surface finish but has lower material utilization and often requires expensive tooling and fixturing. The integration of AM and SM will be extremely **effective if**: Part feature tolerance and surface finish of required critical features (or all features, as required) is achieved by the hybrid process. Depending on the application requirements of each part, finish machining select surfaces could suffice the design requirement as shown in Figure 39.

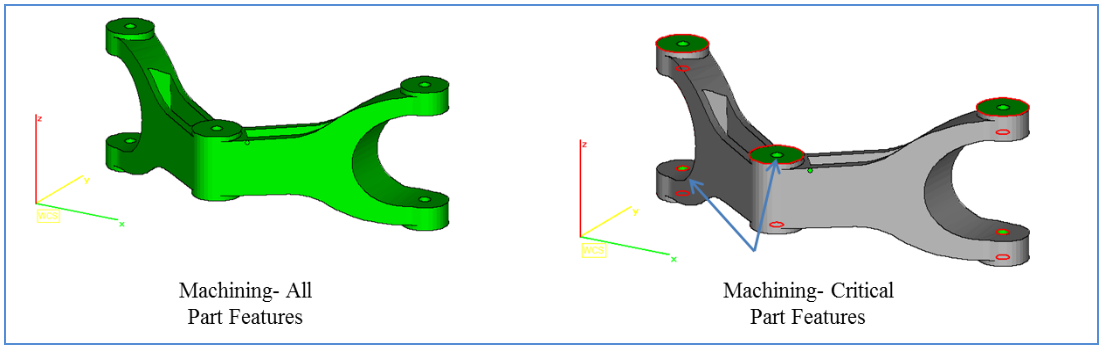

Figure 39: Machining All vs. Critical Part Features

There are several major performance metrics for hybrid manufacturing. Similar to most manufacturing processes, the major engineering objectives relate to material consumption, production time and production cost. From a global standpoint, the major metrics are defined with respect to AIMS. In the following sections, models of the process with respect to specific performance metrics will be presented. The focus here is to detail the three major factors: Material, Production cost and Production time. This helps in comparing AIMS with traditional and existing AM processes and also would lead to identifying the most impactful cost factors.

3.7.1 Metric (0.1): Minimize {Material Consumption, V_{total}}

One objective for production is to minimize the amount of material consumed (V_{total}) which consists of the AM-part volume (AM_{pv}) and any loss of material in AM such as powder loss during handling (ε_{AM}). The AM-part volume consists of the final part volume (P_v), CNC-RP fixture volume (Fix_v), support material for overhanging surfaces during AM (S_v) and the machining allowance which will be machined (δ_v).

This amount of material used is constrained by the orientations during the AM build (ori_{AM}) and CNC-RP (ori_{CNC_RP}) which are dictated by the physical constraints of maximum build and machining volume correspondingly. An objective is to address the sustainability and the higher cost of expensive alloys that are often processed using AM processes. The following basic relationship can be derived:

$$\mathrm{Min}\{V_{total}\} = f_1(\delta_v) \tag{3.9}$$

Where, the minimum total material consumption is a function of machining allowance for a given part and fixture volume.

$$V_{total} = AM_{pv} + \varepsilon_{AM} \tag{3.10}$$

Where, the total material consumption is a sum of total part volume consumed in AM and any material loss during handling (e.g., powder handling loss).

$$AM_{pv} = P_v + AM_{sv} + Fix_v + \delta_v \tag{3.11}$$

Subject to constraints; ori_{AM} AND ori_{CNC_RP}

Where, the total AM material consumption is a sum of desired part volume (fixed), wafer or volume support used to support overhanging surfaces in AM, CNC-RP fixture volume and finally, the machining allowance. The total AM volume is subject to physical constraints of maximum build volume (based on orientation) and maximum fixture size (that can be clamped in CNC-RP).

Figures 40 and 41 below describe the total volume and identify the AM-part volume with machining allowance $(P_v + \delta_v)$, support volume (AM_{sv}) along with the CNC-RP fixture (Fix_v). It should be noted that the orientation constraints in AM and CNC-RP are influenced by the physical volume available for processing the AM-made part (AM_{pv}) in **both** AM and the CNC-RP machine tool.

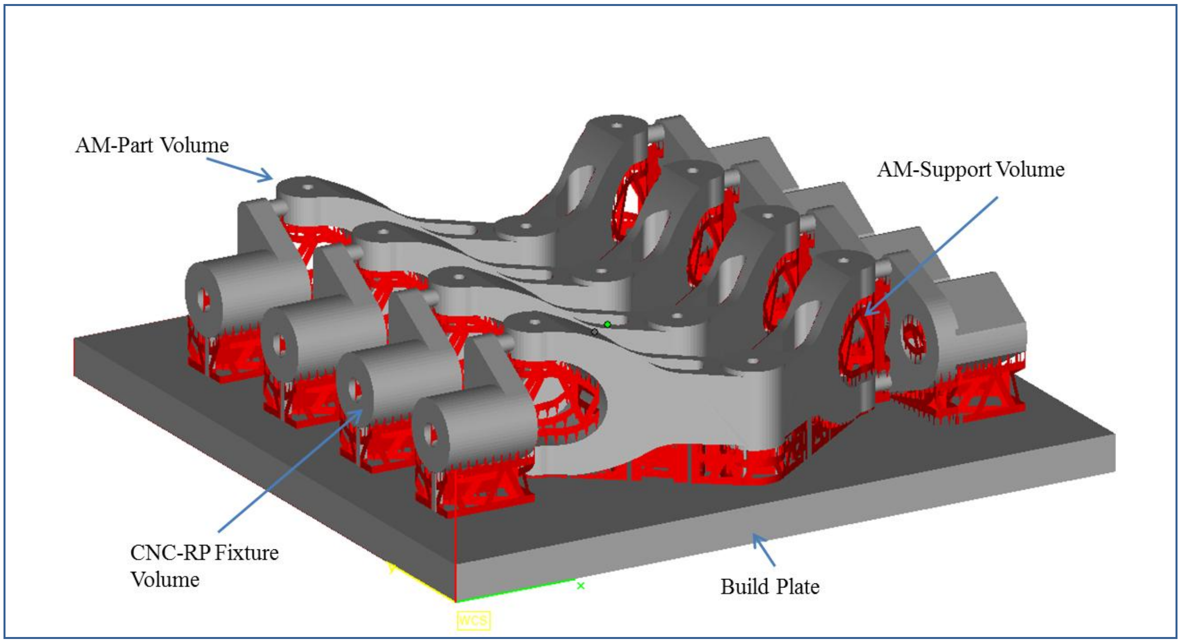
AM-Part Volume
AM-Support Volume
CNC-RP Fixture Volume
Build Plate
WCS

Figure 40: Material Consumption

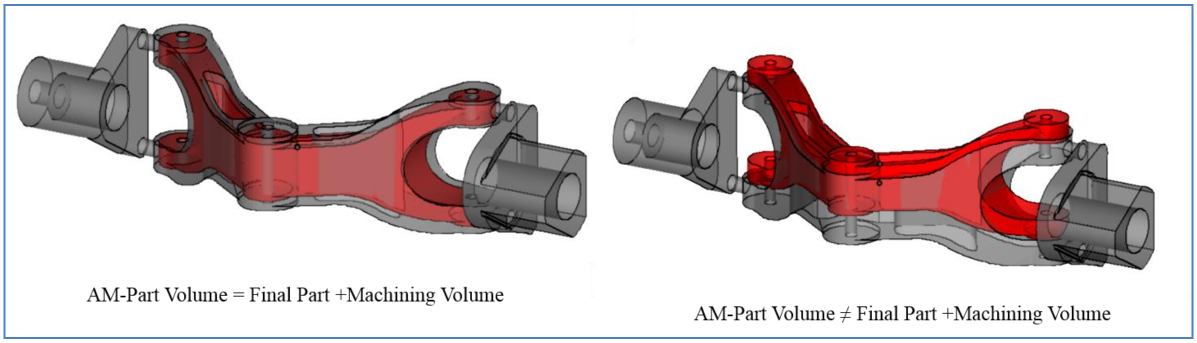
AM-Part Volume = Final Part +Machining Volume
AM-Part Volume ≠ Final Part +Machining Volume

Figure 41: Machining Allowance for CNC-RP

It can be noted that, since the final part volume is pre-defined based on the CAD model, the total material consumption (without any handling loss) can be re-defined as:

$$AM_{pv} = f_1'(AM_{sv}, Fix_v, \delta_v) \tag{3. 12}$$

Subject to constraints; ori_{AM} AND ori_{CNC_RP}

Where, the total AM material consumption is a function of desired part volume (fixed), wafer or volume support used to support overhanging surfaces in AM, CNC-RP fixture volume, and the machining allowance.

3.7.2 Metric (0.2): Minimize {Production time, T_{total}}

Another objective for AIMS is to minimize the total production time (T_{total}) which consists of AM-processing time (T_{AM}) and CNC-RP hybrid time, i.e. finish machining (T_{CNC_RP}).

In the case of AM, the processing time is impacted by the build orientation (ori_{AM}) because the total build height influences the number of layers and AM-part volume (AM_{pv}). The overall CNC-RP time (T_{CNC-RP}) is a function of the machining allowance (δ_v), material removal rate (MRR), machinability, and tooling time $(T_{tooling})$ respectively. Hence, the following relationship can be derived:

$$\text{Min}\{T_{total}\} = f_2(T_{AM}, T_{CNC-RP}) \tag{3.13}$$

Where, the minimum total production time is a function of the sum of AM time and finish CNC-RP time for a given part. Since the AM time depends on the part orientation and part volume, it can be further expressed as:

$$T_{AM} = f_2'(ori_{AM}, AM_{pv}) \tag{3.14}$$

Where, the total AM production time to produce the near-net part is dependent on the orientation of the part (build layers) and the total AM-part volume (including machining allowance). In the case of CNC-RP:

$$T_{CNC-RP} = f_2''(\delta_v, MRR, T_{tooling}) \tag{3.15}$$

Where, the total CNC-RP production time is a function of machining allowance, the material removal rate and tooling time. In other words, it is desired to have a build orientation with the least AM-time and minimal machining allowance with higher material removal rate. If the machinability of the material is high, the *MRR* will be large leading to reduced machining time and lower tool wear and subsequently, less time spent on tool changes.

3.7.3 Metric (0.3): Minimize {Production cost, T_{cost} }

A third objective is to minimize the total production cost (T_{cost}) which consists of minimizing the material consumption (V_{total} based on Obj 0.1) and the total processing time and tooling (T_{total} based on Obj 0.2). The cost of the material (C_{mat}) and the machinability ($MRR,\ T_{tooling}$) varies based on material, whereas the cost of production (C_{AM}, C_{CNC-RP}) differs based on AM (based on the AM process employed) and CNC-RP. Hence, we can express the relationship as follows:

$$\mathrm{Min}\{T_{cost}\} = f_3(V_{cost}, T_{total}) \tag{3.16}$$

Where, the total production cost is a function of total material cost and cost associated with production time and tooling.

$$V_{cost} = f_3{}'(V_{total}, C_{mat}) \tag{3.17}$$

As shown above, the total material cost depends on the cost of the material (\$/volume) and the overall volume of material consumed (part volume, AM-support volume, machining allowance and CNC-RP fixtures)

$$T_{total} = f_3{}''(T_{AM}, C_{AM}, T_{CNC-RP}, C_{CNC-RP}, MRR,\ T_{tooling}) \tag{3.18}$$

Where, production time cost is a function of operation cost associated with both AM and CNC-RP stage. Further, depending on the material removal rate, the tooling cost (cost of tool and tool change time) is impacted.

In the AM stage, it can be noted that the build orientation (least AM-time), build volume and operating cost influences the AM cost. It is desired to orient the part along the minimum build height and with minimal part volume. In the case of CNC-RP, it is desired to consume the minimal total volume (minimum machining allowance) of AM material with lower cost and higher machinability. Lower machinability leads to longer machining time and greater tool consumption. Subsequently, the tooling cost and tool change time increases.

Based on the three performance metrics (minimizing material consumption, production time, and total AIMS cost), the following sub-objectives can be correspondingly derived. Sub-objective 1.0 is directly associated with minimizing the material consumption. This would influence the material cost, machining volume and machining time (also, tool consumption). Sub-objective 2.0 focuses on the fixturing design for CNC-RP, namely the geometry and volume of the fixtures. This would influence the material consumption (fixture volume), fixture strength to withstand machining forces and deviation associated with the fixture-jaw interaction.

The sub-objective of increasing the machinability (*MRR*) and lowering the tool wear is beyond the scope of this research. Sub-objective 3.0 integrates the minimal machining allowance required and the impact of fixture design to determine the minimal amount of part overgrowth required prior to AM- processing. This is critical because the part should be overgrown to accommodate the impact of fixture geometry, size and its impact on deviation along with the influence of the part volume. The final sub-objective is to determine the fixture accuracy requirement for a given AM process (and its accuracy based on orientation) and subsequently, the part overgrowth required based on tolerance specifications required in the final hybrid part.

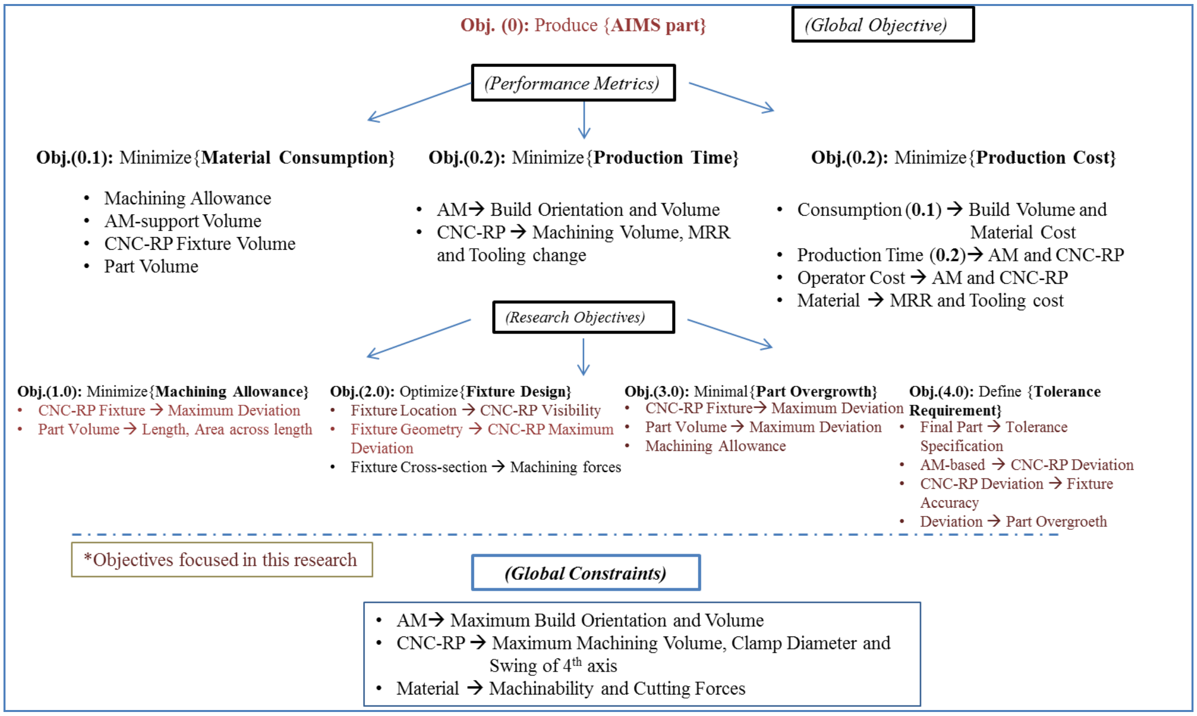
Obj. (0): Produce {AIMS part}
(Global Objective)
(Performance Metrics)
Obj.(0.1): Minimize{Material Consumption}
Machining Allowance
AM-support Volume
CNC-RP Fixture Volume
Part Volume
Obj.(0.2): Minimize{Production Time}
AM→ Build Orientation and Volume
CNC-RP → Machining Volume, MRR and Tooling change
Obj.(0.2): Minimize{Production Cost}
Consumption (0.1) → Build Volume and Material Cost
Production Time (0.2)→ AM and CNC-RP
Operator Cost → AM and CNC-RP
Material → MRR and Tooling cost
(Research Objectives)
Obj.(1.0): Minimize{Machining Allowance}
CNC-RP Fixture → Maximum Deviation
Part Volume → Length, Area across length
Obj.(2.0): Optimize{Fixture Design}
Fixture Location → CNC-RP Visibility
Fixture Geometry → CNC-RP Maximum Deviation
Fixture Cross-section → Machining forces
Obj.(3.0): Minimal{Part Overgrowth}
CNC-RP Fixture→ Maximum Deviation
Part Volume → Maximum Deviation
Machining Allowance
Obj.(4.0): Define {Tolerance Requirement}
Final Part → Tolerance Specification
AM-based → CNC-RP Deviation
CNC-RP Deviation → Fixture Accuracy
Deviation → Part Overgroeth
*Objectives focused in this research
(Global Constraints)
AM→ Maximum Build Orientation and Volume
CNC-RP → Maximum Machining Volume, Clamp Diameter and Swing of 4th axis
Material → Machinability and Cutting Forces

Figure 42: List of Major and Local Objectives.

The list of global AIMS metrics and local objectives associated with this study is detailed in Figure 42 above. Further, economic models to evaluate the performance metrics of the AIMS system and impact of cost components are presented in Chapter 6.

Summary

In this chapter, a novel hybrid approach in AIMS is presented and feasibility experiments that were conducted to demonstrate the proposed hybrid approach are illustrated. The major cause of inaccuracies associated with the approach, namely, AM-part accuracy and surface roughness and their effects on CNC-RP inefficiency are noted. Also, this chapter outlines the various research components required to develop the AIMS system.

A framework associated with process flow for the proposed unique hybrid system, where process planning for the subtractive stage is incorporated in the initial stages of the AIMS process is described. Further, based on the nature of the process components, physical and software architectures that are required to develop AIMS are distinguished. Hence, it is important to identify the global/overall objectives associated with AIMS development such that hybrid-made parts can be created with accurate part features irrespective of part geometry, build orientation, AM-process and material (which all have unique shrinkage properties). Finally, local objectives associated with this study are presented.

CHAPTER 4: METHODOLOGY

Introduction

In this chapter, part location analysis will be presented for parts that have been redesigned with sacrificial machining fixtures that have been created in an AM process. The fixturing feature's accuracy and surface characteristics of the sacrificial fixtures (work-holding) are analyzed. A geometric model that uses the maximum fixturing deviations, coupled with tolerance chain links to the part features (and machine envelope) is developed. It is important to analyze and model the inaccuracies and surface roughness of the fixture surfaces because they represent how the workpiece is presented to the machine tool. In an ideal CNC-RP set-up, the location of a desired part feature is related to the machine coordinate system through the physical linkage of the stock. In the case of AIMS, the toolpath generated for finishing operations for the machining of part features is constrained and located through the sacrificial fixtures. Further, in the case of AIMS the orientation of the near-net AM part is predefined and hence, design principles for the location and geometry of the sacrificial fixtures are also defined. Section 4.1 details a model for quantifying the maximum fixture deviation as a function of the fixture accuracy (maximum-minimum deviation) and surface characteristics. Section 4.2 presents the design principles associated with the fixture design. Section 4.3 presents the approach employed to analyze the part deviation and overgrowth and the interaction between fixture deviation and part geometry.

4.1. Fixture Deviations

Any process produces part features with surface roughness/texture and size variability. Due to the nature of many AM processes, there can be part and build orientation dependent shrinkage and size characteristics. To accommodate fixturing errors, most fixtures and fixture surfaces are typically specified with a tolerance of a magnitude less than the most critical part tolerance; however because of the manner in which AIMS has been designed, the fixture surface for machining, comes directly from a surface produced in an AM process where there can be considerable deviation in work-holding surfaces as shown in Figure 43.

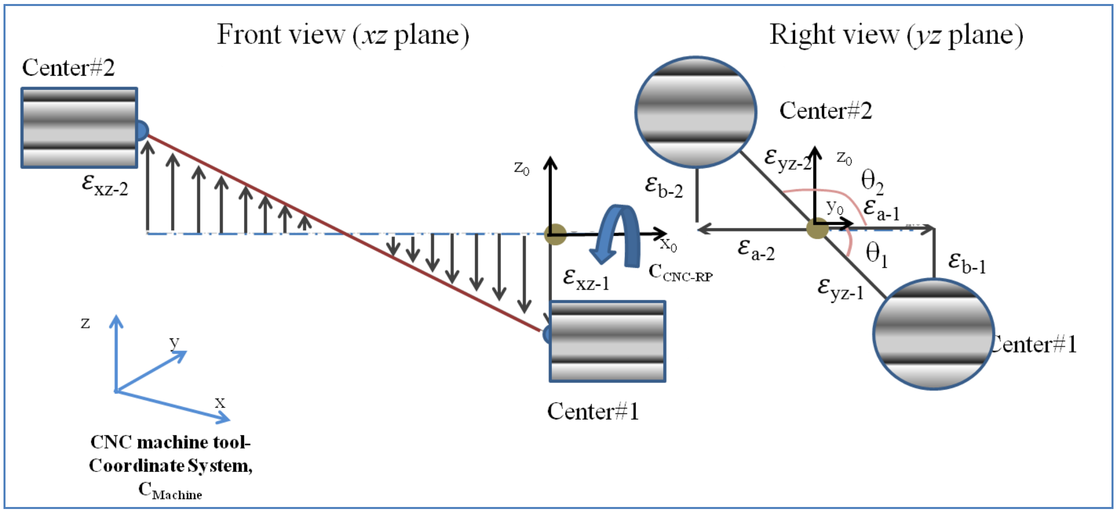
Front view (*xz* plane)
Right view (*yz* plane)
Center#2
ε_{xz-2}
z_0
x_0
ε_{xz-1}
C_{CNC-RP}
z
y
x
CNC machine tool-
Coordinate System,
$C_{Machine}$
Center#1
Center#2
ε_{yz-2}
z_0
θ_2
ε_{b-2}
y_0
ε_{a-1}
ε_{a-2}
θ_1
ε_{b-1}
ε_{yz-1}
Center#1

Figure 43: 2D Vector Model-Distance between Fixtures

A greater deviation of the part geometry (ε_{CNC-RP}) during CNC-RP as shown in Figure 43 yields a larger machining allowance. The deviation of the part geometry is influenced by two dependent variables; magnitude of deviations associated with the CNC-RP fixture due to surface roughness and fixture accuracy (ε_{Fix}), and the part volume (ε_{Pv}), i.e. length and geometry.

The deviation caused by the inaccuracy and surface roughness of the fixtures $(\varepsilon_{yz-i}, \Theta_i)$ is shown as a vector model in Figure 43 where *i* = 1 and 2 (for the head and tail-end of the indexer). Locating the part with respect to the sacrificial fixtures produced in the AM process will likely result in axial misalignment of the part. Hence, it is critical to analyze the magnitude of deviations at the fixture centers' in order to model the maximum part deviation about the machine axis. This will subsequently be used to determine the amount of part overgrowth required to produce the final part.

There are two major components associated with the fixture deviation, namely fixture accuracy and the surface characteristics/texture of the fixture that is in contact with the work-holding chuck. In this study, two different fixture geometries are considered namely; Circular and tri-planar faced as shown in Figure 44. The hypothesis is that tri-planar faces will assist in constraining a rotational degree of freedom when fixturing the part since; the work-holding 3-jaw chuck has an included angle of 120º. Geometric models to characterize the total axial misalignment will be developed and examined.

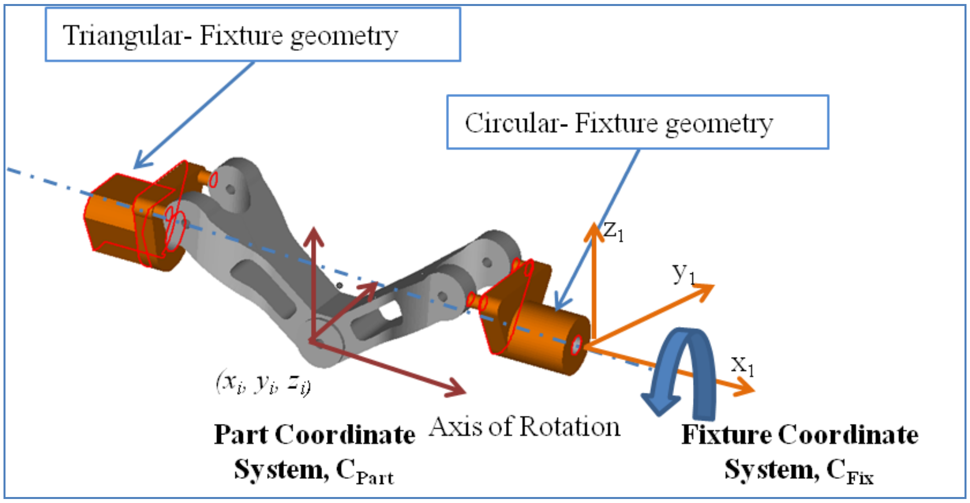
Triangular- Fixture geometry
Circular- Fixture geometry
z1
y1
x1
(xi, yi, zi)
Part Coordinate System, CPart
Axis of Rotation
Fixture Coordinate System, CFix

Figure 44: Fixture Geometries

The approach to integrating the influence of both the factors is based on the objective to identify the ‘maximum deviation’ of the fixture’s true location with respect to the machine axis using least square fit of actual contact surfaces that are measured. Hence, in this study, the maximum deviation of the fixtures’ form accuracy namely; the max-min of the planar faces and the circular profile of the fixtures are recorded. Further, profile characteristics of the AM-made contact surfaces are then super-imposed onto the ‘absolute’ maximum deviation contact profiles as shown in Figure 45 below.

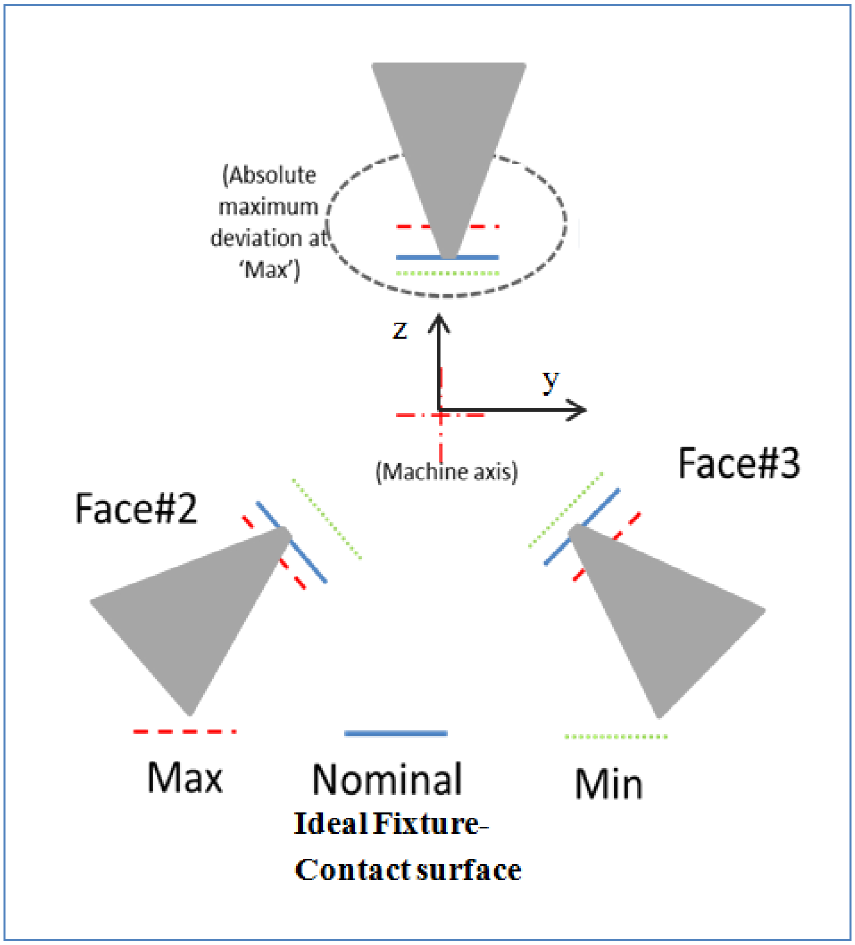
(Absolute maximum deviation at 'Max')
z
y
(Machine axis)
Face#2
Face#3
Max
Nominal
Min
Ideal Fixture-Contact surface

Figure 45: 2D Interaction of Feature Form Inaccuracy and Surface characteristics

In the case of circular fixtures, similar to the tri-planar faces the contact surfaces are limited by the contact surface based on the jaw profile and the surface profile distribution. In the case of tandem 3-jaw chuck, we know that the distance between the jaw contact surfaces are physically limited to the radius of the nominal diameter of the part that is being clamped. For instance, in the case of clamping a perfectly polished ground stock in a tandem 3-jaw chuck, the distance between the three contacts surfaces will ideally be the radius of the stock.

However, in the case of ‘maximum’ deviation analysis in AIMS the distance between the contact surfaces and the machine axis can be described as shown in Figure 46.

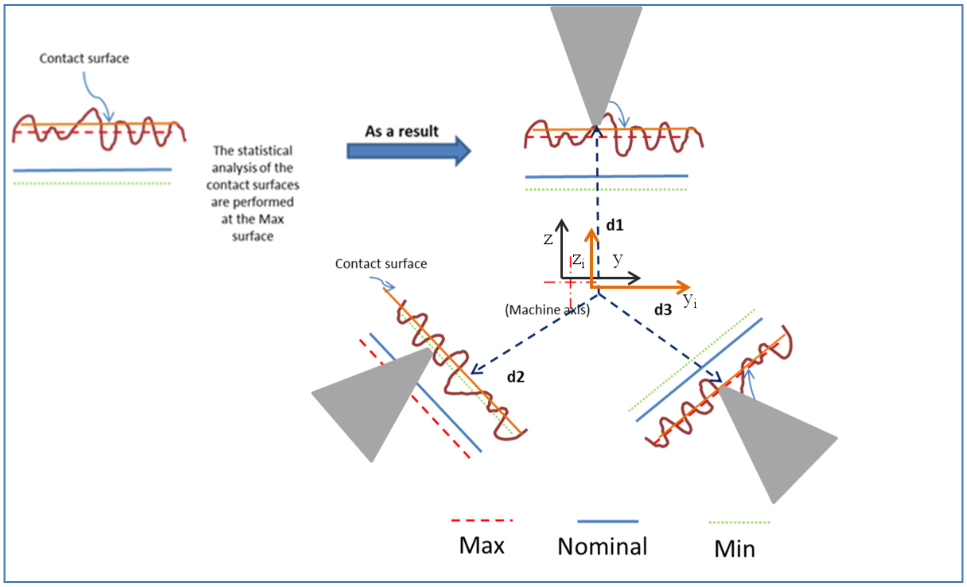
Contact surface
The statistical analysis of the contact surfaces are performed at the Max surface
As a result
Contact surface
d1
d2
d3
z
y
zi
yi
(Machine axis)
Max
Nominal
Min

Figure 46: 2D Contact Surfaces across the 3-jaw Chuck with respect to the Machine Axis

The following sub-sections detail the methodology employed to characterize the form deviations and surface characteristics.

4.1.1 Form Accuracy

For this study, a CMM was used to record and calculate the form feature accuracy and a non-contact Laser profilometer is used to record and analyze the surface texture characteristics. Automated recording and measurement was programmed using the PC-DMIS software with a Renishaw CMM machine.

The programs are provided in Appendix-1 for reference. Least square methods where employed to derive the maximum and minimum deviations from the calculated average plane shown in Figure 46. Figure 47 shows the reasoning behind collection of fixture contact points and the representation of the positive-negative deviations from the average plane and diameter.

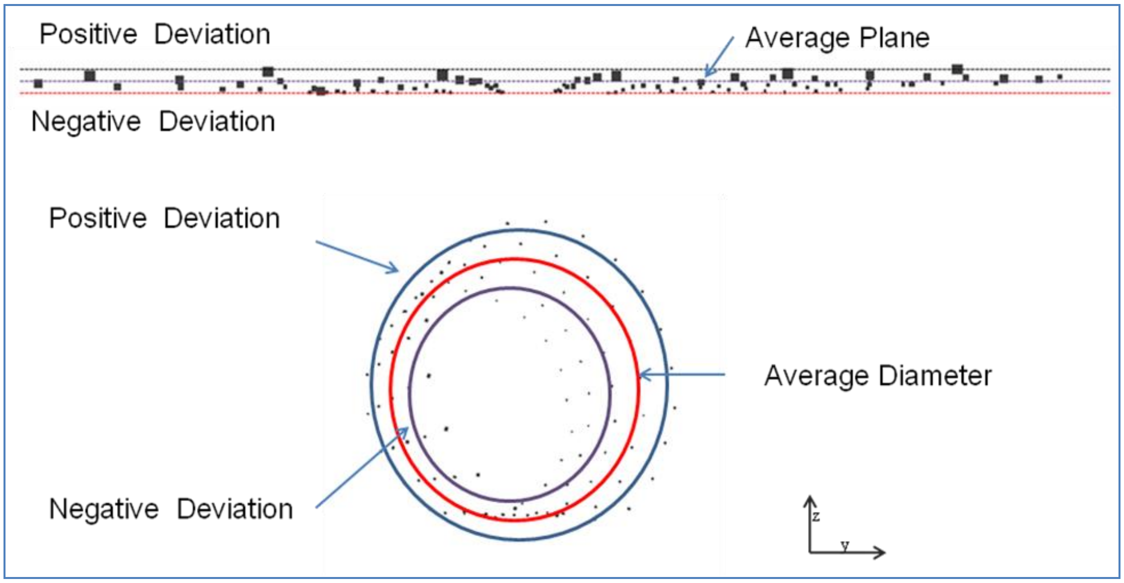
Positive Deviation
Average Plane
Negative Deviation
Positive Deviation
Average Diameter
Negative Deviation
z
y

Figure 47: Maximum-Minimum Deviation

The Renishaw Ruby probe used had a diameter of 4 mm which is assumed to suffice since, initial profilometer data showed frequencies of peak-to-peak of several magnitude lower than 4 mm. In the case of cylinders, 5 levels of measurements at z-spacing of 2.54 mm and 20 uniformly spaced data points were collected at each z-level based on the results from a preliminary sensitivity study. The average diameters of the cylinders that were measured ranges from about 17 mm to 58 mm. The Figure 48 shows a sample average diameter scatter plot performed on a circular support.

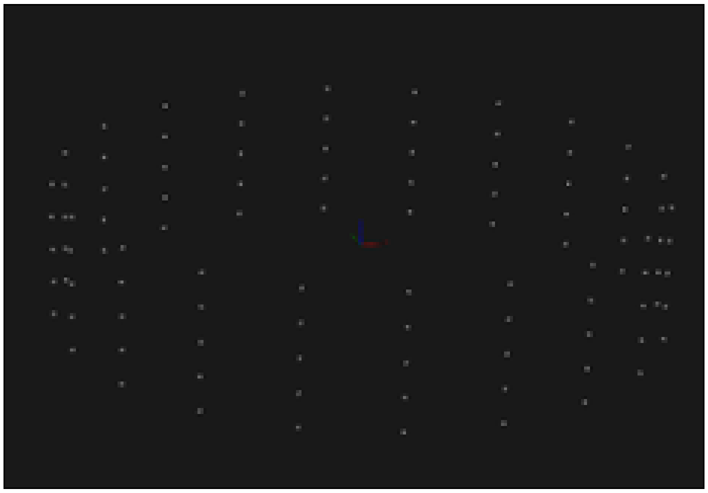

Figure 48: Cylindrical Fixture – Form Measurement

In the case of tri-planar features, 10 levels of z-spacing at 2.54 mm and 10 uniformly spaced data points at each z-level were collected to calculate the positive and negative deviations from the average plane. The following Figure 49 shows sample nominal tri-planes calculation performed on tri-planar fixture geometry.

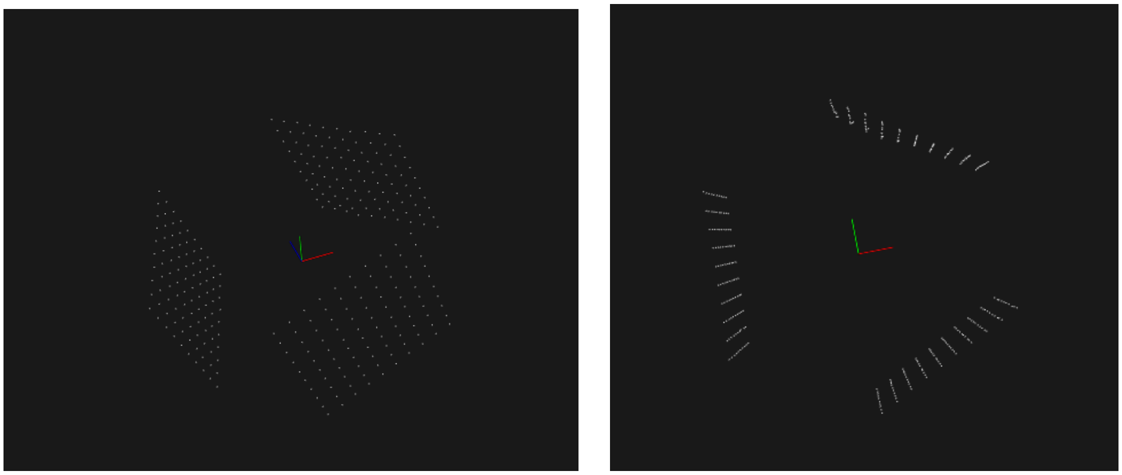

Figure 49: Tri-planar Fixture – Form Measurement

The methodology employed to determine the positive and negative deviations of the contact surface was described. However, in addition to fixture form inaccuracy, surface characteristics need to be included. The surface deviations can be added to the contact deviation to determine the maximum possible fixture deviations.

4.1.2 Surface Characteristics

In the case of AIMS, the AM-made fixture surfaces often have wafer-supports that are attached to it for over-hanging edges. Upon, manually removing those structures the surfaces are often subjected to operations such as peening or grinding. In the case of contact between a nominally smooth (precision-machined chuck jaws) and a rough surface (AM-made part), we can analyze the contact based on the Greenwood and Williamson (G-W) approach [1] which presents the interaction between two nominal surfaces to determine the actual contact surface.

The assumptions of G-W are appropriate in the case of AIMS due to the presence of a rough surface with a number of asperities with a composite radius, with varying magnitude of profile height and being a Gaussian surface. It is also assumed that there is no sliding between the two contact surfaces as shown in Figure 50 below and hence, we consider only elastic contact between the surfaces. Since, the separation distance in elastic contacts is greater than elastics-plastic contact; this would result in slightly higher estimation of required part overgrowth ensuring that the part can be successfully produced.

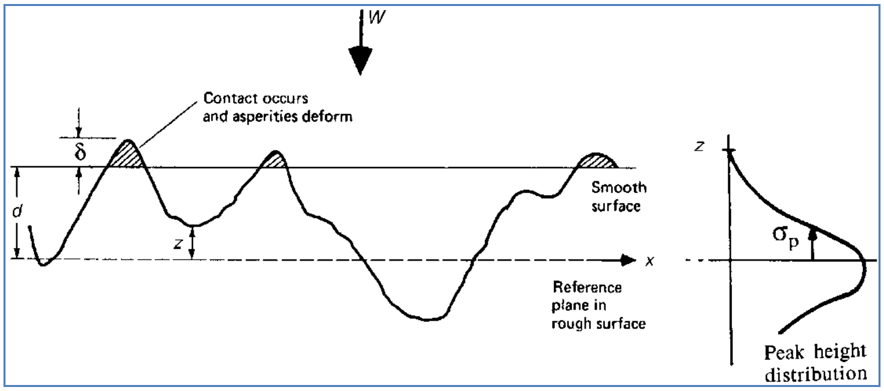
W
Contact occurs
and asperities deform
δ
d
z
Smooth
surface
x
Reference
plane in
rough surface
z
σp
Peak height
distribution

Figure 50: Contact between Smooth and Rough Surface

Given a separation distance *d*, mean real pressure p_r, real area of contact A_{re}, number of contact spots, *n* and mean asperity real area of contact as a function of separation *d*, the probability of making contact at any given asperity of height *z* can be defined as:

$$P(z > d) = \int_d^\infty p(z)\, dz \tag{4.1}$$

And for a given number of asperities *N*, $\delta = z\text{-}d$, large spherically tipped asperities of same radius $R_{p,}$ the expected area of contact is defined as [1]:

$$A_{re} = \pi NR_p \int_d^{\infty} (z-d)p(z)\, dz \tag{4.2}$$

And with *D* as the dimensionless separator and assuming that the contact occurs at the larger asperities (given jaw diameter and surface profile) [1],

$$\sigma_p = \sigma = \frac{(\pi * n)}{(A_{re} * R_p)} * \frac{F_1\ (D)}{F_0\ (D)} \tag{4.3}$$

And the function for dimensionless separator can be resolved as shown below, where, $p^*(s)$ is the standardized peak-height probability density function.

$$F_m\ (D) = \int_D^{\infty} (s-D)^m\, p^*(s)\, ds \tag{4.4}$$

In order to identify the contact surface, we need to identify the diameter of the large spherical asperities, real area of contact and corresponding sampling of number of points. For this purpose, MicroTrak MT-250 diffuse Laser sensor was mounted on a motion controlled table controlled by isel MC-4 controller. MicroTrak 7000 laser displacement sensor was used to record data through a National Instruments-DAQ system as shown in Figure 51. The programs are attached in Appendix-2.

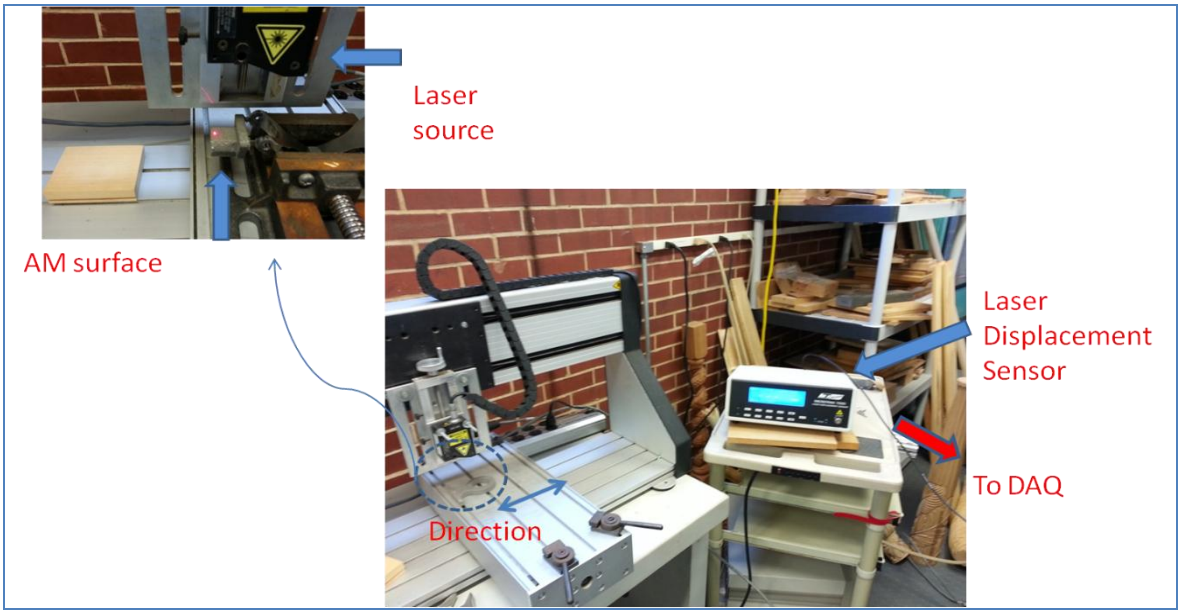

Figure 51: Surface Profile Measurement

Using the calibrated laser profilometer, 16 AM-made surfaces from the Arcam EBM (Model A2) where measured. The recorded raw data in the case of non-planar surfaces (e.g. tri-planar faces #2 and #3) were de-trended to accommodate for the angularity. The standard area analyzed was 10 mm x 10 mm with 6 scans at an interval of 1.25 mm to estimate the average profile of the surface. Figure 52 shows a scanned profile of a face in a tri-planar fixture followed by filtered data. Filtering of raw data is required to eliminate the effects of tilt (de-trending) and is performed based on auto-thresholding at 3000Hz.

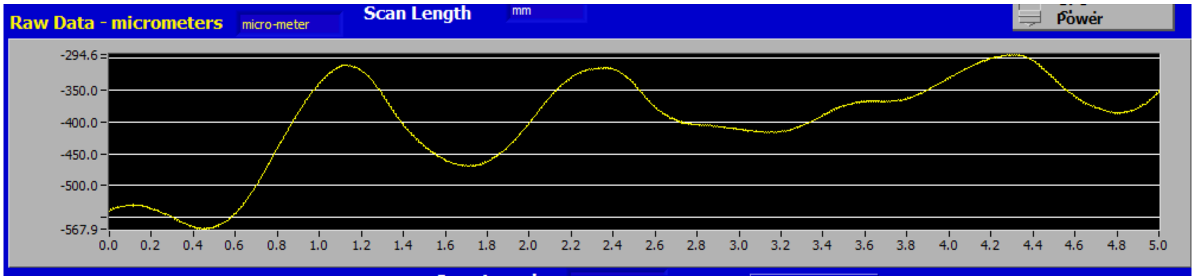

Figure 52: Raw Data of a Surface Scan #1

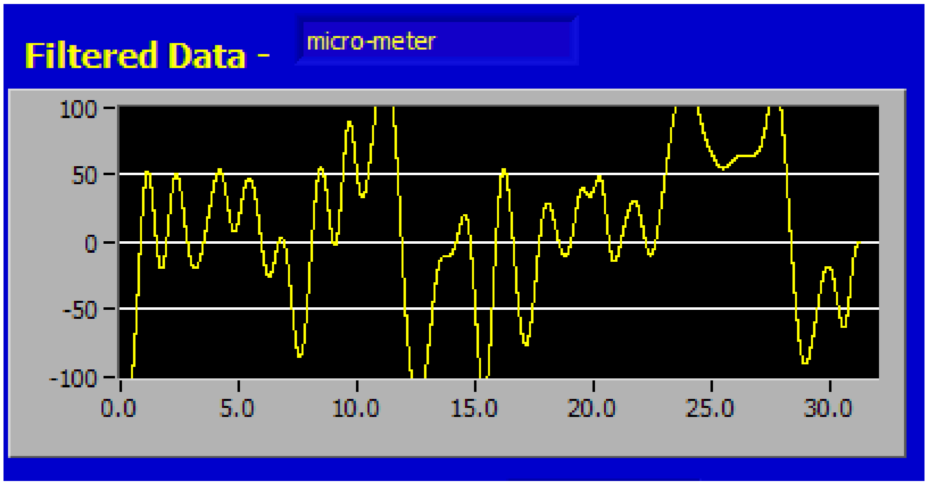

Figure 53: Filtered Data of all the Scans of the surface

The deviations determined from the post-processed surface profile are added to the maximum minimum deviations as described in Section 4.1 to determine the fixture location with respect to the machine axis. This section has addressed the texture of AM produced surfaces, and has specifically looked at how a cylindrical jaw will interact with the surface irregularities. In the next section, the effects of the location of the sacrificial fixture will be addressed. The section begins with a brief discussion of design of these sacrificial fixtures so that limitations for their position can be better understood.

4.2. Fixture Design Principles

In this section, some basic design rules in the design of fixtures that will be added to the part design prior to AM processing are presented. Since the fixturing features for CNC-RP are integrated in the AM part, it is important to consider the 'critical surfaces' in selecting the geometry and location of the fixturing features. It influences the accessibility of the cutting tool to finish machine the critical surfaces and also, impacts the material consumption and build time in AM. For instance, depending on the AM process selected (EBM-S12, EBM-A2, DLMS, etc.), the total build volume and orientations available will vary. Also in AIMS, the visibility analysis for CNC-RP is performed prior to processing in AM and hence, the possible fixture locations and geometry are known prior to the AM build.

The influence of selecting the fixture locations and design on secondary CNC fixturing is shown in Figure 43. It is obvious that accessibility to machine the identified critical features is feasible when the fixtures do not interfere with the cutting tool-part features (e.g. assembly holes cannot be reached in the second design) as shown in Figure 54.

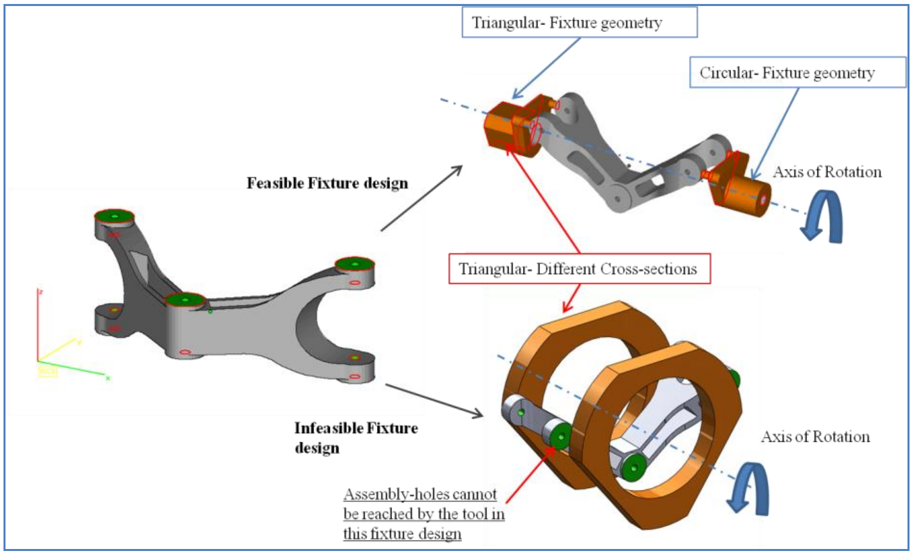
Triangular- Fixture geometry
Circular- Fixture geometry
Feasible Fixture design
Axis of Rotation
Triangular- Different Cross-sections
Infeasible Fixture design
Axis of Rotation
Assembly-holes cannot be reached by the tool in this fixture design

Figure 54: Influence of Critical Features on Fixture Design

The fixture design (Fix_v) consists of two major considerations, namely location (Fix_{loc}), its geometry in terms of the fixture geometry (Fix_{gi}), where i=1 (circular), 2 (triangular)… and cross-sectional area of each fixture (Fix_{ai}). In this study, the length of fixture-contact is not considered.

The fixture locations' restrict the part visibility (Θ_{CNC-RP_i}) during CNC-RP. Further, the fixture designs (location and volume) are constrained by the maximum machining forces (F_{CNC-RP}) during machining and the available build volume-orientation in AM (ori_{AM}) and the machining volume in CNC-RP (ori_{CNC-RP}).

$$Minimize\ \{Fix_v\} = f(Fix_{loc}, Fix_{gi}, Fix_{ai}) \tag{4.5}$$

Subject to constraints; Θ_{CNC-RP_i} AND ori_{AM} AND ori_{CNC_RP} AND F_{CNC-RP}

The influence of part visibility (Θ_{CNC-RP_i}) for CNC-RP on the fixture design can be restricted to visibility of only critical surfaces (as in Figure 55) or orientations with maximum visibility that can be built within the AM part volume and fixtured in the CNC-RP setup. Another design criterion for fixture location in the part includes the cutting tool length required to machine, since tools with higher length/diameter ratio suffers from chattering and deflection.

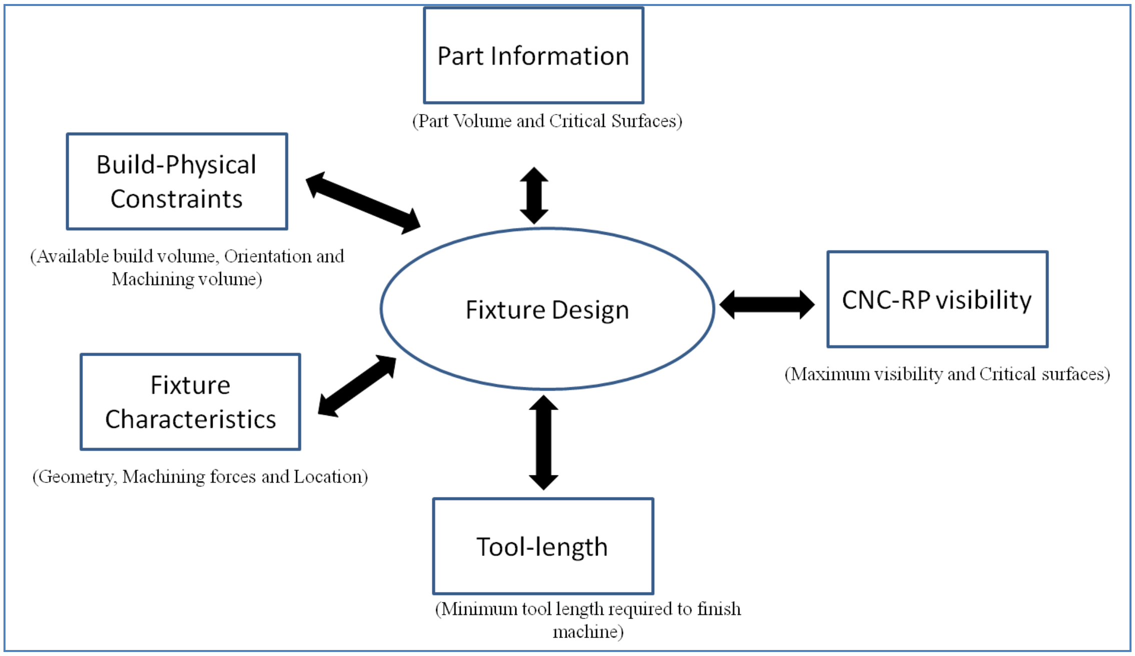
Part Information
(Part Volume and Critical Surfaces)
Build-Physical Constraints
(Available build volume, Orientation and Machining volume)
Fixture Design
CNC-RP visibility
(Maximum visibility and Critical surfaces)
Fixture Characteristics
(Geometry, Machining forces and Location)
Tool-length
(Minimum tool length required to finish machine)

Figure 55: Fixture Design Principles

Based on the major criteria presented in Figure 55, the following heuristics is presented for the design of fixtures in AIMS:

1) Part Information → P_v and Critical surfaces (Primary and Secondary)
    - CAD file of the desired part with critical surfaces (i) identified

2) Visibility Analysis → CNC-RP
    - Analysis for machining accessibility of critical surfaces, (θ_{CNC-RP_i})
    - Analysis of maximum visibility and minimum number of orientations after aligning the part to machine critical surfaces
3) Tool-length considerations → Deflection and Accessibility
    - Minimum tool length required to machine critical and/or all surfaces ($Min\text{-}T_i$)
    - Analysis for additional rotational orientations to reduce the tool length required (lesser chattering and tool deflection)
4) Fixture considerations → Location and Cutting forces
    - Selection of fixture geometry and size, $(Fix_g \text{ and } Fix_a)$ based on mis-alignment analysis, (ε_{yz-i})
    - Estimation of cutting forces for the considered machining parameters, part geometry and mechanical support required through fixture support, (F_{CNC-RP})
    - Location of the fixture supports on non-critical surfaces (since such surfaces require manual removal and finishing), (Fix_{loc})

5) Build-Physical constraints → Orientation

- Analysis of build orientation in AM process (θ_{AM}) for given AIMS part (AM_{PV}) which includes the desired part with attached sacrificial fixtures and compensated for machining allowance

In this study, the parts are manually analyzed by identifying the critical surfaces as shown in Figure 39 followed by performing the visibility analysis. Cutting forces analysis and tool length considerations are not included in this work. Fixture design is analyzed for the mis-alignment and its location on non-critical surfaces. Finally, the impact of build orientation (which could impact the fixture part geometry and cross section) are studied.

4.3. Part Deviation and Overgrowth

Based on the models presented in Sections 4.1 and 4.2, the maximum deviations associated with the CNC-RP fixture (ε_{Fix}) for a given part geometry are determined. As a result, the tool-path generated for each rotational orientation are not effective in finish machining the desired part and often, gouges into the part and damaging it permanently. This part deviation is associated with the part volume (ε_{P_v}) i.e., dependent on the length of the part (l) and the cross-sectional area of the part along the length $(a(l))$ as shown in Figure 56. Therefore, the total deviation that occurs after the part is fixtured into the CNC machine is a combination of the errors associated with the fixturing and the part volume as illustrated in Figure 56.

The deviation along the part length (in *xz* plane) varies for the uniform part volume based on the fixture error $(\varepsilon_{xz-i}, \varepsilon_{yz-i}, \Theta_i)$ as shown in Figure 56 (a-b) and (c-d).

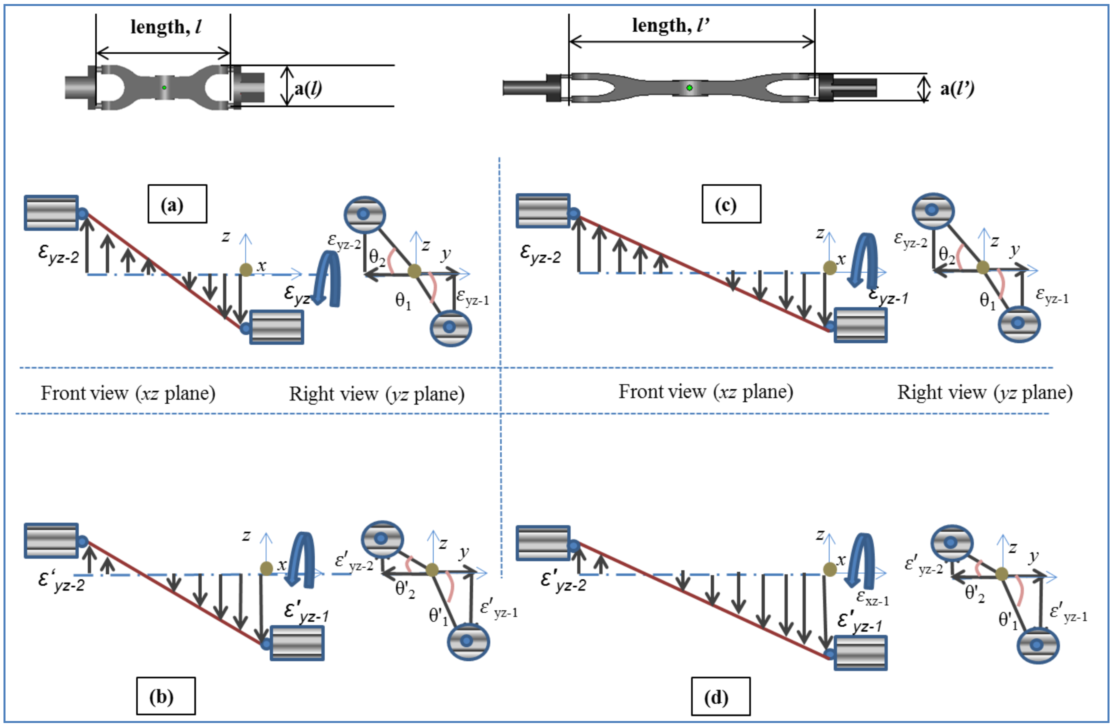
length, *l*
a(*l*)
length, *l'*
a(*l'*)
(a)
(c)
(b)
(d)
ε_{yz-2}
ε_{yz-1}
ε_{xz-1}
z
x
y
θ_1
θ_2
Front view (*xz* plane)
Right view (*yz* plane)
ε'_{yz-2}
ε'_{yz-1}
θ'_1
θ'_2

Figure 56: Interactions between Fixture Error and Part Geometry

The total deviation varies for uniform fixture errors based on the part geometry $(l, a(l))$ as shown in Figure 56 (a-c) and (b-d). The objective is to identify the part overgrowth required in the total AM produced part volume, for the maximum part deviation and can be expressed as:

$$\text{Minimal}\{\delta_v\} = f_4(max_{\varepsilon_{CNC-RP}}) \tag{4.6}$$

Where the minimal machining allowance, δ_v (Eq. 6) required in producing the part is a function of maximum part deviation associated with fixturing the near-net part in CNC-RP.

$$max_{\varepsilon_{CNC-RP}} = f_4'(\varepsilon_{Fix}, \varepsilon_{Pv}) \tag{4.7}$$

Where the maximum CNC-RP error (Eq. 4.7) is a function of error associated with near-net CNC-RP fixtures (Eq.8) and the AM-made part volume across the two fixtures (Eq. 4. 9).

$$\varepsilon_{fix} = f_4''(\varepsilon_{xz-i}, \varepsilon_{yz-i}, \Theta_i) \tag{4.8}$$

Where, referring to Figure 56, the error associated with the near-net CNC-RP fixtures, is a function of the misalignment with respect to the machine rotational axis.

$$\varepsilon_{Pv} = f(l, a(l)) \tag{4.9}$$

Where, referring to Figure 56, the error associated with the part volume/geometry, is a function of the misalignment along the machine rotational axis and the part cross-section. Therefore, the objective is to determine the minimum part overgrowth required for a given part volume which is based on its orientation in CNC-RP and fixture deviation which is based on fixture geometry as shown in Eq.10 below.

$$Minimum\ \{\Delta_v\} = f(\delta_v\ , Fix_{gi}, Fix_{ai}) \tag{4.10}$$

This is based on the findings from the previous sub-objectives namely; machining allowance required based on the CNC-RP fixture error and part volume, and the impact of fixture design on the combined fixture-part volume.

In this study, the part overgrowth is limited to global surface offset (across all surface facets) for the magnitude of maximum part deviation across all facets. However, with further studies, we can optimize the overgrowth based on each individual surface facet and also, based on part orientation in AM (downward vs. upward facing surfaces, etc.).

The deviation caused by the inaccuracy and surface roughness of the CNC-RP fixtures $(\varepsilon_{CNC-RP}, \Theta_i)$ is shown as a vector model in Figure 56 where i = 1 and 2 (for the head and tail-end of the indexer). Given the part orientation in the CNC-RP setup, it can be observed that the maximum part deviation always occurs at the end of the part geometry, l for the maximum fixture deviation $(\varepsilon_{CNC-RP}, \Theta_i)$, where $\Theta_i$could vary from 0-180º due to axial symmetry when the part is rotated about the axis during machining. Hence, the global part deviation including material for finishing in the Cartesian coordinate system of the part, $\mathbf{C}_{\mathbf{Part}}$ can be defined as,

$$\delta_{vx} = (\varepsilon_{CNC-RP} \times Sin\, \Theta_i) \tag{4.11}$$

$$\delta_{vy} = (\varepsilon_{CNC-RP} \times Cos\, \Theta_i) \tag{4.12}$$

$$\delta_{vz} = (\varepsilon_{CNC-RP} \times Sin\, \Theta_i) \tag{4.13}$$

Since, we are solving for the maximum possible part deviations, the overall part surface offset can be applied for the maximum of the two axial symmetrical (Θ_i) at 0º and 180º.

4.4. 2D Part Deviation CMM Analysis

We know that from Section 4.1, that the location of the fixture coordinate system is determined by identifying the intersection of the lines from the contact surface with respect to the CNC-RP coordinate system as shown in Figure 43.

The tandem 3-jaw chucks used in this study have intersecting lines at an included 60º. In an ideal work set-up the intersection would be at (0, 0). However, because of the change in actual contact surfaces due to surface roughness and fixture geometry we get unequal deviations ($d_1 \neq d_2 \neq d_3$). With the known slopes and contact point for the lines corresponding to the jaws, we can formulate the intersecting lines to determine the actual fixture location. Referring to Figure 45, we can express the corresponding contact surface lines as:

$$y_i = d_i z_i + c_i \tag{4.14}$$

Where for Plane#1 contact substituting, $y_1 = 0$, $z_1 = d_1$ and d_1,

$$c_1 = {d_1}^2 \tag{4.15}$$

Where for Plane#2 contact substituting, $y_2 = d_2$ Cos30º, $z_2 = d_2$ Sin30º and d_2,

$$c_2 = {d_2}^2 \text{ Sin } 30^o - d_2 \text{ Cos } 30 = \frac{{d_2}^2}{2} - \frac{\sqrt{3}d_2}{2} = -\ 0.3651\ d_2 \tag{4.16}$$

Where for Plane#3 contact substituting, $y_3 = -d_3$ Cos30º, $z_3 = -d_3$ Sin30º and d_3,

$$c_3 = -{d_3}^2 \text{ Sin } 30^o + d_3 \text{ Cos } 30 = -\frac{{d_3}^2}{2} + \frac{\sqrt{3}d_3}{2} = 0.3651\ d_3 \tag{4.17}$$

Table 1 summarizes the intercept values for the tri-planar deviations. They indicate the location and intercept of each plane with respect to the fixed center of the 3-jaw chuck.

Table 1: Intercepts for the Jaw contact lines

Average Radius (mm)	**Plane#1**	**Intercept**	**Plane#2**	**Intercept**	**Plane#3**	**Intercept**
	d1 (mm)	**c1**	**d2 (mm)**	**c2**	**d3 (mm)**	**c3**
12.685	12.735	162.1802	12.80	-4.67145	13.025	4.755428
7.58	7.7	59.29	7.78	-2.84048	8.19	2.990169
7.475	7.6275	58.17876	7.63	-2.7848	7.78	2.840478
7.94	8.1	65.61	8.10	-2.95731	8.26	3.015726
8.38	8.5325	72.80356	8.53	-3.11522	8.685	3.170894

In order to validate this method, the first approach that was employed was to manually induce known deviations d_i using precision shims in a 3-jaw chuck of machined tri-planar fixture and cylindrical fixtures with an average diameter of 38.1 mm (1.5”) with square and cylindrical features as shown in Figure 57 below.

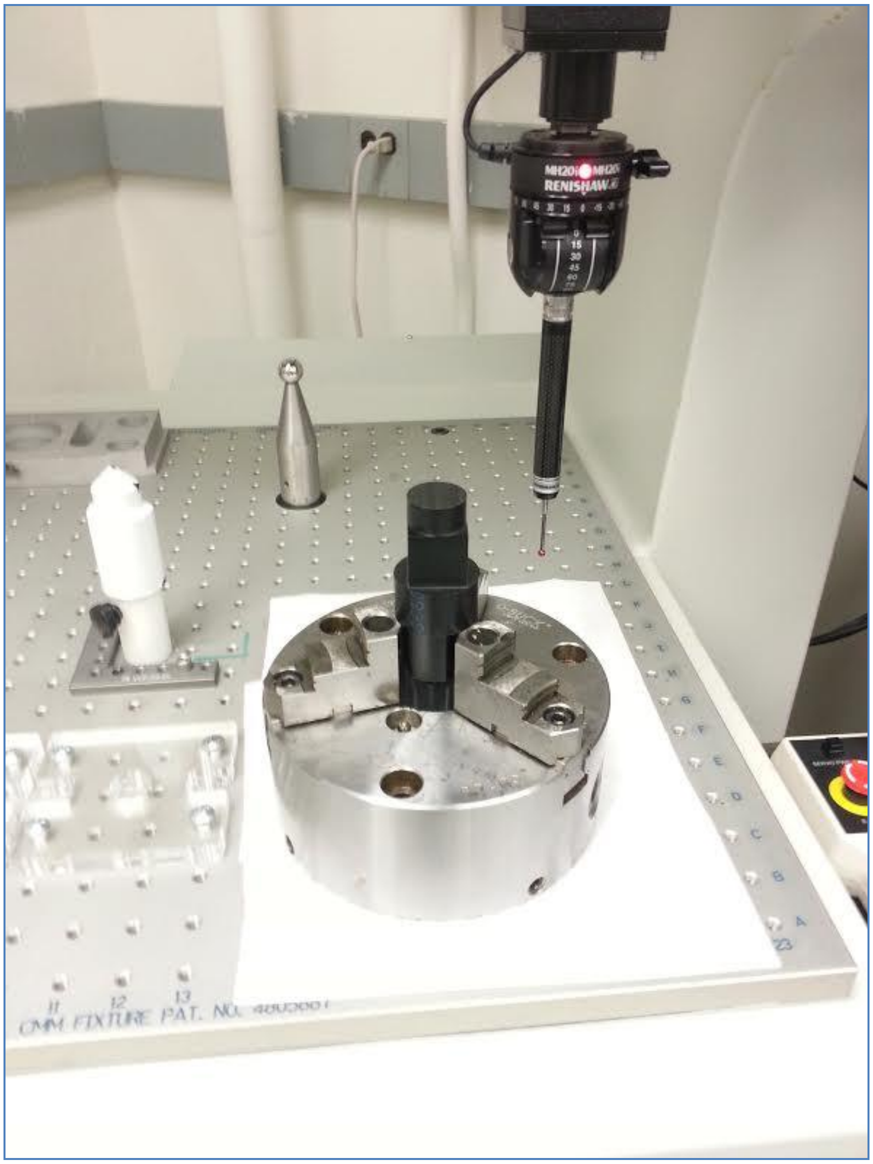

Figure 57: Evaluation of Fixture Inaccuracies

The CMM routine used to collect data on the AM-made parts where used to determine the location of the fixture center with respect to the center of the chuck. The deviations induced at the jaw contact surfaces is a full factorial combination of 0 mm, 0.254 mm, 0.381mm, and 0.508 mm (0”, 0.01”, 0.015” and 0.02”).

Table 2 summarizes the expected and measured deviation of the location of the center and the corresponding error.

Table 2: Expected vs. Measured Fixture Inaccuracies

Deviation	**Expected**	**Measured**	**Error**
mm	(mm)	(mm)	(mm)
0-0-0.254	0.1544	0.1720	-0.0176
0-0-0.381	0.1892	0.2331	-0.0439
0-0-0.508	0.3278	0.3336	-0.0058
0.254-0.254-0.508	0.1544	0.1563	-0.0019
0.254-0.254-0.254	0.0000	0.0524	-0.0524
0.381-0.381-0	0.1892	0.1377	0.0515
0.381-0.381-0.381	0.0000	0.1516	-0.1516
0.381-0.508-0.254	0.2299	0.2567	-0.0268
0.381-0.508-0.381	0.3137	0.3052	0.0085
0.381-0.508-0.508	0.4940	0.5233	-0.0293
0.508-0.508-0	0.2273	0.1929	0.0344
0.508-0.508-0.508	0.0000	0.1361	-0.1361

There were errors associated with expected and measured deviation. This can be attributed to using a polymer part (which is subject to plastic deformation during clamping) and would have induced dislocation of the fixture upon clamping. Hence a 3D deviation model which considers deviation at both the centers based on elastic deformation model (e.g. metal fixtures) is required.

4.3. 3D Between-Centers Fixture Deviation

In the case of AIMS, the deviations associated with work-holding occur at both fixturing ends. Further, unlike the preliminary 2D CMM analysis, the set-up of AIMS includes recording of work-offset in the *x*-direction as shown in Figure 58 which shows an exaggerated deviation of the fixturing and referencing surfaces:

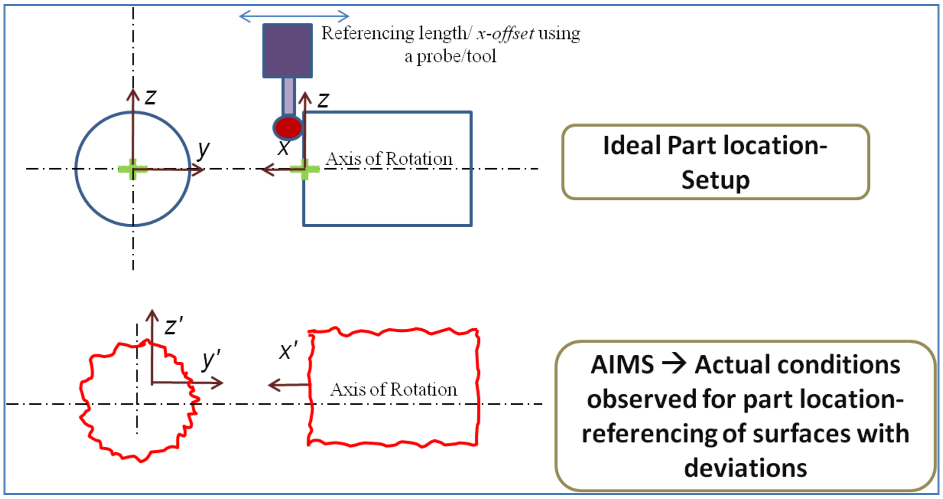
Referencing length/ *x-offset* using a probe/tool
z
y
z
x
Axis of Rotation
Ideal Part location-Setup
z′
y′
x′
Axis of Rotation
AIMS → Actual conditions observed for part location-referencing of surfaces with deviations

Figure 58: Impact of referencing from near-net metal additive parts

Hence, when compared to the basic model in Figure 43 the fixture deviations associated with AIMS is extended into a 3D model as shown in Figure 59:

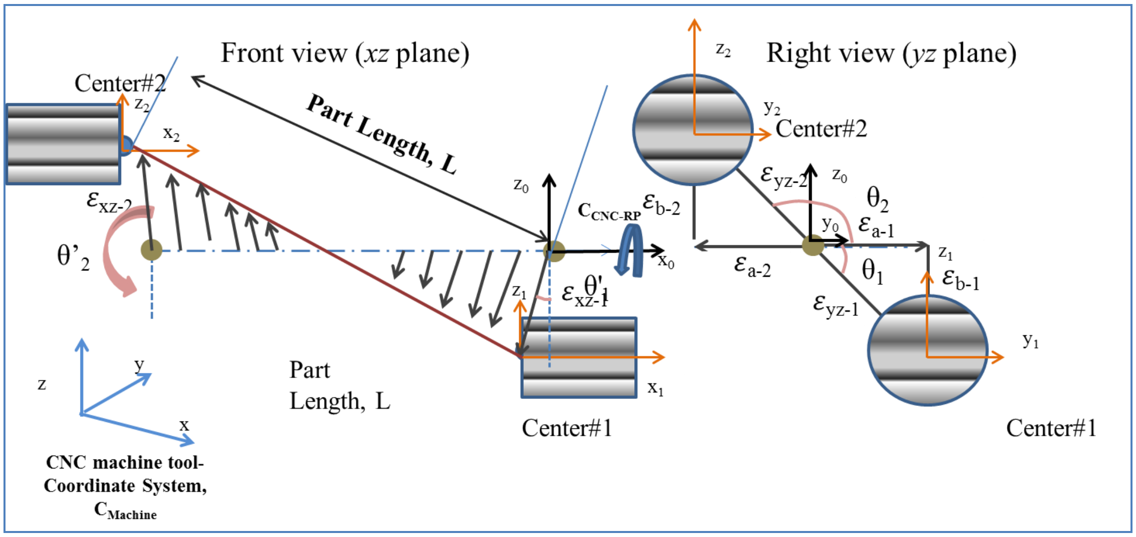
Front view (xz plane)
Right view (yz plane)
Center#2
z_2
x_2
Part Length, L
ε_{xz-2}
θ'₂
z_0
C_{CNC-RP}
ε_{b-2}
x_0
z_1
ε_{xz-1}
θ'₁
x_1
Center#1
Part
Length, L
z
y
x
CNC machine tool-
Coordinate System,
$C_{Machine}$
z_2
y_2
Center#2
ε_{yz-2}
z_0
θ₂
y_0
ε_{a-1}
ε_{a-2}
θ₁
z_1
ε_{b-1}
ε_{yz-1}
y_1
Center#1

Figure 59: 3D Fixturing Deviation parts

Hence, the fixture coordinate system for both the centers (x_{c-i}, y_{c-i}, z_{c-i}) with respect to the CNC-RP coordinate system ((x_0,y_0,z_0) which is the work-offset) presented in Eq. 3.1 can be modified as:

$$\begin{bmatrix} x_{c-i} \\ y_{c-i} \\ z_{c-i} \end{bmatrix} = \begin{bmatrix} 1 & 0 & 0 & (-\varepsilon_{xz-i}\ Cos\ \theta'_i) \\ 0 & 1 & 0 & (-\varepsilon_{yz-i}\ Cos\ \theta_i) \\ 0 & 0 & 0 & (-\varepsilon_{yz-i}\ Sin\ \theta_i) \\ 0 & 0 & 0 & 1 \end{bmatrix} \times \begin{bmatrix} x_0 \\ y_0 \\ z_0 \end{bmatrix} \tag{4.18}$$

And can be simplified into,

$$x_{c-i} = x_0 \times (-\varepsilon_{xz-i}\ Cos\ \theta'_i)\ , \tag{4.19}$$

$$y_{c-i} = y_0 \times (-\varepsilon_{yz-i}\ Cos\theta_i) \tag{4.20}$$

$$z_{c-i} = z_0 \times (-\varepsilon_{yz-i}\ Sin\theta_i) \tag{4.21}$$

It should be noted that the total part length, L does not change because of 3D deviations, since it is physically limited by the as-AM produced part dimensions. Once the maximum deviation of the fixtures at both the centers are identified, this information can be used to determine the location of the part coordinate datum (x_i,y_i,z_i). For instance, the cases of ideal and actual set-up with fixture deviations, part coordinate datum can be expressed as shown in Figure 60.

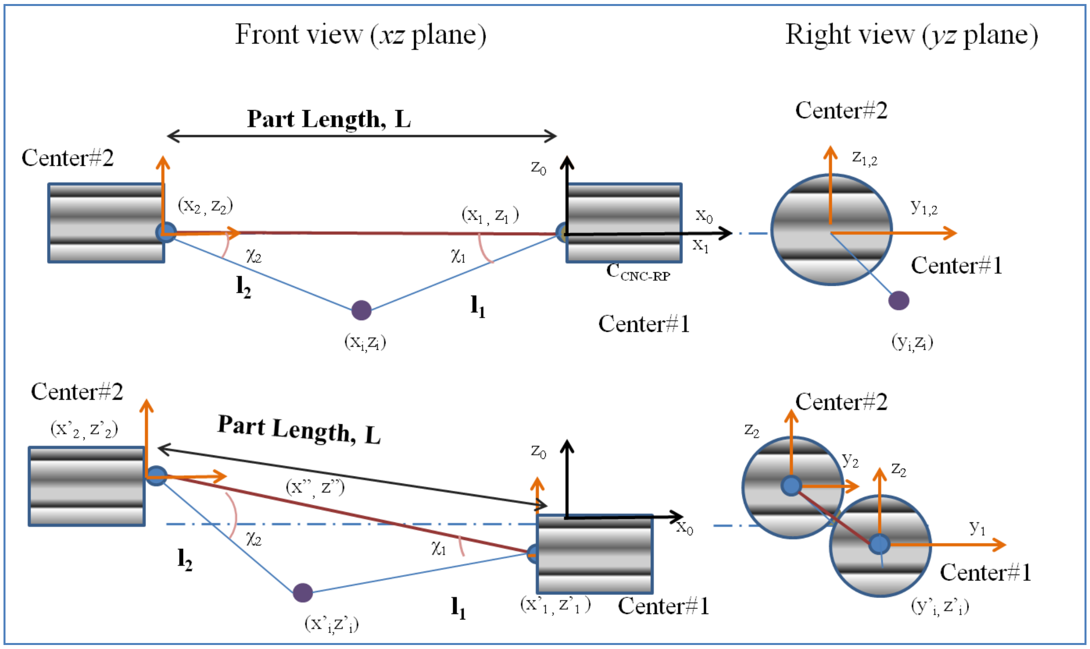
Front view (xz plane)
Right view (yz plane)
Part Length, L
Center#2
(x2 , z2)
(x1 , z1)
z0
x0
x1
χ2
χ1
l2
l1
CCNC-RP
(xi,zi)
Center#1
Center#2
z1,2
y1,2
Center#1
(yi,zi)
Center#2
(x'2 , z'2)
Part Length, L
(x'', z'')
z0
x0
χ2
χ1
l2
l1
(x'i,z'i)
(x'1 , z'1)
Center#1
Center#2
z2
y2
z2
y1
Center#1
(y'i, z'i)

Figure 60: Part Coordinate System w.r.to Fixturing Deviation parts

The next step is to identify the deviation of part coordinate system (x_i,y_i,z_i) with respect to the fixture deviations at both the centers. This approach is considered because, the deviation of individual part features can be subsequently determined based on the datum call-out. Eq. 4.14 can be used to calculate the deviation of the fixture centers corresponding deviations (y'_{ci}, z'_{ci}). However, in the case of deviation along *x*-direction, we need to consider the fixed length of the part. The following procedure is used to determine the deviation of the datum system x'_i for given fixture deviations at the fixtures. It should be noted that the selection of datum location for the ideal setup below is for demonstration. With known part end locations and datum (as in the case of the validation in further sections), this method is applicable for all part feature and datum designs. From the basic engineering drawing, we can determine **L, l_1, l_2 , χ_1 and χ_2 .** From Eq. 4.14 y_{c-i}', z_{c-i}' and by measuring the deviation in the contact surface along *x*-axis x_{c-i}', we can express the modified part deviation, with the known nominal lengths of **l_1** and **l_2** (to fixture centers) as:

$$l_1 = \sqrt{(x_i' - x_1')^2 + (z_i' - z_1')^2} \tag{4.22}$$

$$l_2 = \sqrt{(x_i' - x_2')^2 + (z_i' - z_2')^2} \tag{4.23}$$

By solving, the simultaneous quadratic equations in Eq. 4.22-4.33, we can identify the intersection of two circles centered at the two fixtures, which will provide the *x*-coordinates of the new location of the part datum. The results from Eqs.4.14 and 4.23, provide the deviated datum location for an orientation in CNC-RP. Further, the location of any deviated point (px''_i, py''_i, pz''_i) within the part specifications with respect to the deviated fixture coordinate system is given as,

$$\begin{bmatrix} px''_i \\ py''_i \\ pz''_i \end{bmatrix} = \begin{bmatrix} 1 & 0 & 0 & x_i' \\ 0 & 1 & 0 & y_i' \\ 0 & 0 & 0 & z_i' \\ 0 & 0 & 0 & 1 \end{bmatrix} \times \begin{bmatrix} px_i \\ py_i \\ pz_i \end{bmatrix} \tag{4.24}$$

And based on values from Eq. 4.24, the deviated part location can be expressed as,

$$px''_i = (x'_i - px_1) \tag{4.25}$$

$$py''_i = (y'_i - py_1) \tag{4.26}$$

$$pz''_i = (z'_i - pz_1) \tag{4.27}$$

Subsequently, after determining the maximum possible deviation for a given part design (for all machining orientations), minimum machining allowance can be added to the total deviation. This will provide the part design that will be produced in an AM machine.

Summary

In this chapter, models were developed that can be used to assess the location/positional deviation of a part made on an AM process when it is fixture in a machine tool for machining. Models describing the geometric location of the part were developed and measurement of part features was undertaken to validate the models. From these measurements, one could estimate the deviation of the fixtures and subsequently, deviation of part volume based on part geometry and location from the fixtures. In addition to these models, heuristics required in fixture design in terms of its location and geometry is developed. The interaction between the surface roughness and the location of deviated contact plane was also described and modeled. Based on preliminary studies, the model was extended to 3D deviation with the constraint of constant part length. Finally, the methodology employed in determining the part deviation is presented.

References

1) Whitehouse, D.J., “Handbook of Surface Metrology”, CRC Press, 1994, ISBN-13: 978-0750300391

CHAPTER 5: RESULTS AND ANALYSIS

Introduction

This chapter is focused on validating the models developed in Chapter 4. The results of measured error are compared to the modeling maximum for fixture inaccuracies and corresponding part deviation. Also, analysis on selection of fixture geometry and AM-build orientations based on surface analysis is also provided. The interactions between part deviation and part-fixture geometry are also analyzed when the part is held between two centers with varying contact surfaces at each ends.

5.1. Fixture Deviation Analysis

This section details fixture inaccuracies and surface characteristics of the near-net shape AM parts measured using a CMM and laser profilometer as shown in Section 4.1 from Chapter 4.

5.1.1 Fixture Inaccuracy

The CMM measurements of the fixture geometry inaccuracies for sacrificial cylinder fixture geometry are shown in Table 3 showing the deviation of the maximum-minimum fixture diameter from the average diameter for 11 EBM built cylindrical features.

Table 3: Cylinder Form Inaccuracy

Filename	Average diameter	Maximum diameter	Minimum diameter	Maximum deviation	Minimum deviation
	mm	mm	mm	mm	mm
CT_13P	16.95	17.50	16.78	0.55	0.71
CT_12P	18.68	19.79	18.27	1.11	1.52
CT_19P	18.69	20.07	18.11	1.38	1.97
CT_4P	42.93	43.17	42.72	0.24	0.45
CT_8P	42.96	43.20	42.72	0.24	0.48
CT_2P	42.96	43.42	42.61	0.46	0.81
CT_16P	48.88	49.56	48.22	0.68	1.34
CT_11P	48.96	49.61	48.67	0.65	0.94
CT_1P	49.99	50.48	49.64	0.49	0.84
CT_10P	55.74	56.03	55.43	0.30	0.60
CT_3P	57.89	58.42	57.61	0.53	0.81

For the measured data of average diameter of EBM made cylinderical features, it was observed that the absolute deviation was always higher with the minimum contact plane from the nominal surface as shown in Figure 61. This could primarily be attributed to the non-unifom shrinkage that occurs during the EBM processing. Hence, to identify the ‘maximum deviation’ of the actual fixture coordinate system, $\mathbf{C_{Fix}}$ with respect to the $\mathbf{C_{CNC\text{-}RP}}$ we need to consider contact surfaces with the jaws at max-max-min contact deviation from the nominal plane in AIMS. It can be seen that positive (or over) deviation is greater than negative (or under) deviation. This is because when using contact-probe of CMM to quantify the deviations, the contact probe diameter (4mm in this study) could be larger to find sharp protrusions (positive deviations) than valleys (negative deivations).

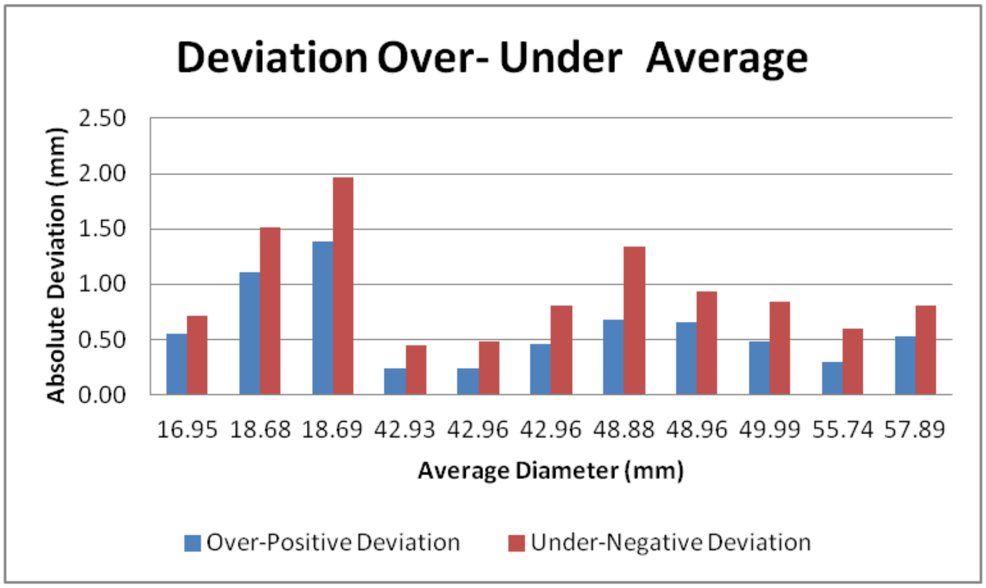

Figure 61: Maximum-Minimum Deviation

For the unit normal of each plane towards the center, each plane can be represented as $ax+by+cz+m$, where the planar equation refers to the nominal plane location. Similarly, the CMM measurement for tri-planar fixture geometry is shown in Table 4 referring to Figure 47, where the equations represent each plane.

Table 4: Fixture characterization of Tri-planar faces

Name	**Equation of plane1**	**Equation of plane 2**	**Equation of plane 3**	**Nominal diameter (mm)**
TT_14AP.csv	(0.01)x + (-1.00)y + (-0.00)z + (113.53)	(-0.87)x + (0.50)y + (0.01)z + (233.03)	(0.86)x + (0.50)y + (-0.00)z + (-415.12)	25.37
TT14A_H10_R10_S0.05.csv	(-0.03)x + (-1.00)y + (0.00)z + (139.17)	(-0.84)x + (0.53)y + (0.01)z + (203.28)	(0.88)x + (0.47)y + (-0.01)z + (-412.55)	15.16
TT14B_H10_R10_S0.05.csv	(0.88)x + (0.47)y + (0.01)z + (-396.06)	(-0.85)x + (0.52)y + (-0.01)z + (208.98)	(-0.03)x + (-1.00)y + (0.01)z + (141.59)	14.95
TT15_H10_R10_S0.05.csv	(0.77)x + (-0.64)y + (0.02)z + (-220.31)	(-0.94)x + (-0.35)y + (-0.00)z + (398.49)	(0.17)x + (0.99)y + (-0.02)z + (-266.52)	15.88
TT18_H10_R10_S0.05.csv	(-1.00)x + (0.03)y + (-0.02)z + (382.15)	(0.45)x + (-0.89)y + (-0.01)z + (-55.37)	(0.52)x + (0.85)y + (0.03)z + (-341.71)	16.76

Correspondlingly, the measured positive-over and negative-under deviation of the planes on the inscribed circle were determined based on the collected data and is presented in the following Table 5 and Figure 62. Similar to the observed deviations in measurements of the average diameter of cylinders (Figure 61), the positive deviation from average value is greater than negative deviation in the case of tri-planar faces.

Table 5: Plane Positive and Negative Deviation

Nominal Diameter (mm)	**Plane#1**		**Plane#2**		**Plane#3**		**Total Deviation**	
	Positive	**Negative**	**Positive**	**Negative**	**Positive**	**Negative**	**Over Nominal Deviation**	**Under Nominal Deviation**
25.37	0.07	0.05	0.11	0.07	0.16	0.04	0.34	0.16
15.16	0.12	0.11	0.20	0.16	0.30	0.18	0.61	0.44
14.95	0.15	0.11	0.26	0.21	0.27	0.20	0.68	0.52
15.88	0.16	0.09	0.21	0.17	0.22	0.16	0.58	0.41
16.76	0.15	0.10	0.16	0.21	0.38	0.21	0.70	0.53

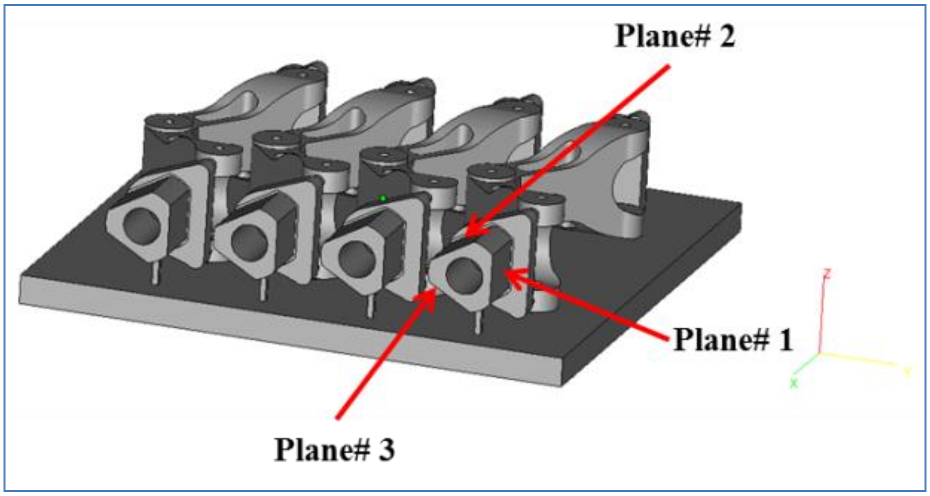

Figure 62: Maximum-Minimum Deviations- Plane# 3 and Plane#1

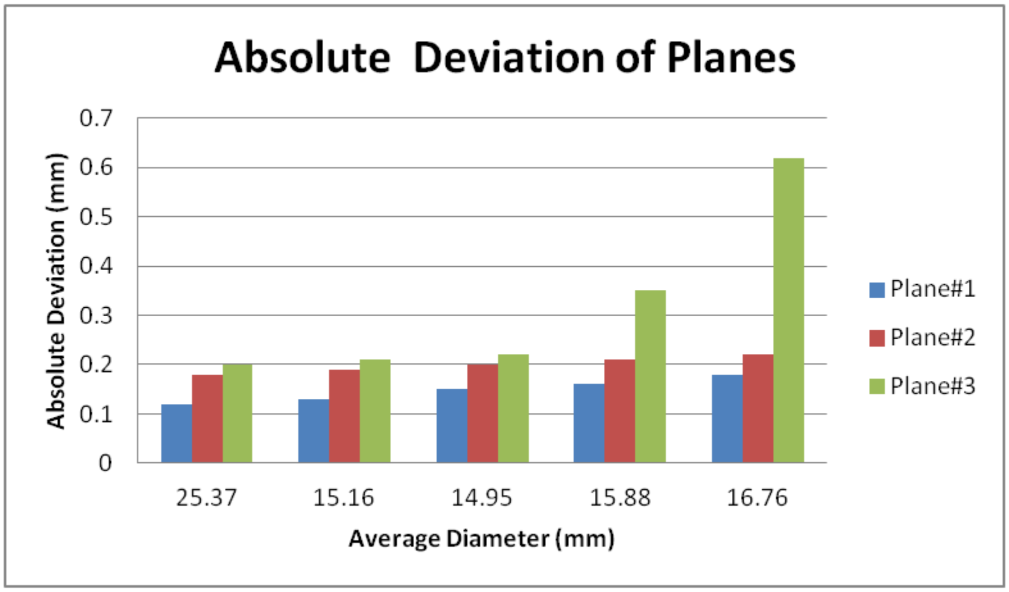

Figure 63: Total Absolute Deviation of the Planes

It can be derived that in order to capture the negative deviations, the probe diameter should be much smaller and/or other non-contact techniques could be applied. The total absolute deviation of each of the planes is represented in Figure 63.

It was found that the plane with minimum absolute deviation from the nominal surface was the plane #1 built along the build direction shown in Figure 64 and this is due to the absence of any wafer support material (plane #3) and staircase effects of subsequent layers (plane #2). On the contrary, the downward facing plane #3, which had wafer support attached prior to AIMS, has the maximum absolute deviation and could be attributed to the residual wafer support edges and presence of sintered metal powder on the surface. Hence, analysis on fixture deviation due to orientation in AM build envelope is performed for the two orientations shown in Figure 64 below. Based on the analysis, the location of the fixtures *i*, are re-oriented such that *i=1* is on the upward face and in the other case, has wafer supports attached to it being the downward facing surface.

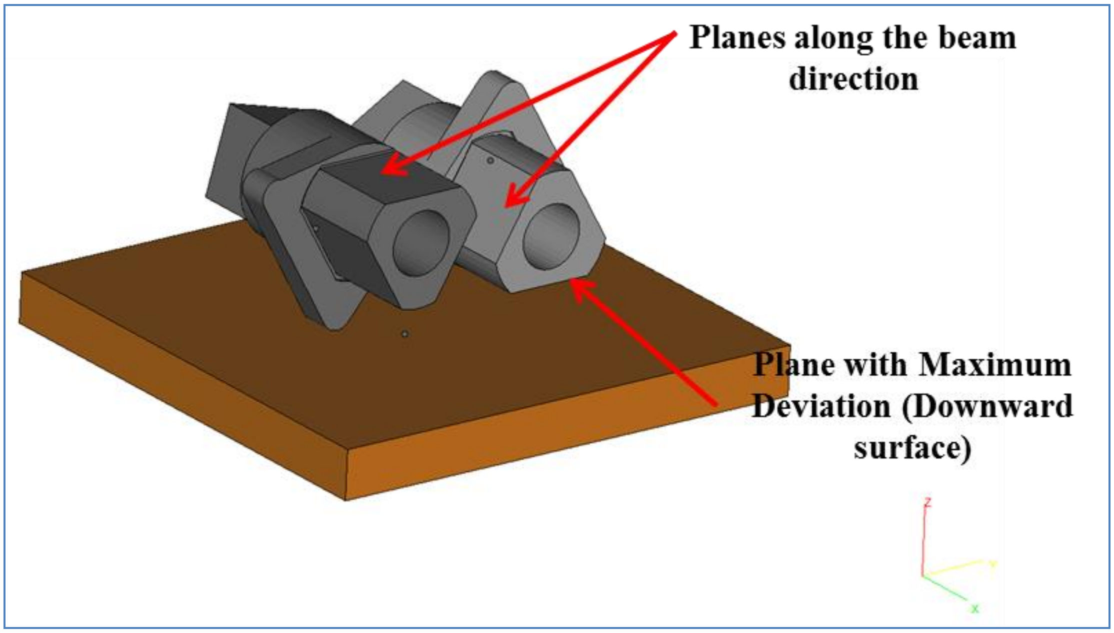
Planes along the beam direction
Plane with Maximum Deviation (Downward surface)
z
y
x

Figure 64: Reorientation of Tri-planes

5.1.2 Surface Characteristics

This section details the surface characteristics measure to determine the contact surface of the jaws with the contact surface. As detailed in the section 4.1.2, the following data were recorded from the characterization on the laser profilometer. Table 6 and Table 7 note the average separation distance for all the trials from the reference plane in the rough surface for tri-planar and cylindrical fixtures.

Table 6: Separation Distance of Tri-planar surfaces

Plane #1	Asperities (N)	Large Asperity Radius (mm)	Contact spots (n)	Real Contact Area (mm2)	Seperation Distance (mm)
1	18	0.05	4	0.0353	0.0563
2	17	0.03	3	0.0120	0.0425
3	15	0.04	3	0.0188	0.0500
4	14	0.03	2	0.0099	0.0525
Plane #2	**Asperities (N)**	**Large Asperity Radius (mm)**	**Contact spots (n)**	**Contact Area (mm2)**	**Seperation Distance (mm)**
1	16	0.07	3	0.0615	0.0933
2	16	0.07	2	0.0615	0.1400
3	15	0.07	3	0.0577	0.0875
4	16	0.06	3	0.0452	0.0800
Plane #3	**Asperities (N)**	**Large Asperity Radius (mm)**	**Contact spots (n)**	**Contact Area (mm2)**	**Seperation Distance (mm)**
1	18	0.12	4	0.2035	0.1350
2	17	0.09	3	0.1081	0.1275
3	19	0.08	5	0.0955	0.0760
4	22	0.09	4	0.1399	0.1238

Table 7: Separation Distance of Cylindrical fixture

Cylinder	Asperities (N)	Large Asperity Radius (mm)	Contact spots (n)	Contact Area (mm2)	Seperation Distance (mm)
1	10	0.08	5	0.0502	0.0400
2	11	0.04	3	0.0138	0.0367
3	10	0.05	4	0.0196	0.0313
4	14	0.09	4	0.0890	0.0788

The impact of surface deviations can be superimposed on the form inaccuracy of the fixtures using:

$$\varepsilon_{Fix-i} = \max \left| \text{Average}_{\text{Min-Max}} \right| + \text{Separation Distance } (D_i) \qquad (5.1)$$

Based on the average separation distance for each of the planes from the four trials, the maximum contact surface deviation can be superimposed on the three planes from the CMM studies resulting in the actual contact deviation as shown in Table 8 below.

Table 8: Total Deviation including Surface Roughness and Form Inaccuracy

Nominal Diameter (mm)	Plane#1		Plane#2		Plane#3		Total Deviation	
	Max1	Min1	Max2	Min2	Max3	Min3	Max Deviation	Min Deviation
25.37	0.07	0.05	0.11	0.07	0.16	0.04	0.34	0.16
15.16	0.12	0.11	0.20	0.16	0.30	0.18	0.61	0.44
14.95	0.15	0.11	0.26	0.21	0.27	0.20	0.68	0.52
15.88	0.16	0.09	0.21	0.17	0.22	0.16	0.58	0.41
16.76	0.15	0.10	0.16	0.21	0.38	0.21	0.70	0.53

In order to evaluate the proposed hypothesis that tri-planar surfaces have lesser feature deviation when compared to the cylinders of similar average diameters (15-18mm) the following Figure 65 is presented. It is proven that tri-planar surfaces have relatively lesser total contact surface deviation and variability when compared to cylindrical surfaces. Hence, in the case of AIMS it is preferred to incorporate tri-planar fixture design during the processing of CAD to minimize fixture deviation and subsequently, part deviation during machining.

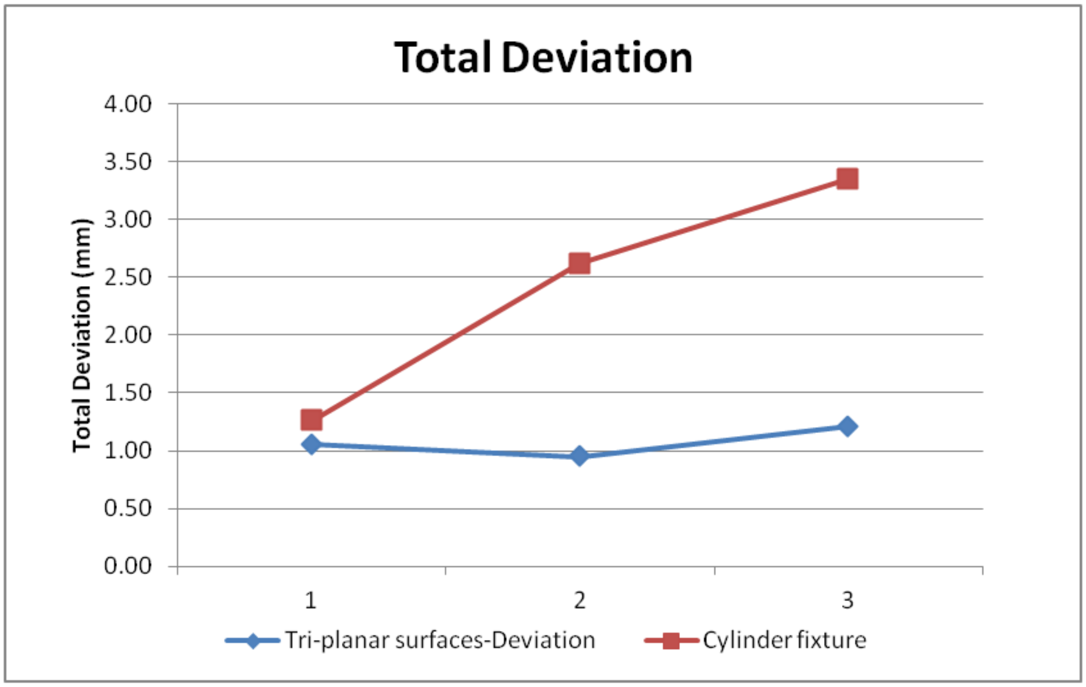

Figure 65: Total Deviation of the Fixture designs for average diameters of 15-18 mm.

5.2. Part Deviation Analysis

Since the average diameter of each measured cylinders and the tri-planar features vary, an alternative method is required to analyze the model. This includes measuring the average dimensions of one AM part (e.g. EBM) of the following functional part with assembly features which will be produced using the fixture design shown in Figure 66. In this analysis, a laser based DMLS AM and EBM process were used to create the fixture, characterize the corresponding accuracy of the features and determine the part feature deviations by varying the contact surface location (to simulate varying fixture deviations). The deviation of the part features were calculated using the fixture deviation-part datum models presented in Chapter 4.

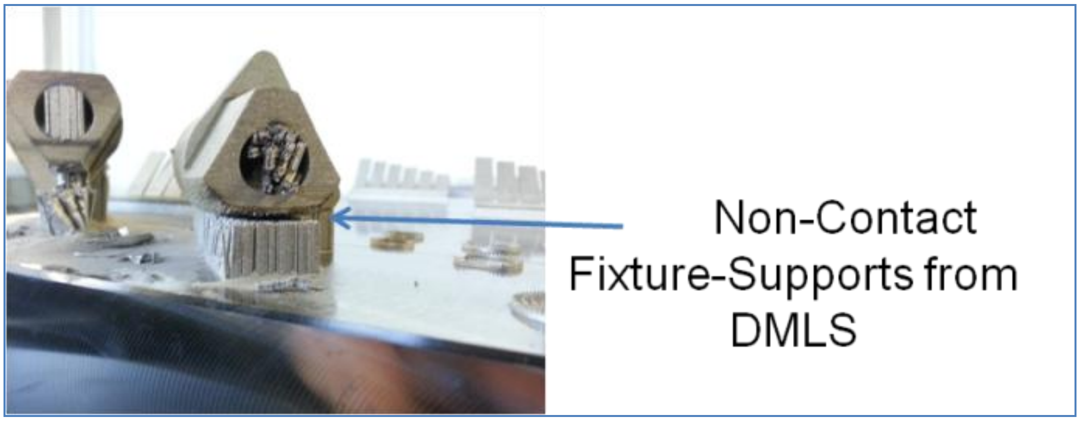
Non-Contact
Fixture-Supports from
DMLS

Figure 66: Downward Tri-plane Fixture Defects- DMLS

After evaluating the fixture deviations for the two different orientations as shown in Figure 67, the design with no downward facing tri-plane made of Ti64 in EBM was used. Only critical features that are of interest in this study are provided a tolerance.

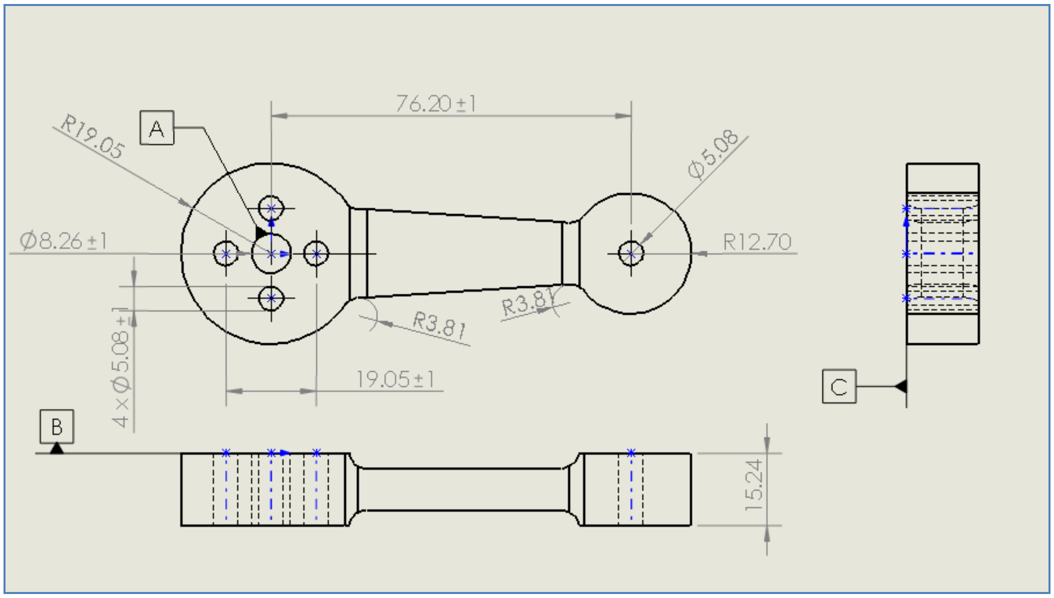
R19.05
A
76.20±1
Ø5.08
Ø8.26±1
R12.70
R3.81
R3.81
4×Ø5.08±1
19.05±1
B
C
15.24

Figure 67: Part Design for Validation

The nominal part features shown in Figure 67 were qualified using the AIM™ non-contact measurement system for the specified 6 cylindrical features. The AIM™ system enables the incorporation of analysis within a machining center using high speed measurement sensor such as laser, ultrasound sensors, eddy current sensor, etc. For this study, Keytence LK-H052 laser scanner with LK-G50010 controller was used to collect information on the features. It was mounted on a Renishaw PH10MQ indexing head which was controlled by PHC-10-2 controller. The entire set-up was mounted on to the spindle of a Miltronics VM-16 CNC machining center as shown in Figure 68.

The rationale for using a laser scanner is that it eliminates errors associated with using contact probe on a near-net AM surface which has deviations associated with the referencing surface. Using a laser scanner to establish the average dimensions enables us to analyze the impact of inducing known deviations at the fixture contact surfaces using shims. The resolution of the AIM™ is about 0.001” and has (patent-pending) synchronization and 3D alignment between sensors and NC position. The AIM™ system’s control box contains the timing circuit and signal cables which is interfaced to a computer network through Ethernet connection.

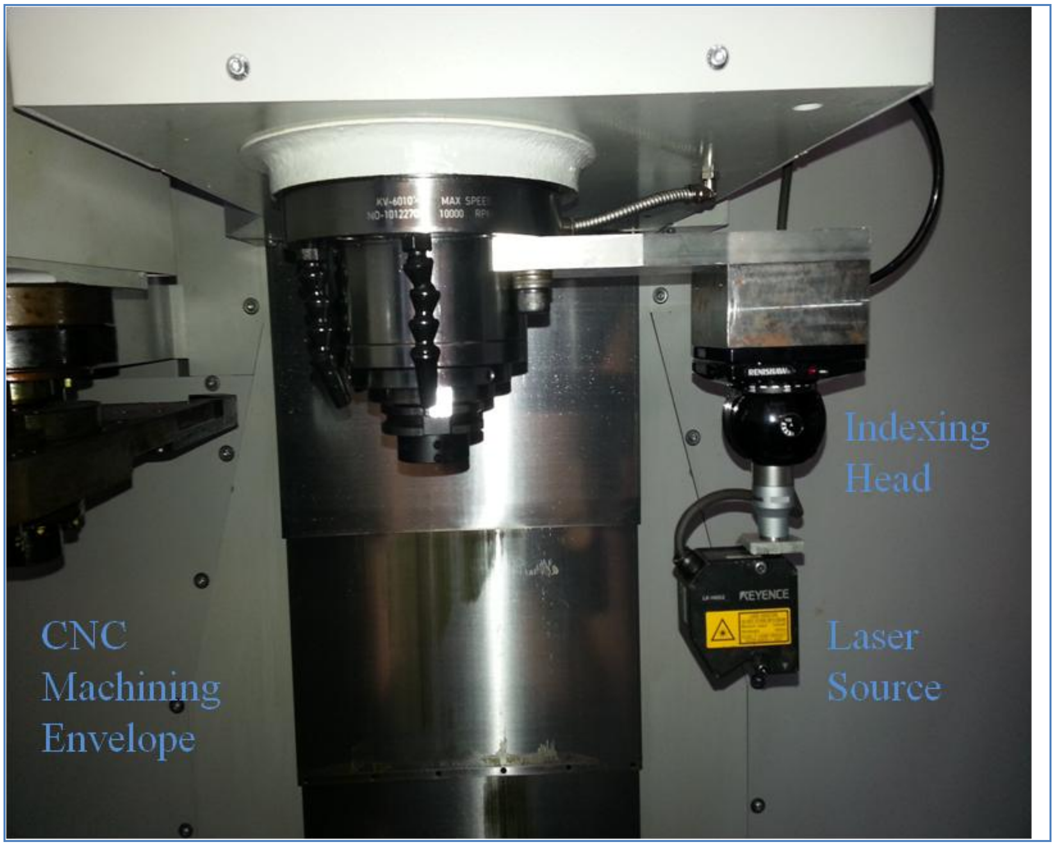

Figure 68: Non-Contact Scanner in CNC Machine

Custom fixtures with flat surfaces at an included angle of 60° that would be in contact with the faces of the tri-planar fixtures were created. NC toolpath was generated using SolidCAM to control the linear motions of the machine and 4th and 5th axis controls were used to control the rotations of the laser scanner. The CAD file used for the AM-process was used to create the toolpath, which had a machining allowance of 0.127 mm (0.005”). It is important to compensate for this machining allowance, since all the surfaces of the part were not machined. One of the set-ups with shims at only Center#2 is shown in Figure 69.

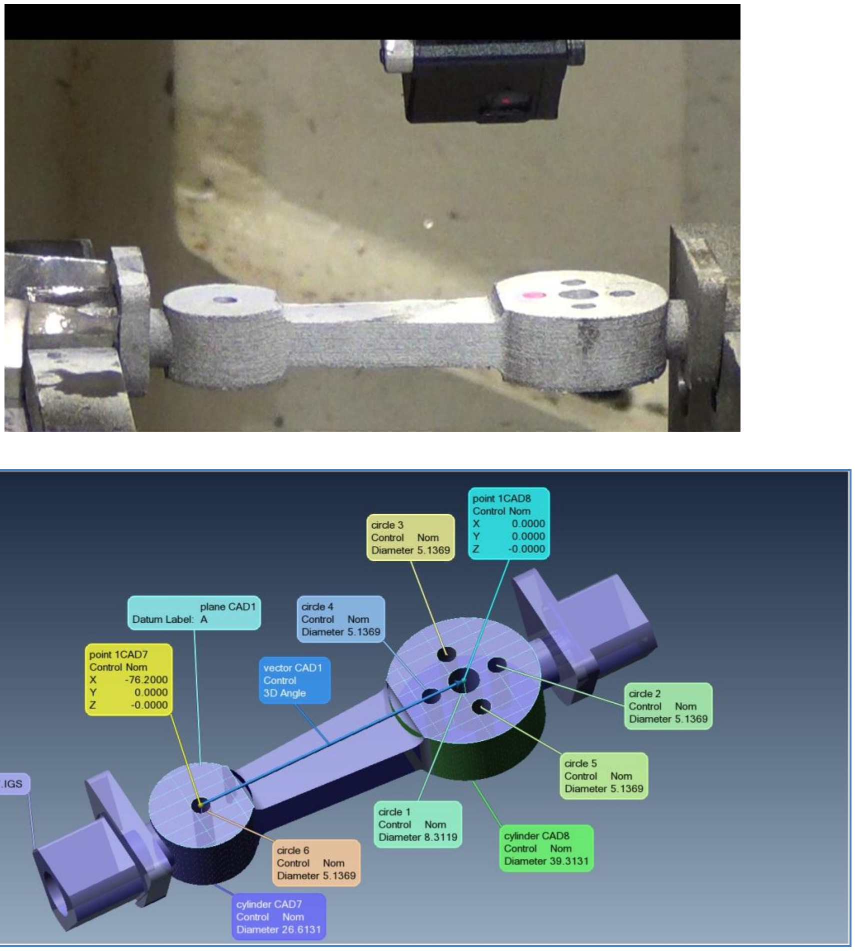
circle 3
Control Nom
Diameter 5.1369
point 1CAD8
Control Nom
X 0.0000
Y 0.0000
Z -0.0000
plane CAD1
Datum Label: A
circle 4
Control Nom
Diameter 5.1369
point 1CAD7
Control Nom
X -76.2000
Y 0.0000
Z -0.0000
vector CAD1
Control
3D Angle
circle 2
Control Nom
Diameter 5.1369
mc-validation80_M7.IGS
circle 5
Control Nom
Diameter 5.1369
circle 1
Control Nom
Diameter 8.3119
cylinder CAD8
Control Nom
Diameter 39.3131
circle 6
Control Nom
Diameter 5.1369
cylinder CAD7
Control Nom
Diameter 26.6131

Figure 69: AIMS Part Fixtured between Centers

The pre-machine hole diameters after scanning the nominal part is shown in Figure 70. The toolpath consists of continuously scanning the circumference of the cylinders at *z*-levels of 5 mm. The AIM™ system's synchronizes the toolpath with the collected information on the part location using the laser sensor. The scanning rate was about 2048 points/second at a feed rate of 3.048 m/min, which amounts to data collection every 0.0354 mm of linear travel (not accounting for acceleration and deceleration due to change in momentum during travel). Figure 69 shows the superimposed data on the original CAD file.

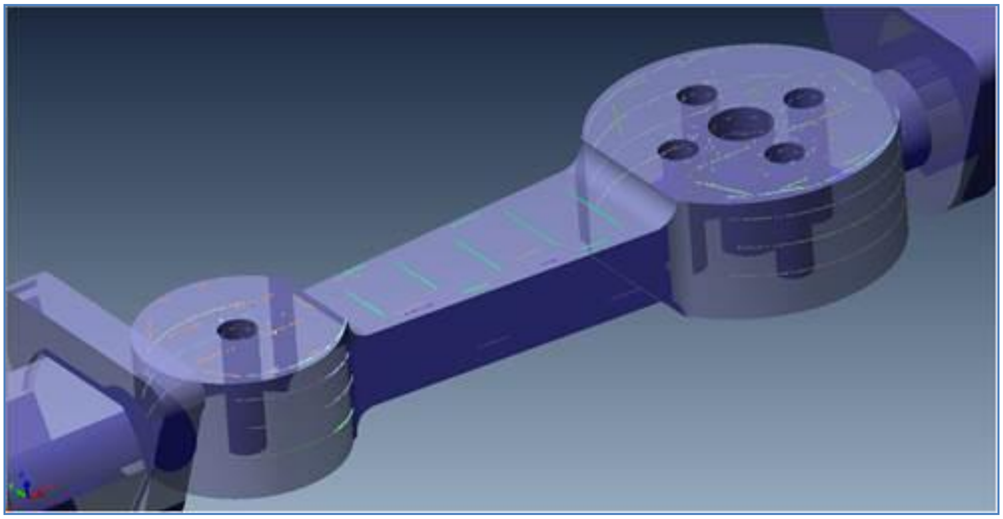

Figure 70: Toolpath superimposed on the CAD part

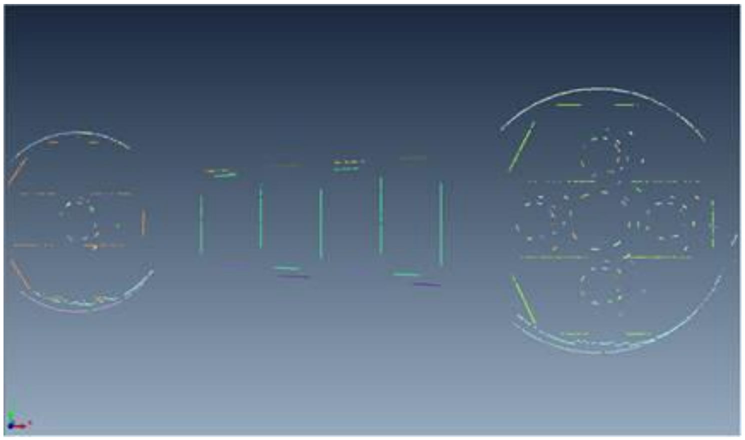

Figure 71: Raw Cloud Point from a Scan

An example of the raw cloud point data of the EBM part with machined critical features is shown in Figure 71. Point cloud engineering software tool of Innovometric Polyworks V10 was used to process the raw point cloud. Extraneous points that were located more than 2 mm from the features were manually removed.

For each of the six features, automated least-square fit was performed to determine feature location and dimensions. Then, to replicate CMM's 3-2-1, feature-based alignment was performed in Polyworks using the generated plane (Plane CAD1), line (Vector CAD1) and center of the feature 1 (Point 1CAD) shown in Figure 69. This does not compensate for the machining allowance not accounted for the alignment plane. The measurements for the nominal part are provided in Tables 9 and 10. The location of the centers of the critical features was in accordance with the datum (center of the larger critical feature) is shown in Figure 67. The measured nominal-target dimension was calibrated for the critical features and recorded in the following tables.

Table 9: Location of the centers for the nominal part

Deviations (mm)		Hole Centers Locations (mm)						
Center# 2	Center# 1	Point	X	ΔX	Y	ΔY	Z	ΔZ
Nominal	Nominal	10000-1	0.128	0.000	-0.070	0.000	0.000	0.000
		10000-2	9.710	0.000	-0.059	0.000	0.000	0.000
		10000-3	0.272	0.000	9.506	0.000	0.000	0.000
		10000-4	-9.270	0.000	0.006	0.000	0.000	0.000
		10000-5	0.206	0.000	-9.584	0.000	0.000	0.000
		10000-6	-75.604	0.000	0.129	0.000	0.000	0.000

Table 10: Measured diameters of the features

Deviations (mm)		Hole Diameters and Cylindricity		
Center# 2	Center# 1	Cylinder	Diameter	∆Diameter
Nominal	Nominal	10000-1	8.537	0.000
		10000-2	5.444	0.000
		10000-3	5.404	0.000
		10000-4	5.320	0.000
		10000-5	5.320	0.000
		10000-6	5.482	0.000

5.3. Estimation of Fixture Deviation

Following the notations provided in the Section 4.3. The major dimensions L, l_1, l_2, χ_1 and χ_2 are identified for the nominal part without any induced deviations at the fixtures. In this nominal part, there are no deviations at the fixtures and hence, the location of the other features with respect to the datum can be determined based on specifications.

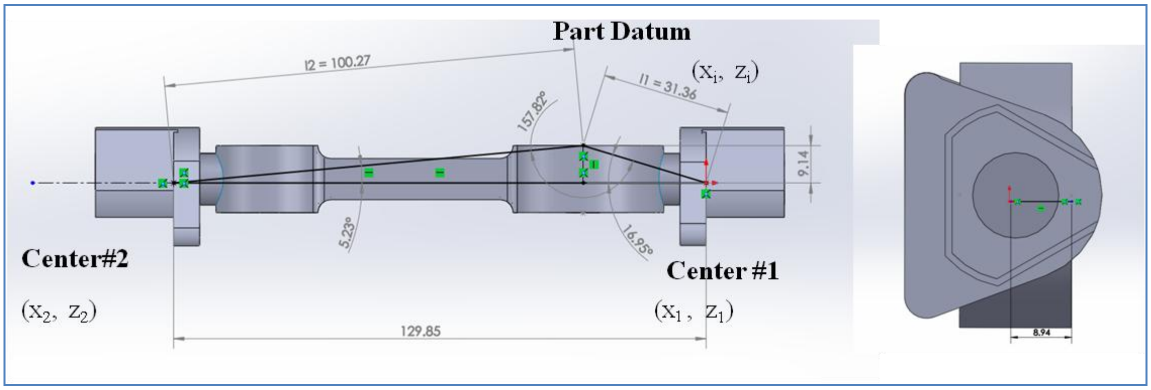

Figure 72: Location of the Datum w.r.to Fixtures

In the case of fixture deviations, prior to estimating the deviations for the identified features (#2-5), the location of the part datum feature#1 ($x_{i,}z_i$) needs to be determined. First, we estimate the variations of the fixture centers for different combinations of deviations caused at the fixtures using combinations of shims with thickness 0.254 mm and 0.508 mm (0.01” and 0.02” respectively). Given the build orientation of this part in EBM as shown in Figure 62, the total maximum deviation for the contact plane along *x*-axis is derived from the measurements presented in Table 5 for the nominal diameter of the fixture of 18 mm as 0.07 mm $(-\varepsilon_{xz-i}\ Cos\ \theta'_i)$.

Based on the equation 4.14, the deviations of the centers (y_{c-i} and z_{c-i}), will be calculated for the different combinations of deviations by similarly fitting a circle to the three contact points and identifying the center.

Table 11: Deviation of Fixture at Center#2

	Center#2 Contact Points						Deviated Center #2	
Deviations	**Plane# 1**		**Plane# 2**		**Plane# 3**		**y2'**	**z2'**
Center#2	y	z	y	z	y	z	mm	mm
0.508-0-0	0	9.508	-1.3878	-4.5	4.5	-1.3878	-0.1406	0.2659
0-0-0	0	9	-1.3878	-4.5	4.5	-1.3878	0	0
0.508-0.508-0	0	9.508	-1.46613	-4.754	4.5	-1.3878	-0.3898	0.163
0.254-0.508-0	0	9.254	-1.46613	-4.754	4.754	-1.3878	-0.048	0.0019
0.254-0.254-0	0	9.254	-1.42697	-4.627	4.5	-1.3878	-0.1928	0.0813
0.254-0-0	0	9.254	-1.3878	-4.5	4.5	-1.3878	-0.0703	0.1331

The set of random combinations of shim thickness used for center#2, the contact points for the contact surfaces with the fixture and corresponding location of the deviated center is shown in Table 11. Similar procedure was followed for the deviations of the fixture in center#1, with a different set of shim thickness combination and the results are shown in Table 12.

Table 12: Deviation of Fixture at Center#1

	Center#1 Contact Points						**Deviated Center #1**	
Deviations	**Plane# 1**		**Plane# 2**		**Plane# 3**		**y1'**	**z1'**
Center#1	y	z	y	z	y	z	mm	mm
0-0-0.508	0	9	-1.3878	-4.5	4.754	-1.46613	0.3048	0.0314
0-0.508-0.508	0	9	-1.46613	-4.754	4.754	-1.46613	0.0724	0.1369
0-0.508-0.508	0	9	-1.46613	-4.754	4.754	-1.46613	0.0724	0.1369
0-0-0	0	9	-1.3878	-4.5	4.5	-1.3878	0	0
0.508-0.508-0	0	9	-1.46613	-4.754	4.5	-1.3878	-0.2393	0.1037
0-0-0	0	9	-1.3878	-4.5	4.627	-1.42697	0	0

5.4. Estimation of Part Datum Deviation

Following the estimation of fixture location deviations, part datum deviation can be calculated from the procedure outlined in Section 4.3. Based on Eq. 4.22 - 4.33, and for sets of shim deviations experiments for different fixture deviations (x_{c-i}', y_{c-i}' z_{c-i}') the deviation of datum locations can be determined. For instance, for the third set of deviations in both centers#1 and 2, the quadratic equations can be re-written as:

$$(x_i' - 0.07)^2 + (z_i' - 0.1369')^2 = 31.36^2 \text{ mm} \tag{5.2}$$

$$(x_i' - 129.92)^2 + (z_i' - 0.1630')^2 = 100.27^2 \text{ mm} \tag{5.3}$$

In this case, x_i'= 30.0696 mm, and we know from Figure 72, x_i= 30.00 mm. Hence, the deviation is 0.0696 mm and including the machining allowance (0.127 mm), Δx_i'=0.1966.

Similarly, from y_i'= 8.94 mm and z_i'= 9.14 and using Eq. 4.18, along with the machining allowance:

$\Delta y'_i$ = 0.0724 * cos (90-16.95+ 0.127= 0.1482 mm and

$$\Delta z'_i = 0.1369 * \text{Sin } (90\text{-}16.95) + 0.0.127 = 0.2581 \text{ mm}$$

A summary of the estimation of fixture location deviations, part datum deviation is shown in Table 13:

Table 13: Estimation Part Datum Location Deviation

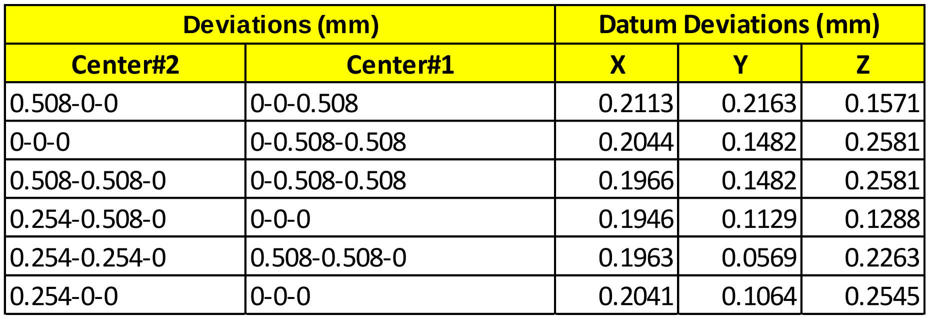

Deviations (mm)		**Datum Deviations (mm)**		
Center#2	**Center#1**	**X**	**Y**	**Z**
0.508-0-0	0-0-0.508	0.2113	0.2163	0.1571
0-0-0	0-0.508-0.508	0.2044	0.1482	0.2581
0.508-0.508-0	0-0.508-0.508	0.1966	0.1482	0.2581
0.254-0.508-0	0-0-0	0.1946	0.1129	0.1288
0.254-0.254-0	0.508-0.508-0	0.1963	0.0569	0.2263
0.254-0-0	0-0-0	0.2041	0.1064	0.2545

5.5. Analysis

The summary of measured deviation from scanning is shown in Table 14 below.

Table 14: Measured Datum Location (10000-1)

Deviations (mm)		Hole Diameters and Cylindricity			
Center# 2	Center# 1	Cylinder	Diameter	ΔDiameter	Cylindricity
Average	Average	10000-1	8.537	0.000	0.213
		10000-2	5.444	0.000	0.218
		10000-3	5.404	0.000	0.275
		10000-4	5.320	0.000	0.264
		10000-5	5.320	0.000	0.267
		10000-6	5.482	0.000	0.284
0.508-0-0	0-0-0.508	10001-1	8.471	-0.066	0.174
		10001-2	5.345	-0.099	0.205
		10001-3	5.332	-0.072	0.253
		10001-4	5.266	-0.054	0.189
		10001-5	5.240	-0.080	0.142
		10001-6	5.305	-0.177	0.206
0-0-0	0-0.508-0.508	10002-1	8.461	-0.076	0.194
		10002-2	5.335	-0.109	0.222
		10002-3	5.417	0.013	0.330
		10002-4	5.263	-0.057	0.169
		10002-5	5.232	-0.088	0.155
		10002-6	5.358	-0.124	0.366
0.508-0.508-0	0-0.508-0.508	10003-1	8.450	-0.087	0.215
		10003-2	5.316	-0.128	0.203
		10003-3	5.320	-0.084	0.281
		10003-4	5.255	-0.065	0.186
		10003-5	5.221	-0.099	0.182
		10003-6	5.303	-0.179	0.321
0.254-0.508-0	0-0-0	10004-1	8.478	-0.059	0.189
		10004-2	5.383	-0.061	0.232
		10004-3	5.373	-0.031	0.258
		10004-4	5.276	-0.044	0.198
		10004-5	5.268	-0.052	0.204
		10004-6	5.284	-0.198	0.236
0.254-0-0	0.508-0.508-0	10005-1	8.446	-0.091	0.184
		10005-2	5.314	-0.130	0.222
		10005-3	5.303	-0.101	0.342
		10005-4	5.260	-0.060	0.209
		10005-5	5.213	-0.107	0.197
		10005-6	5.303	-0.179	0.238
0.254-0.254-0	0-0-0	10006-1	8.442	-0.095	0.170
		10006-2	5.347	-0.097	0.231
		10006-3	5.328	-0.076	0.252
		10006-4	5.261	-0.059	0.192
		10006-5	5.260	-0.060	0.155
		10006-6	5.285	-0.197	0.425

The error in estimation of the datum deviation with respect to the fixture deviations are shown in Table 15 below:

Table 15: Estimation Error

Deviations (mm)		Error in Estimation(mm)		
Center#2	Center#1	X	Y	Z
0.508-0-0	0-0-0.508	0.0603	-0.0877	-0.5099
0-0-0	0-0.508-0.508	0.1104	-0.1018	-0.5619
0.508-0.508-0	0-0.508-0.508	-0.0914	-0.1448	-0.9019
0.254-0.508-0	0-0-0	-0.0304	-0.1021	-0.0602
0.254-0.254-0	0.508-0.508-0	0.1833	-0.4561	-0.9597
0.254-0-0	0-0-0	-0.0319	-0.0266	0.0495

The accuracy of the scanning system is about 0.0508 mm (± 0.001”), hence accounting for that, actual error can be computed as:

Table 16: Actual Error

Deviations (mm)		Error in Estimation(mm)		
Center#2	Center#1	X	Y	Z
0.508-0-0	0-0-0.508	0.0095	-0.1385	-0.5607
0-0-0	0-0.508-0.508	0.3746	-0.1526	-0.6127
0.508-0.508-0	0-0.508-0.508	-0.1422	-0.1956	-0.9527
0.254-0.508-0	0-0-0	-0.0812	-0.1529	-0.1110
0.254-0.254-0	0.508-0.508-0	0.1325	-0.5069	-1.0105
0.254-0-0	0-0-0	-0.0827	-0.0774	-0.0013

Summary

In this chapter, a series of experiments where undertaken to demonstrate how the as-built part datum accuracy compares to the analytically derived models.

The part fixture deviations and surface characteristics models were analyzed. The part was demonstrated for different location errors at either centers associated with fixturing from features with size tolerances of about 1 mm. Each part was located twelve times in the fixtures with known fixturing deviations to calculate the part datum locations.

It was found that there is significantly more fixturing error associated with the circular fixture design. Also, it was analyzed that the orientation of the fixture during AM build is very important in minimizing the overall part deviation during the finishing stage. Based on the analysis, this was tested using two independent processes and it was validated that fixturing errors are minimal when there are no downward facing surfaces in the fixture design. Further, a mechanical part with assembly specifications was analyzed for the optimal fixture orientation.

The developed model which identifies the datum deviation can be used to estimate the part features deviation for other part designs. In this study, deterministic approach was pursued by causing known deviations on a near-net surface. In the future, recording of large samples of fixture surface roughness and size accuracy ‘as-built’ based on the build orientation will enable determine the variance associated with the appropriate AM process. This can be incorporated into the model to predict the deviation of datum location based on each part design. A logical next step would be to incorporate desired machining allowance and/or pass to the part feature deviations. In conclusion, this study demonstrated an analytical model to determine a part datum -feature deviation based on deterministic deviations at the jaw-contact surfaces. This model can be used to include variance associated with the fixturing surface and it could minimize the amount of part deviation and associated machining allowance.

CHAPTER 6: AIMS PERFORMANCE METRICS

Introduction

In this chapter, the economics of hybrid manufacturing will be addressed. Specifically, AIMS performance in terms of production time, cost and material utilization is studied. Cost models are developed for processing of low volume batch production (1-4) through AIMS and true CNC-RP. In this case, the cost model for AIMS is employed using EBM as the AM component; however, other AM processes can be easily adapted e.x. DMLS and SLM. For generality, conventional manufacturing processes which require custom fixturing and tooling are not analyzed since fixture development cost can be so variable. Also, AIMS and CNC-RP provide the same final process performance (machining accuracy and finish) and neither process requires custom tooling, again a highly variable cost component.

The impact of cost components and AM-based process constraints namely, 'part overgrowth' due to fixturing deviations as detailed in previous chapters are studied through sensitivity analysis. Finally, brief discussions on major criteria that impact the overall AIMS performance metrics of unit cost are also listed. One major component of hybrid manufacturing that is NOT addressed here is that of design for AM or hybrid. Recently, a focus has been reported where mechanical designs can be significantly improved (mechanical strength) by using geometric shape features that have been difficult or impossible to produce using traditional manufacturing methods.

These new designs use less material and require less time on an AM process than tradition geometric shapes. We will not consider this aspect of engineering design for hybrid manufacturing, but will note that when this is properly applied, it will skew the economics more in favor of AM produced parts.

6.1. Metrics Model

The following section describes the economic models to evaluate unit cost and manufacturing time as function of part and support volume for the following systems:

(1) Subtractive Manufacturing- CNC-RP

(2) Hybrid Manufacturing AIMS-

  a. Additive Manufacturing-EBM

  b. CNC-RP (finishing)

The development of the cost model consists of material and manufacturing cost (including setup and tool costs) components. The time for preparation of process parameters in terms of NC codes (CNC-RP) and additive manufacturing process files are approximately the same (and small < 60 minutes) and hence, engineering cost is not included in the model. However, in highly complex geometries it is recommended to include this cost. The cost model is material and activity-based, and the notations for all the major cost factors detailed in Table 10.

In order to develop the cost model, the following nomenclatures are used to develop a mathematical model for AIMS (using EBM) and CNC-RP is presented in Table 17.

Table 17: Nomenclature for cost models for additive, subtractive and hybrid processes

Major Notations	**Unit**	**Comments**
General factors		
C_{unit}	\$	Cost per unit
Pv	mm^3	Part volume
SPv	mm^3	Support volume- sacrificial supports
$C_{process}$	\$/hr	Operating cost for each process
C_{mat}	\$	Cost of material in each process
t_{build}	hr	Time to fabricate the part in additive process
$t_{setup\_process}$	hr	Setup time in each process
$t_{post\_process}$	hr	Post-processing time in each process
CNC-RP specific factors		
Sv	mm^3	Volume of bar stock
t_{hog}	hr	Time for hogging operation
t_{rough}	hr	Time for roughing operation
t_{finish}	hr	Time for finishing operation
t_{tool_life}	hr	Cutting tool life duration
t_{tool_change}	hr	Time for changing tool and tool set-up time
ΔV	mm^3	Total volume removed at each stage in CNC-RP
MRR	mm^3/hr	Material Removal Rate at each stage in CNC-RP
$C_{tooling}$	\$/tool	Cost of cutting tools
nt	--	Number of tool changes in each stage
$C_{tooling}$	\$/tool	Cost of cutting tools
EBM specific factors		
n_{EBM}	--	Number of layers in EBM fabrication
ρ	kg/mm^3	Density of metal powder used
t_{EBM}	hr	Total build time in EBM
t_{plate}	hr	Time to preheat the start plate to required temperature before fabrication
t_{cool}	hr	Time to cool the build volume, retrieve part and recycle unused powder

6.2. Additive Manufacturing Model

In the case of additive manufacturing, unit cost can be simplified as a function of set-up time, part height (i.e., number of layers), summation of cross-sectional area of each layer and post-processing time. Hence, in a part with *n* layers, where t_{build_i} is the build time for layers $i = 1, 2, \ldots$ n, the total manufacturing time and unit cost are formulated as:

$$C_{unit} = C_{material} + (C_{add} \times t_{add}) \tag{6.1}$$

$$t_{add} = t_{setup\_add} + \sum_{i=1}^{n} \left(t_{build\_i}\right) + t_{post\_proce} \tag{6.2}$$

The generic model provided can be adapted to many layer by layer manufacturing methods depending on individual cost components in each layer (e.g. different part and support generation parameters) and corresponding setup and post-processing time such as sintering. In the following sections, this model is extended to two specific systems: CNC-RP and EBM-CNC-RP hybrid process.

6.3 CNC-RP Cost Model

In the case of CNC-RP, the manufacturing cost is a function of; cost of the stock, total machining time and the tooling cost. The machining time is determined from the total volume of metal to be removed from the stock (ΔV) for a given metal removal rate (MRR), i.e. $\Delta V/MRR$. Further, based on tool geometry, feed rates and depth of cut the metal removal rate will vary in hogging, roughing and finishing stages. The setup time ($t_{setup\_CNC\text{-}RP}$) is assumed to be uniform irrespective of the part volume (because the stock is fixtured across two chucks). Further, the material cost (S_v – Stock volume) is based on part orientation (cylinder with minimum diameter equal to diagonal of part).

The post-processing step in CNC-RP is the removal of sacrificial supports which takes negligible time and is not considered in the cost model derived from equations 6.1- 6.2 as shown below:

$$C_{unit} = (S_v \times C_{mat\_CNC-RP}) + (C_{CNC-RP} \times t_{CNC-RP}) + (C_{tooling} \times n_{stage}) \tag{6.3}$$

$$t_{CNC-RP} = t_{setup\_CNC-RP} + t_{hog} + t_{rough} + t_{finish} \tag{6.4}$$

$$nt = \frac{(\Delta V)}{MRR} \times \left(\frac{1}{t_{tool\_life}}\right) \tag{6.5}$$

$$t_{stage} = \frac{(\Delta V)}{MRR} + (nt \times t_{tool\_change}) \tag{6.6}$$

At every ‘stage’ of CNC-RP (hogging, roughing and finishing) there are two time components namely; machining time and tool change operations equations 6.5-6.6. Subsequently, the unit cost of CNC-RP made part as shown in equation 6.3 is derived from manufacturing time equation 6.4, material cost and tooling cost.

6.4 AIMS Cost Model

The developed hybrid process has two steps: EBM and the ‘finishing’ stage of CNC-RP. First, a cost model for EBM is developed by integrating EBM-specific process steps for the total build time in equation 6.2.

$$\sum_{i=1}^{n} (t_{build\_i}) = t_{plate} + t_{raking} + t_{preheating} + t_{melt\_i} + t_{support\_i} + t_{postheating} \tag{6.7}$$

In this process parameter based cost model, the total build time as shown in equation 6.7 is further expanded to differentiate individual operations in each layer *i* namely; preheating of the plate, raking of the metal powder, preheating the powder bed, melting the contour (or edges) and part volume, support structures and finally, post-melting scan. Constant plate preheating, raking, preheating and post-heating durations are assumed.

For each layer *i*, the melting and support generation time are formulated based on EBM process parameters as shown below in equations 6.9-6.10.

$$t_{mel\_i} = \sum_{i=1}^{n} \left(\frac{Contour\ scan\ length}{Contour\ Speed}\right) + \sum_{i=1}^{n} \left(\frac{Melt\ scan\ length}{Melt\ Speed}\right) \tag{6.9}$$

$$t_{support\_i} = \sum_{i=1}^{n} \left(\frac{Support\ scan\ length}{Support\ Speed}\right) \tag{6.10}$$

In the case of EBM, the post-processing involves cooling down of the build chamber, part retrieval and recovery/recycling of unused powder. Hence, the overall cost-time of EBM component in this hybrid process is defined as:

$$t_{EBM} = t_{setup\_EBM} + \sum_{i=1}^{n} \left(t_{build\_i}\right) + t_{cool} \tag{6.11}$$

$$C'_{EBM} = (\eta \times (P_v + SP_v) \times \rho \times C_{kg}) + (C_{EBM} \times t_{EBM}) \tag{6.12}$$

Unlike complete CNC-RP, the subtractive stage of the hybrid system consists only of finishing stage. Since the sacrificial fixtures used in subtractive stage are considered as ‘EBM-made part volume’, there is no additional material cost associated with the subtractive stage.

The ‘near net’ part from EBM is the stock volume and hence the cost-time CNC-RP component in this hybrid process is defined as:

$$C_{Hybrid} = \left(C_{CNC-RP} \times \left(t_{setup\_CNC-RP} + t_{finish}\right)\right) + \left(C_{tooling} \times n_{finish}\right) + C'_{EBM} \qquad (6.13)$$

6.5. Case Study

The cost models are analyzed using a case study of the example part shown in Figures 73 and 74. The unit cost and time are determined for manufacturing the case study part through CNC-RP and AIMS.

Also, the impact of low-volume batch production is investigated. The material selected for this study is Ti64, which is representative of metal alloys processed through additive methods. The part geometry selected in this study is typical of an additive manufacturing part and when processed through traditional machining would require multiple refixturings.

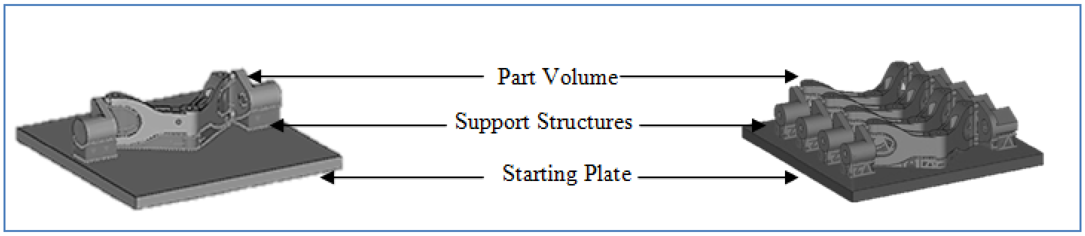

Figure 73: Unit and batch production of sample part in EBM

For the process variables for CNC-RP, it was assumed that the operating cost was $ 25/hr with stock setup time of 10 minutes and tool change of 10 minutes including qualification of tool length.

The cutting tool is assumed to be four flute carbide flat end mills with diameters of 25.40 mm, 6.35 mm and 3.18 mm for hogging, roughing and finishing respectively. The machining parameters were estimated for the surface speed of 508 mm/s with chip load of 0.05 mm in the case of hogging and roughing and 0.03 mm in the case of finishing. The layer thickness (depth of cut) considered were 5.08 mm, 0.51 mm and 0.127mm in the case of hogging, roughing and finishing operation respectively. The stock volume for this study was a cylinder with a diameter of 63.50 mm and a length of 203.20 mm and valued at $ 400 per bar. The average tool life was assumed to be 100 minutes of machining time and tooling cost of $20/tool.

In the case of EBM, the operating cost was estimated at $ 104/hr and the layer thickness used was 0.07 mm. The setup time in EBM including pumping the pressure in the build chamber down to the appropriate vacuum level and preheating the EBM plate was assessed as 90 minutes. The cost of the EBM powder used was $ 300/kg and a 5 % loss in powder during handing was also considered. Figure 74 shows the build slices (a) and an individual layer (b). Individual layer showing the support and melt features. Constant beam speed conditions throughout melting and support generation are assumed in this study, although it is recognized that in reality the EBM adapts the beam speed throughout the process.

However, the proposed model can be used for varying process condition to replicate the exact physical build conditions across each layer. In this experiment, multi-spot Arcam A2 was used and the effective contour speed was 17.18 mm/s and support speed was 50 mm/s. In the case of melting, the beam overlap of 0.20 mm was used and hence the effective beam travel distance per unit is defined by total melt area per overlap. Constant raking duration per layer (10 seconds), preheating (12.5 seconds) and post-heating duration (12.5 seconds) per layer are assumed. During this experiment, the melt beam speed used was 500 mm/s and total number of layers was 528. The total cooling time for the build and part retrieval was estimated at 1200 minutes.

In the analyzed caste study, the total melt area of a unit part was calculated as 152,255mm^2 and the total contour distance was found to be 21,605 mm. In the case of support structures, the total support distance were calculated as 7,766 mm.

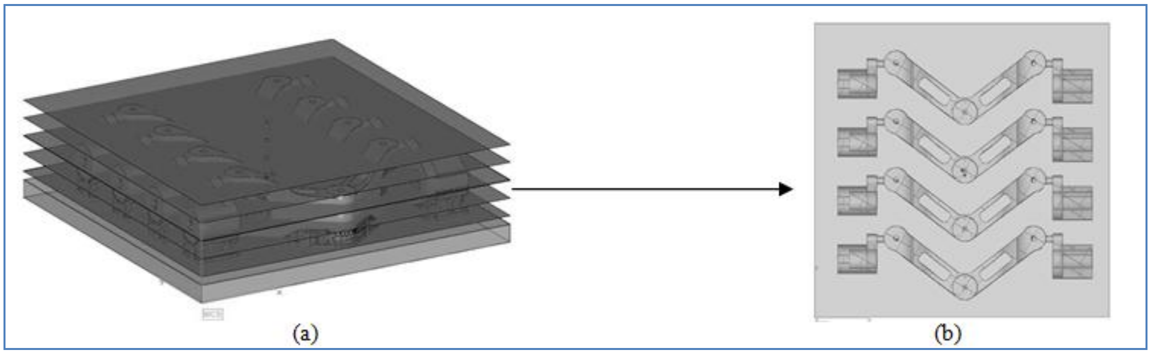

Figure 74: (a) EBM build slices and (b) Individual layers

During batch production using CNC-RP, the process plan is repeated according to the batch size since stock is replaced after each run. In contrast, the number of parts in a single build can be increased in additive processes subject to build envelope restrictions as shown in Figure 74. In such batch runs using EBM, the processing time for set-up, plate pre-heating, raking, layer pre-heating and post-heating does not change.

However, the layer processing time varies based on the area and perimeter of the cross-sectional geometry of each layer. Therefore, the hybrid system could benefit from batch production in additive stage in some cases followed by ‘finishing’ operation of every ‘unit’ in the batch separately in repeated CNC-RP operation.To summarize this study, in order to compare CNC-RP and AIMS, individual batch sizes of 1, 2, 3 and 4 are considered in this study. Referring to equation 6.3, the independent variables associated with CNC-RP are material cost, machining time and cutting tool cost. In the case of EBM-based AIMS referring to equation 6.3, the independent variables associated with AIMS are material cost, production time and cutting tool cost.

6.6 Results

In CNC-RP, the hogging-roughing and finishing stages for the CNC machining parameters for Ti-6Al-4V resulted in the processing time and cost shown in Table 18.

Table 18: Breakdown of CNC-RP operation and tooling cost

CNC-RP stage	**Setup time (hrs)**	**Machining time (hrs)**	**Number of tool changes**	**Tooling cost ($)**	**Tool change time (hrs)**	**Stage time (hrs)**	**Operating cost ($)**	**Total cost including material ($)**
Roughing and Hogging	0.17	14.04	8	160	1.33	15.37	417.50	1358.25
Finishing		9.38	5	100	0.83	10.21	276.00	
Total CNC-RP	0.17	23.42	13	260	2.17	25.59	698.25	

In the case of CNC-RP, lower material removal rate contributes to higher machining time. This is representative of machinability of alloys used in aerospace applications such as Ti-6Al-4V and superalloys such as Inconel 625. Such alloys have desired high temperature strength when compared to other metals with superior machinability such as Aluminum alloys and Stainless Steel. These alloys are also extremely difficult to machine, which leads to higher tool wear resulting in consumption of multiple cutting tools. In addition, the cost of stock for those alloys is significantly higher than other commonly used material such as Aluminum, Stainless Steel and Brass. In the case of batch production through CNC-RP process, the unit price remains the same because the process is repeated for each stock. In the case of additive stage of EBM in hybrid process, the unit price varies as shown in the following Table 19 for unit and batch production. It can be observed that increasing batch size reduces the unit cost.

This can be attributed to the significant amount of time required in EBM for cool-down and part retrieval. The material cost of alloys used in EBM (and other AM processes) is often greater than wrought stock due to preparation of material through atomization, etc.

Table 19: EBM cost-component in unit and batch production

Batch Size	**Setup-Plate time**	**Build time**	**Cool time**	**Total time**	**Material cost**	**Total cost**	**Unit cost**
	(hrs)	**(hrs)**	**(hrs)**	**(hrs)**	**($)**	**($)**	**($)**
1	1.50	6.53	20.00	28.03	104.23	3019.54	3019.54
2	1.50	12.48	20.00	33.98	138.97	3672.93	1836.47
3	1.50	18.43	20.00	39.93	185.30	4337.91	1445.97
4	1.50	24.38	20.00	45.88	247.07	5018.32	1254.58

The hybrid process results as shown in Table 20 includes the setup of ‘near-net’ part in CNC-RP, finish machining and tool change time and costs

Table 20: Hybrid process unit and batch production

Batch Size	**Hybrid Process**						
	EBM stage			**CNC-RP**		**Total Cost ($)**	**Unit Cost ($)**
	Time (hrs)	**Material Cost ($)**	**EBM Cost ($)**	**Time (hrs)**	**CNC-RP Cost ($)**		
1	28.03	104.23	3,019.54	10.38	359.50	3,483.27	3,483.27
2	33.98	138.97	3,672.93	20.76	619.00	4,430.90	2,215.45
3	39.93	185.30	4,337.91	31.14	878.50	5,401.71	1,800.57
4	45.88	247.07	5,018.32	41.52	1,138.00	6,403.39	1,600.85

From Figure 75, it is recognized that the batch size does not impact the unit cost when producing a part only through CNC-RP (including hogging and roughing).

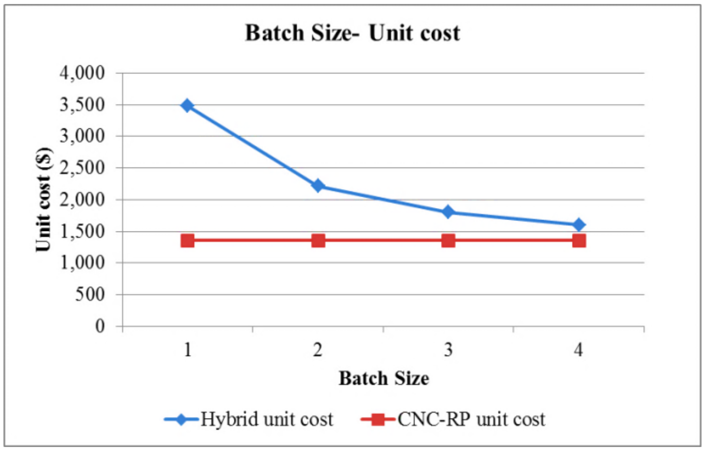

Figure 75: Unit cost through batch production in CNC-RP and Hybrid process- AIMS

From Table 20, it is evident that the capability to fabricate in batches can reduce the unit cost in the EBM stage in this example. This is primarily due to the time involved in raking, preheating and post-heating in each layer and importantly, the cool down time as shown in Figure 76.

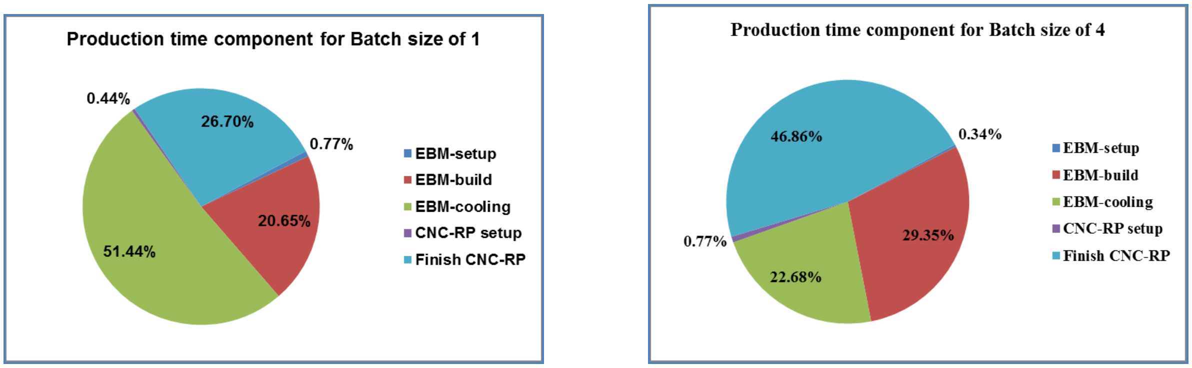

Figure 76: Time Components in the AIMS production based on batch size

By increasing the number of parts that can be accommodated in the AM build, the significant cooling time is amortized across the units in the batch.

6.7 Sensitivity Analysis- Influence of Cost Components

The following sensitivity analysis studies the major factors based on the case study in order to evaluate the impact of the cost components. The variables include; cost of material, operating cost, machining allowance, material removal rate-MRR ratio and AM production time. The cost of material varies significantly in EBM (and other AM) based on the alloys such as Ti-6Al-4V, Inconel, etc. and also, the method and quantity of production through atomization. In the case of CNC-RP, the cost of machining stock also varies significantly based on the material such as Aluminum and Ti-6Al-4V. The amount of total material removed during finishing operation is based on two factors namely; Part deviation (Referring to Chapters 4 and 5 in the case of AIMS) and the material that is being processed. Higher part deviation in AIMS due to fixture inaccuracies and surface characteristics require greater part overgrowth to successfully produce the part.

Machinability is an important factor for the unit cost, since selection of machining parameters can vary based on the material (Aluminum, Ti-6-Al-4V), available cutting tools (High speed steel, coated carbides) and machine tool. The physical properties of the material being processed influences the recommended depths of cut for finishing operation and the material removal rate for desired surface finish. It should be noted that the MRR ratio is with respect to the previous study. Hence, lower the ratio, greater the MRR when compared to the case study. The total AM production time which is a function of preheat time, rake time, melt time and cooling or heat-treatment time is important, since advancements in AM methods have been improving rapidly. Hence, it is important to analyze the effects of reducing this time component. The unit EBM time component reduces based on batch size as shown in Figure 75. Therefore, this sensitivity analysis of single unit batches includes multiple units in a single build where the unit EBM time is reduced. Also, the unit material cost is a function of the part volume and hence does not vary for different batch sizes.

Further, since AM is relatively new when compared to machining, considerable training and experience is required in the workforce to operate the equipment. As a result, the operator costs are almost four times on average to that of a machinist. Finally, this analysis studies the impact of these variables on the unit cost for hybrid and CNC-RP production. It should be noted that batch production is not considered for CNC-RP since the same process plan is repeated for each unit with a bar stock. The analysis was performed on the same part design detailed in the section 3.4 for the following conditions shown in Table 21.

Table 21: Variable Conditions

Variables	Case-study-Section.3	Level #2	Level #3
EBM material cost ($/kg)	300	30	150
CNC-RP stock cost ($/unit)	400	200	40
Ratio: MRR/MRR-case study	1	0.5	0.1
EBM production time (hr/part)	20	10	2
EBM operating cost ($/hr)	104	66	33
CNC-RP operating cost ($/hr)	25	50	75

The price of atomized Ti64 metal powder for AM is currently around $ 300/kg and it is expected that with gaining popularity of metal AM, the overall production volume will increase and hence the price could reduce. The cost of round stock for machining is higher for superalloys such as Ti64 and lower for Steel and lowest for Aluminum, hence the CNC-RP stock cost is considered at 50 % and 10 % of Ti64 cost. Similarly, the machinability of steel and aluminum are of the same order in terms of MRR. With the development in processing capabilities and techniques (e.g. cool down external to EBM machine volume) would lower the production time. Finally, with growing workforce and skilled operators the operating cost of metal AM such as EBM would reduce in the future. The influence of the major factors on hybrid unit cost is shown in Figure 77. In Figure 77, it was observed that EBM (AM) production time tremendously affects the unit hybrid cost along with production cost. It was found that a 50 % reduction in EBM production time resulted in lowering the unit cost by 40 % and when EBM production time was reduced to 90 %, the overall unit cost was reduced by 72 %.

Similarly, a 36 % reduction in operation cost reduced the unit cost by about 30 %. For the analyzed part design and volume, it was found that material cost had lesser effect on the unit cost where 50 % reduction in material cost resulted only in 8 % reduction in unit cost. Further, increasing the material removal rate (machinability) of the material during finish-machining by 100 % reduced the unit cost by 10%.

This can be attributed to the fabrication of ‘rough stock’ through AM leading to minimal machining. Similarly, reduction machining allowance by 100 % through tighter fixture deviation control lead to reduction in unit cost by 11%. This is because of lesser material removal and also, lower tool wear resulting in a more economical AIMS finishing operation.

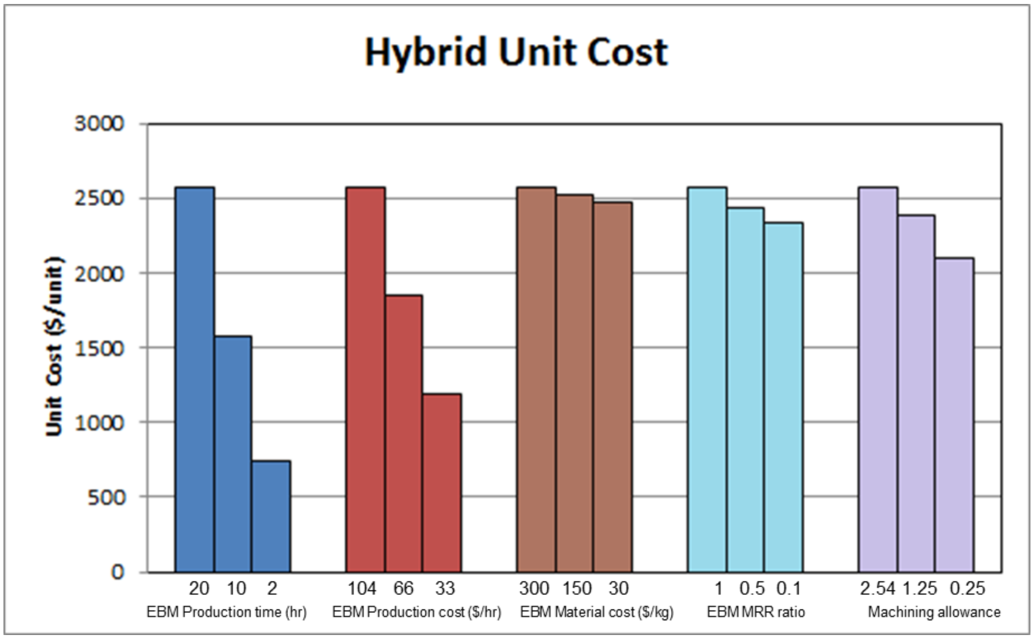

Figure 77: Total Unit Cost for Hybrid Manufacturing

Increasing the machinability (MRR) by 50 % and 100 % in CNC-RP positively influenced the CNC-RP unit cost by 35 % and 52 % respectively as shown in Figure 78. However, reducing the material cost by similar orders had lesser effect on the unit cost (13 % and 25 %), and when compared to the case study, this can be attributed to the significant amount of machining time leading to high tool costs. In other words, machining time is more dominant on unit cost than the material cost because, increased machining time results in higher production cost as well as more tool wear. The values for cost and rates used in the case study were typical costs for the effect of these rates should illustrate typical responses for changes in the manufacturing efficiencies and material costs.

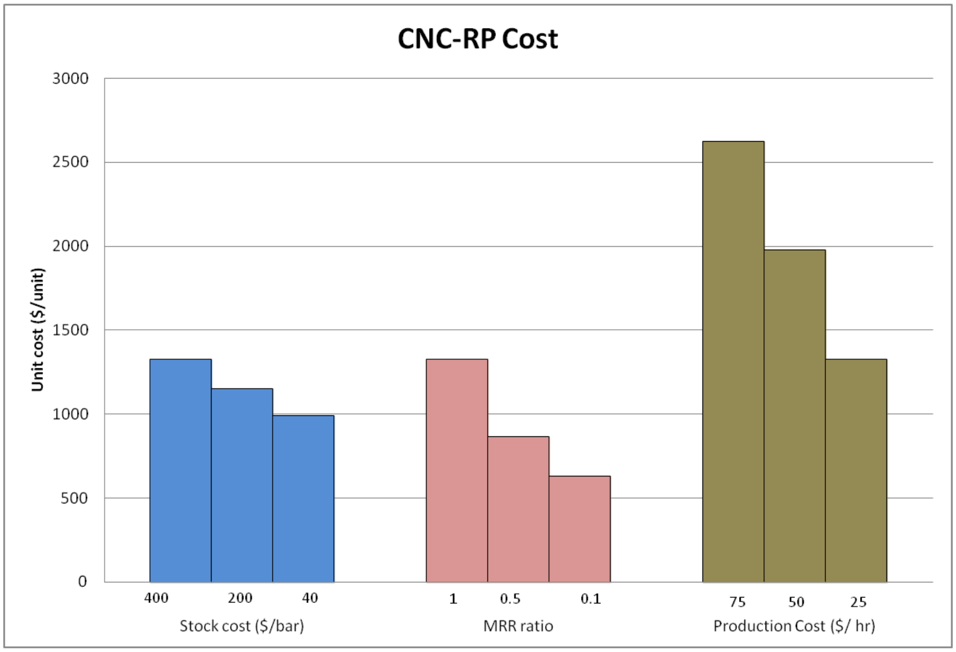

Figure 78: Influence of cost factors on Single-unit CNC-RP

It can be identified from this analysis that the cost of hybrid process can be greatly reduced by reducing the production time and operator cost in EBM (or AM). In the case of CNC-RP, the unit cost can be greatly reduced by increasing the material removal rate significantly. In the case of CNC-RP, the influence of higher MRR is more pronounced than the material cost as shown in Figure 78. This can be attributed to the amount of additional machining time required to machine alloys such as Ti-6Al-4V (MRR ratio = 1) and Brass (MRR ratio > 0.33). In many ways, this study reflects the current state of additive and machining-based manufacturing processes where expensive alloys with part designs requiring multiple fixtures are preferred to be processed through AM (particularly for low volume batches).

Mass production of easier-to-machine alloys like Aluminum, Brass, etc. can be easily processed through machining with higher material removal rate. For the given case-study part design, in order to understand the main and interaction effects between the cost variables, further analysis was performed. As shown in Figure 79, impact of CNC-RP based cost components such as stock cost, MRR and production cost is greater on CNC-RP unit. This can attributed to the machining of the entire part from a bar stock, particularly in the case of materials where the feasible MRR is lower such as Ti64 and other superalloys. It can be seen that the machinability of the material (MRR) ratio has the greatest impact in the case of CNC-RP. With increased machining cost, the unit cost of CNC-RP significantly increases greater in the case of CNC-RP than in AIMS. This can be attributed to elimination of roughing operations through machining a near-net shape part. The impact of material cost is greater in CNC-RP (i.e., stock cost) than in AIMS.

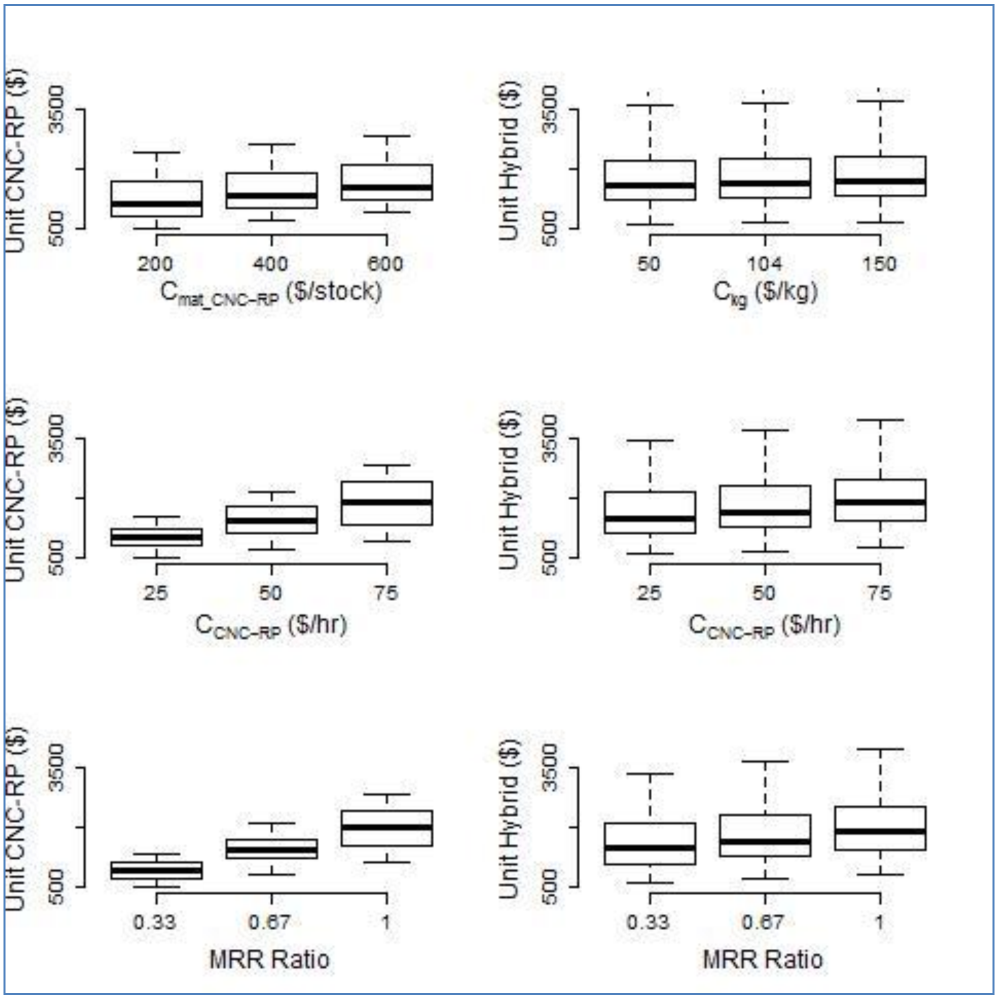

Figure 79: Influence of CNC-RP-related variables: operating cost, material and MRR

Hence, higher material removal rate and lower CNC-RP operating cost would result in lower unit cost as shown in Figure 80. It can be observed that finish machining of a near net AM-part through the hybrid process reduces the influence of machining-based cost components.

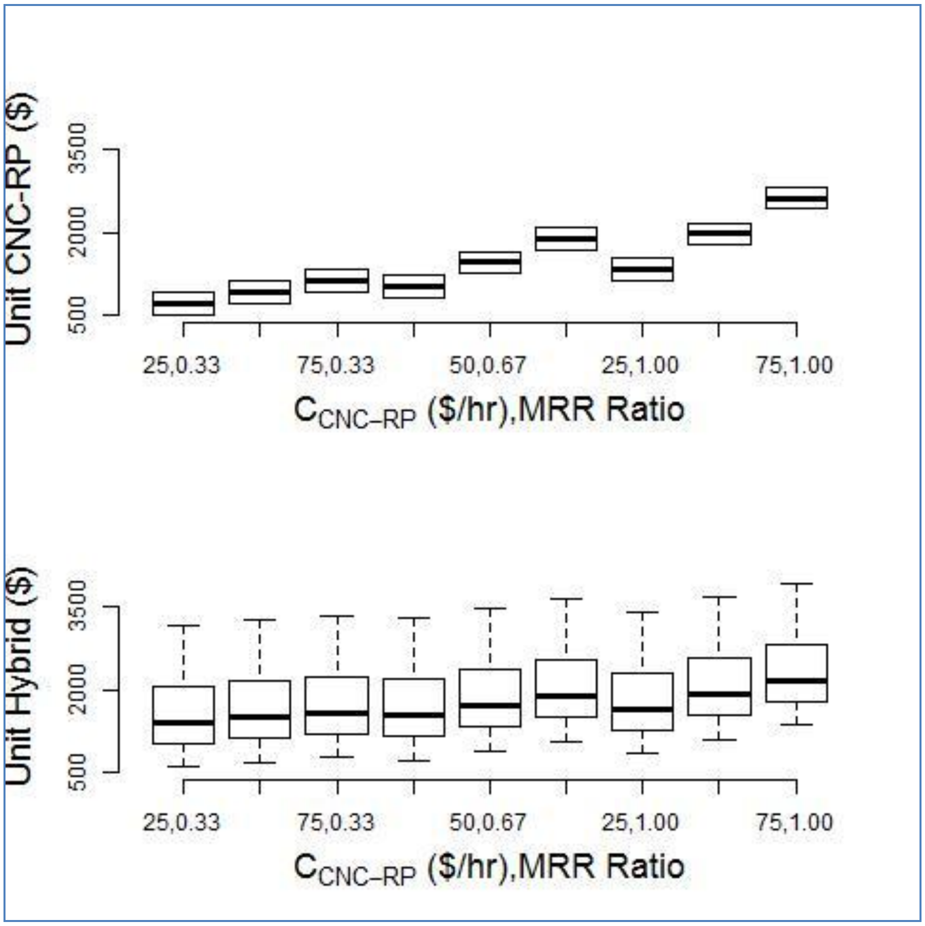

Figure 80: Interaction between production cost and MRR

In the case of hybrid manufacturing as shown in Figure 81, the cool time after the completion of the build has a pronounced effect on the hybrid unit cost. The effect is further increased with higher operating cost.

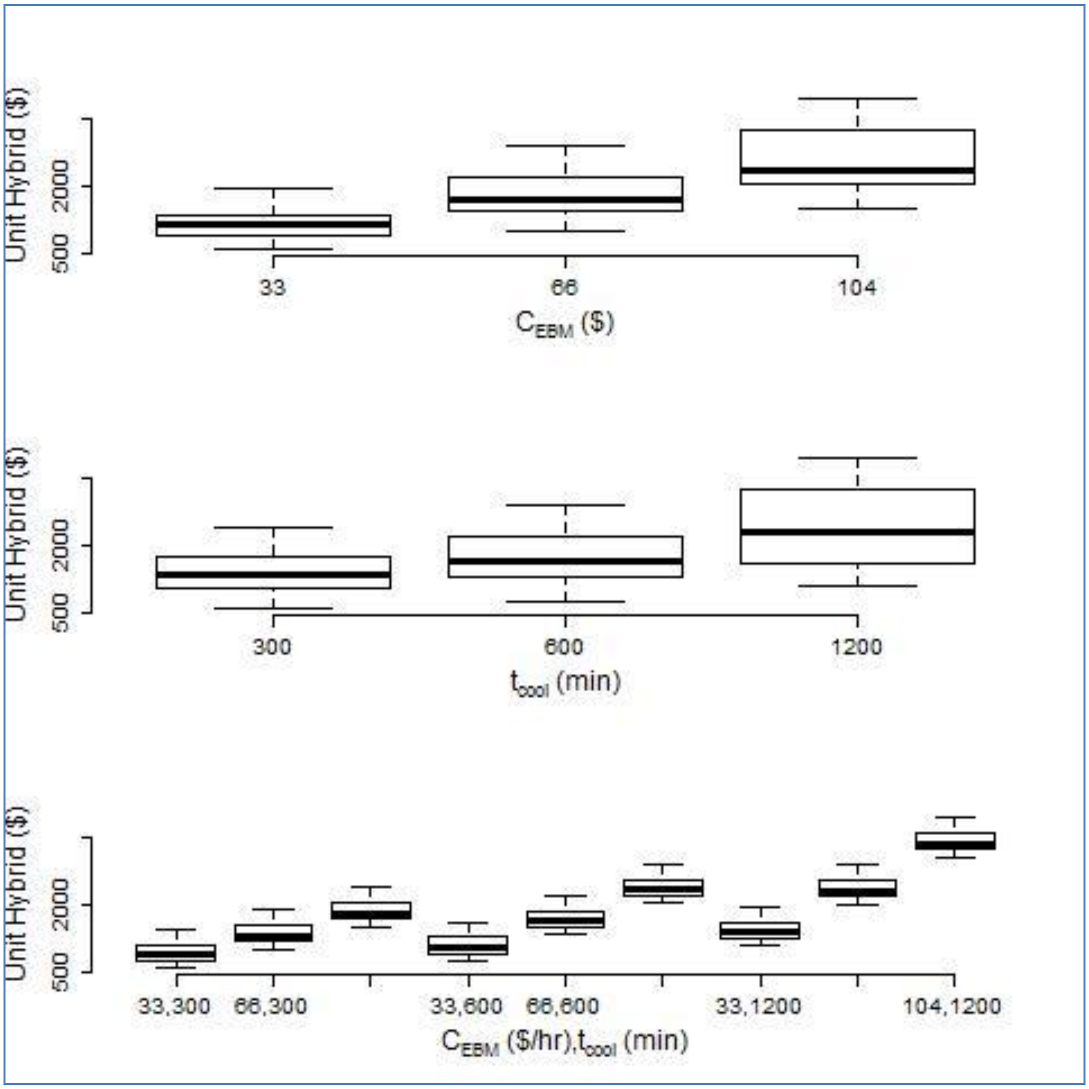

Figure 81: Influence of EBM cool time and EBM operating cost

In the case of AIMS, the analysis above identifies the interaction between the important variables on unit cost for the case study for single-unit and batch production. However, it is important to understand the influence of aspect ratio of the part (i.e. part size) on the unit cost to identify the economical manufacturing method.

Hence, using the same part geometry and cost variables considered in the primary case study, we determined the unit cost for other aspect ratios. The numbers of parts that can be included in a single EBM build (and other additive processes) is limited by the available build volume and build orientation. Further, based on the case study it was identified that batch size does not impact CNC-RP unit cost.

Hence, in this analysis batch size of one that can be accommodated along the shortest build height is only considered for CNC-RP. Since multiple parts can be accommodated in the AIMS system (for given part volume and design), the interaction effects of two main variables in the cost of EBM operation and cooling time (i.e. included in the production time) was also analyzed and shown in Figure 82.

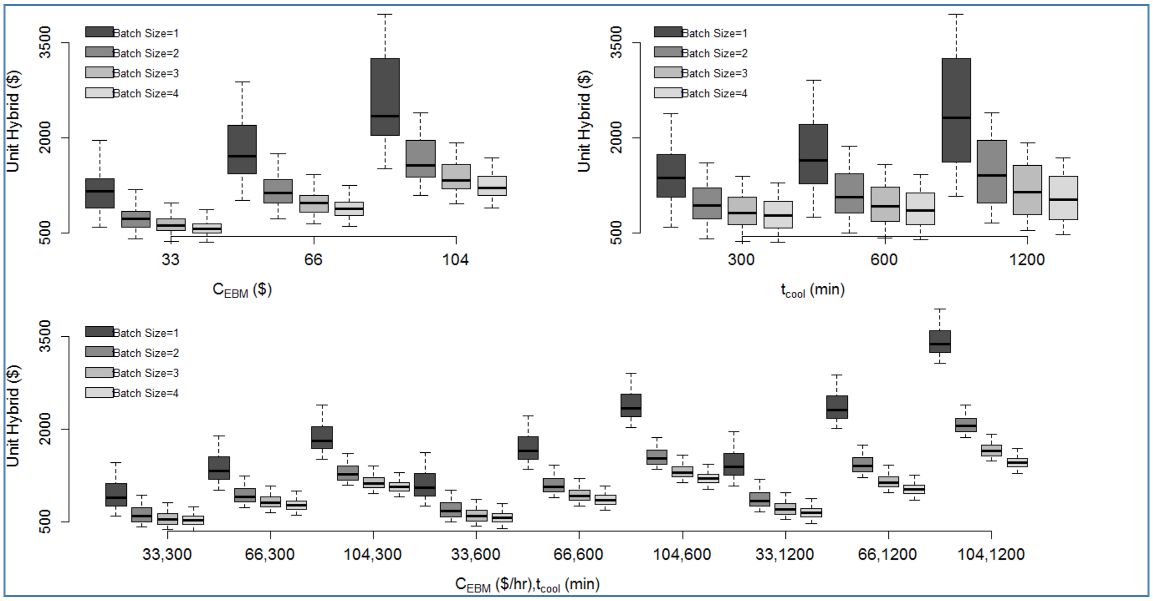

Figure 82: AIMS Unit Cost for different Batch Sizes

It can be identified that the production cost significantly affects the hybrid unit cost and its effects are greater at larger cooling time. In order to test the influence of part size, the case study design was altered and analyzed for the base variables. The following Figure 83 shows the impact of part aspect ratio on the unit cost for batch size of one.

		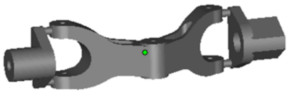	
	Case Study #1	Case Study #2	Case Study #3
Build Orientation			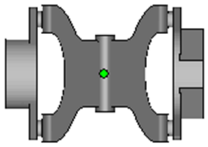
Top view		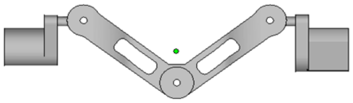	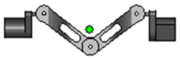
Aspect Ratio	1	1.5	0.5
Maximum-Batch Size	4	1 (with a bigger starting plate)	6
AIMS unit cost (batch size =1)	$ 3483.27	$ 2778.41	$ 4464.53
CNC-RP unit cost (batch size =1)	$ 1358.25	$ 1932.78	$ 1433.38

Figure 83: Unit Cost for different Aspect Ratios

Within AIMS, parts with higher aspect ratio are more cost effective when compared to parts with lower aspect ratio. This can be attributed to the number of build layers in EBM, which impacts the time for raking, pre-heating and post-heating the layer.

On the contrary, the CNC-RP unit cost is affected by the total material to remove and the machining parameters and is more cost effective for parts with parts with lower aspect ratio.

6.7 Discussion

From this study, it is observed that machining duration of CNC-RP only production (including hogging and roughing) is significantly longer than AIMS, (only the finishing stage of CNC-RP).

This could be attributed to the machining parameters such as feed and depth of cut employed for milling alloys such as Ti-6Al-4V. For instance, machining time would be drastically lower in the case of processing relatively softer materials such as Aluminum or Brass. However, since the operation cost of CNC-RP is much lower than the operation cost of relatively newer technologies such as EBM (and other metal AM) the unit cost is lower for a single unit when compared to AIMS. It was also observed that high cooling time (and/or heat treatments) has tremendous influence on increasing the unit hybrid cost.

However, material utilization in terms of part-stock volume of expensive tough to machine materials could become a critical factor based on part geometry while processing solely in CNC-RP. This is important in the case of expensive superalloys used in aerospace and mechanical applications. On the other hand, the hybrid process demonstrated higher material utilization of expensive alloys in EBM **along** with the ability to ‘finish’ machine through CNC-RP.

The benefits were three-fold: (1) addition of sacrificial fixture for CNC-RP in the near-net part eliminated the need for any additional fixtures, (2) employing only 'finish' CNC-RP reduced total machining time (as compared to CNC-RP) and also, lower tooling cost and (3) higher material utilization by using only 'near-net' volume of material (as compared to bar stock in CNC-RP).

It can also be noted that the ability to batch produce 'near-net' part in a single build lowered the EBM-component in the total cost. Another critical factor is the part design limitations with subtractive methods. For instance, it is not feasible to produce non-conventional features such as mesh or lattice structures through CNC-RP.

By integrating such part design within surfaces as shown in Figure 13 and finish machining through CNC-RP, the hybrid process enables increased strength-to- weight ratio along with precision feature and surface accuracy. This is critical particularly in the case of expensive alloys.

In addition, the following relationship can be derived from above:

$$t_{Pre-finishing} = t_{setup-CNC-RP} + t_{hog} + t_{rough} \tag{6.14}$$

and if:

$$C_{RoughStock} = (C_{machining} \times t_{Pre-finishing}) + C_{tool\,(H)} + C_{tool\,(R)} + C_{CNC-RP-stock} \tag{6.15}$$

and:

$$C_{RoughStock} \leq C_{EBM} \tag{6.16}$$

Hence, it is considered optimal to choose the CNC-RP process over the hybrid process (neglecting any geometric constraints) when the cost of rough stock is lesser than that of EBM. Otherwise, the hybrid process provides the least cost solution. Any situation that increases the pre-finishing time i.e., costs of roughing or hogging tooling, or stock costs will shift the decision in the direction of the hybrid process and ‘near-net’ shaping using additive processes. This is intuitive and explains why significant research thrusts in the additive manufacturing arena are towards nickel based super alloys and other difficult to machine materials.

It is also somewhat instructive as to why (again neglecting any geometric constraints) aluminum research in these processes is somewhat muted, as the machinability of aluminum is much greater than that of cobalt chrome and titanium alloys

Other situations may not be as intuitive. Parts that require relatively little hogging or roughing time, such as parts where part volume approaches that of the rough stock size in CNC-RP will favor CNC-RP, and parts where the majority of the material removal is done by the relatively large and rigid hogging tool will again favor CNC-RP. As shown parts with lower aspect ratio (with lower ratio of material removal-stock volume) are preferred to be processed through CNC-RP. Parts with high aspect ratio and thin walls, greater concave areas and small internal features (internal to the convex hull) will favor the hybrid process.

The impact of batch size on the hybrid process is significant because, it is a near-net shaping ‘n’ units of rough stock for finish CNC-RP with a single set-up in EBM and amortized processing time of raking, pre-heating and post-heating of each layer (which consists of ‘*n’* units). Hence, the selection criteria of economical process can further extended as:

$$C_{RoughStock} \geq (C_{EBM})/n \qquad (6.17)$$

If the cost of roughing and hogging through CNC-RP solely for a single unit is greater than processing ‘near-net’ shape EBM-made rough stock in a batch, AIMS is more economical. This criterion should be considered simultaneously for: (1) Batch size, (2) Build orientation and (3) Part shape.

For example, if a larger batch size (~10) of a part with higher aspect ratio is required it would be efficient to select the build orientation along the part length to accommodate the batch size in a single EBM build. For commercial EBM production, we feel that if even one part is being manufactured in an EBM, it will be paired with other parts in the EBM build so that *n* in Eq. 6.17 will be kept as high as possible and the resulting cost will be as low as possible. The ability to address fixturing for subtractive operations prior to fabricating the part provides a unique advantage to analyze the location and geometry of fixtures on non-functional or desired surfaces, the orientation of part fabrication in the additive process can also be adapted to surfaces requiring precision finish (e.g. upward facing surfaces have better finish than downward facing or overhanging surface). Successful implementation of the integrated hybrid system will improve material utilization and eliminate manual finishing processes and the requirement for multiple fixtures.

The AIMS system can be employed through any AM process such as SLS, SLM, etc. One of the highlights of this system is the requirement for a STL/CAD to generate process plan for the entire hybrid system. Such approach can be employed in combining advantages of similar additive and subtractive processes; in this case Electron Beam Melting (EBM) and rapid CNC machining (CNC-RP) are used.

Summary

In this chapter, the AIMS system' economic metrics were demonstrated through a case study of a single part using EBM and CNC-RP where the part is functional load-bearing assembly part made of difficult to machine titanium alloy, Ti-6Al-4V.

It was shown that the decision to use CNC-RP versus the hybrid system is impacted by the machinability and material cost, along with geometric and size considerations of the part. For the part used for our illustration, the hybrid approach is more economically attractive for more expensive and harder to machine materials while CNC-RP is favored for less expensive and easier to machine materials. The hybrid system also becomes less expensive when multiple parts can be produced in the AM process simultaneously (either lot size increases beyond a single unit or pairing with other parts or orders in a single EBM build) subject to build volume-orientation constraints.

CHAPTER 7: CONCLUSIONS AND FUTURE WORK

Introduction

In this chapter, an overall summary of this work is provided along with specific contributions of the research. Also, directions for future research are presented based on this study to fully develop AIMS for automated process planning and production environment.

7.1. Research Summary

In this dissertation, a novel hybrid process called **AIMS** (Additive Manufacturing Integrated with Subtractive Methods) was presented. Based on the major advantages and limitations of additive and subtractive manufacturing principles presented in Chapter 1, an argument for integrating the additive with subtractive manufacturing approaches was presented. It was noted that poor surface finish and lack of high part tolerance were the main drawbacks of current AM methods. On the other hand, subtractive methods required custom tooling and fixtures. It was identified that developing a hybrid process that does not interfere with existing AM and SM processes, and can be implemented across all AM processes is the key to successfully developing a rapid 'high precision' hybrid process.

A recent development in SM namely, CNC-RP was shown to emulate 'fixture-less' layer-by-layer approach of AM techniques and its advantages and disadvantages were noted. Further, existing hybrid systems such as LAMP and UC were also reviewed and it was found that the major advantage of existing hybrid methods is the presence of a constant/fixed coordinate system which allows for seamlessly switching between AM and SM operations 'in the same machine environment'.

Finally, motivation for a new hybrid method which can be used in conjunction with any AM process including binder-jetting and powder-bed fusion methods was presented. The AIMS process was presented in detail and the different coordinate systems associated with the part, fixtures, CNC-RP and AM systems were illustrated. Findings from feasibility studies showed that machining allowance added to the part prior to AM processing needs to account for the non-ideal part-toolpath location when near-net AM fixtures are used. Influence of fixturing from inaccuracies in AM processing and surface roughness was presented and the corresponding transformation models were developed. Further, based on the AIMS process model an overarching scope of research and a desired automated process flow required detailed. Process performance metrics for AIMS namely unit cost, production time and material consumption were outlined as function of process variables such as fixture design, build volume constraints and machining allowance required.

In Chapter 4, the objectives associated with this study (1) Novel Modeling of fixture deviations based on fixture accuracy and surface characteristics, (2) Developing of fixture design heuristics and (3) Novel Modeling of part deviation based on part and fixture designs to estimate the part overgrowth required was presented with corresponding methodologies. The contact plane of the fixture with the chuck was analyzed for fixture inaccuracies based on the maximum and minimum deviation of the planes from the nominal surfaces of AM-made fixtures. A heuristic with sets of decision criteria in fixture designing (tri-planar and cylindrical) was presented.

In this study, it was executed manually for the specific part designs that were analyzed. Finally, the interactions between part geometry and the overall fixture inaccuracies were identified to develop a model to estimate corresponding part overgrowth.

In Chapter 5, models developed for part location were validated successfully for EBM built near-net parts. Dependencies concerning design parameters such as part datum location, critical features, part length, fixture geometry were presented. All of these dependencies will be “part specific”. The developed model can be used for alternative part designs and with analysis of other AM fixture surfaces. Analysis of fixturing inaccuracies found that tri-planar fixture designs had better accuracy than cylindrical fixtures. This could be attributed to the presence of wafer support and sintered powder in the downward facing surfaces of a cylinder during its build orientation. Within tri-planar design fixtures, it was found that the contact surfaces which are perpendicular to the build direction had more impact on deviation (one order of magnitude) due to wafer supports on the fixturing deviation. The developed model for part deviation was tested through controlled fixture deviations using precision shims to validate the estimation of the fixture coordinate system. Finally, tri-planar fixtures were developed in alternative AM- (DMLS) build orientations to eliminate the effects of support structures on the contact planes. Subsequently, the part overgrowth estimation was tested for a functional part with tolerance requirements.

Economic models were developed for AIMS and CNC-RP in Chapter 6 to identify the critical process variables that impact the performance metrics and it was found that elimination of hogging and roughing in AIMS reduces the unit cost significantly.

The study also highlighted the advantage of AIMS system for low-volume production particularly in the case of expensive tough-to-process alloys with higher material utilization. The impact of improving fixturing inaccuracies on lowering the overall unit cost in AIMS was also noted.

7.2. Research Contributions

The following presents a summary of the contributions identified from this research:

- Models of the fixture deviation corresponding to a near-net AM process based on form inaccuracy and surface characteristics were developed. This can be further used to evaluate the fixturing errors associated with any AM or ‘casting’-like bulk processes. The models show some obvious findings such as: 1) larger diameter fixture lugs will reduce positional error, 2) spacing the fixture lugs farther apart also reduces fixture positioning error, and 3) shape of the sacrificial lugs can arrest a rotation degree of freedom and assist in location.
- The analytical models developed appear to accurately represent the maximum deviation limits for near-net shape fixturing.
- Part overgrowth criteria based on part geometry with respect to fixture deviations were presented and this is critical to determine fixture-part tolerance stacking inaccuracies. This model can be used to calculate the part overgrowth based on part geometry (aspect ratio, cross-section) with respect to fixture deviations (geometry and location).

- Critical features-based fixture design criteria were developed and can be automated using textured CAD file format to evaluate fixture placements prior to AM and minimize part deviations.
- The influence of fixture design on overall process deviation was presented as a function of fixture geometry and build orientation. This is an important factor since the overall finish-process accuracy is predicated on the fixture deviation and subsequently, the corresponding overgrowth.
- Cost models that can be employed with any AM-process, part-fixture geometries, material and operating costs were developed and the tremendous impact of the developed hybrid method of AM process were illustrated. Most importantly, the significance of AIMS for low volume batches was presented.

7.3. Future Research

For future research, the characterization models that were developed in this model can be adapted to other metal-AM methods such as ExOne systems to estimate fixturing inaccuracies. AM process accuracies can be recorded for varying materials, part geometry, build volume and orientation to develop an empirical model to estimate fixturing deviations.

The part overgrowth parameter can be simultaneously optimized by using reverse engineering of the AM part in the machine coordinate system to identify part feature specific deviation. This can be achieved by using image-based data acquisition systems such as a laser scanner to determine the actual location of part features to generate and/or adapt toolpath to successfully produce the final part.

Also, algorithms can be developed to automate the fixture design using recorded data on different fixture inaccuracies, machining forces based on part geometry and tool parameters. In addition, using a textured or labeled CAD file format can be implemented to identify the critical surfaces to identify fixture locations.

Studies on re-generation of toolpath after each rotational orientation can be performed to eliminate idle toolpath movements due to global part overgrowth and it would help in more efficient finish machining based on real-time estimation of machining volume. Another area of future focus should be the ability to produce thin wall features with appropriate combination of part overgrowth and machining parameters through hybrid manufacturing. This will enhance the applications of AIMS by eliminating deflection issues through robust fixture design. Finally, AIMS could be enhanced by developing hybrid-centric visibility analysis that could be adapted for ‘minimum-tool length’ and ‘critical surfaces’ since unlike conventional CNC-RP bulk of the roughing operations does not exist.

APPENDICES

Appendix 1: Machining Parameters

The machine tool used has a rapid travel speed of 600 mm/s and can produce up to 25kW of machining force. Based on recommendations from Machinery's Handbook, the process parameters for Ti64 using a 9.525 mm 4-flute carbide flat end mill were identified as 910 rpm for a conservative depth of cut of 0.18 mm in accordance with Taylor's rule (layer thickness in CNC-RP).

Appendix 2: Circular Fixture- Calculation

```
#include <fstream>
#include <iostream>
#include <vector>
#include <istream>
#include <ostream>
#include <iterator>
#include <algorithm>
#include <string>
#include <iomanip>

#include <pcl/point_types.h>
#include <pcl/point_cloud.h>
//#include <pcl/PolygonMesh.h>

//#include <pcl/io/vtk_io.h>

#include <pcl/io/pcd_io.h>
#include <pcl/visualization/cloud_viewer.h>
//#include <pcl/visualization/pcl_visualizer.h>
#include <pcl/visualization/point_cloud_handlers.h>
//#include <pcl/io/ply_io.h>

//#include <pcl/sample_consensus/ransac.h>
//#include <pcl/sample_consensus/sac_model_cylinder.h>
#include <pcl/features/normal_3d.h>

//#include <pcl/registration/ia_ransac.h>
#include <pcl/sample_consensus/method_types.h>
#include <pcl/sample_consensus/model_types.h>
#include <pcl/segmentation/sac_segmentation.h>
#include <pcl/ModelCoefficients.h>
#include <pcl/common/common.h>
#include <pcl/common/distances.h>

typedef pcl::PointCloud<pcl::PointXYZ> Pxyz;

int main(int argc, char** argv)
{

   std::ifstream csvpoints;
   if (argc > 0) csvpoints.open(argv[1]);
   else csvpoints.open("cylinder.csv");
   Pxyz::Ptr cylinder(new Pxyz);

   while(csvpoints.good())
   {       pcl::PointXYZ temp;
char dump;
    csvpoints >> temp.x >> dump >> temp.y >> dump >> temp.z;
    cylinder->push_back(temp);
  }

  //Kludge to remove bad last point
  cylinder->erase(--(cylinder->end()));

  //To calculate normals
  //Needed by the parameter estimator for some reason
  pcl::NormalEstimation<pcl::PointXYZ, pcl::Normal> ne;
  pcl::search::KdTree<pcl::PointXYZ>::Ptr tree (new pcl::search::KdTree<pcl::PointXYZ> ());

  pcl::PointCloud<pcl::Normal>::Ptr cloud_normals (new pcl::PointCloud<pcl::Normal>);

  ne.setSearchMethod (tree);
  ne.setInputCloud (cylinder);
  ne.setKSearch (10);
  ne.compute (*cloud_normals);

  //The sacmodel makes sure all the points are good and gives us the cylinder coeffs
  pcl::SACSegmentationFromNormals<pcl::PointXYZ, pcl::Normal> seg;//Create the sac function
  pcl::ModelCoefficients coefficients;
  pcl::PointIndices inliers_cylinder;

  seg.setOptimizeCoefficients (true);//Set up the sac model
  seg.setModelType (pcl::SACMODEL_CYLINDER);
  seg.setMethodType (pcl::SAC_RANSAC); //Consider using different types of sac
  seg.setNormalDistanceWeight (0.2); //Parameters to be tweaked
  seg.setMaxIterations (1000);
  seg.setDistanceThreshold (0.5);
  seg.setRadiusLimits (0.9,1.1);//Set up to match actual cylinder exactly.
  seg.setInputCloud (cylinder);
  seg.setInputNormals (cloud_normals);
  seg.segment (inliers_cylinder, coefficients);

  //Spit out all coefficients (point, direction, radius) and index of inliers.
  //All the points should be inliers
  std::cout << "\nnum inliers:" << (inliers_cylinder.indices).size();
  std::cerr  << "\n\nCylinder coefficients: " << coefficients << std::endl;

  //Convert coefficient forms
  Eigen::Vector4f line_pt, line_dir, rad;

  line_pt[0] = coefficients.values.at(0);//A point on the line
  line_pt[1] = coefficients.values.at(1);
  line_pt[2] = coefficients.values.at(2);
  line_pt[3] = 0;
```

```
line_dir[0] = coefficients.values.at(3);//Vector along line direction
line_dir[1] = coefficients.values.at(4);
line_dir[2] = coefficients.values.at(5);
line_dir[3] = 0;

float radius = coefficients.values.at(6);

//Compute distances to the axis of the cylinder
std::vector<double> distances;
for(Pxyz::iterator i = cylinder->begin(); i != cylinder->end(); i++)
{
   Eigen::Vector4f pt(i->x,i->y,i->z,0);
   distances.push_back(sqrt(pcl::sqrPointToLineDistance(pt,line_pt,line_dir)));
}

//Computing metrics
//Peak and valley
double peak( *(std::max_element(distances.begin(),distances.end())) - radius),
       valley( *(std::min_element(distances.begin(),distances.end())) - radius);

//Computing cylindricity
double cylin(peak - valley);

//Computing other metrics - absolute average, average and rms
double absavg(0);
double davg(0);
double msq(0);
for(std::vector<double>::iterator i = distances.begin(); i<= distances.end(); i++)
{
   absavg += fabs(*i - radius);
   msq += pow((*i - radius),2);
   davg += *i - radius;
}

absavg = absavg / distances.size();
davg = davg / distances.size();
msq = sqrt(msq/distances.size());

//Computing sample variance
double var(0);
for(std::vector<double>::iterator i = distances.begin(); i<= distances.end(); i++)
{
   var += pow((*i - davg),2);
}
var = var/distances.size();

//Open file for writing - use argv for name
if (argc > 1)
```

```
      {
       for (int i = 2; i < argc; i++)
       {
          if ((strcmp(argv[i],"-f") == 0) && (i < (argc - 1)))
          {
             ofstream cylinders;
             cylinders.open(argv[i + 1], ios::out | ios::app);

             /*
             cylinders << "\nFile: " << argv[1] << "\nRadius: " << radius << "\nPeak: " << peak
                << "\nValley: " << valley << "\ncylindricity: " << cylin << "\nRMS: " << msq
                << "\nAverage absolute deviation: " << absavg
                << "\nAverage deviation: " << davg << "\nVariance: " << var << std::endl;
             */

             cylinders <<  radius*2 << "," << (radius + peak)*2 <<"," << (radius + valley)*2  <<
std::endl;
             cylinders.close();
             break;
          }
       }
   }

   //Else just pipe to output

   std::cout << "\nFile: " << argv[1] << "\nRadius: " << radius << "\nPeak: " << peak
      << "\nValley: " << valley << "\ncylindricity: " << cylin << "\nRMS: " << msq
      << "\nAverage absolute deviation: " << absavg << "\nAverage deviation: "
      << davg << "\nVariance: " << var << std::endl;

   /*while(!viewer.wasStopped())
   {
   }*/
}
```

Appendix 3: Tri-Planar Fixture- Calculation

```
#include <fstream>
#include <iostream>
#include <vector>
#include <istream>
#include <ostream>
#include <iterator>
#include <algorithm>
#include <string>

#include <pcl/point_types.h>
#include <pcl/point_cloud.h>
//#include <pcl/PolygonMesh.h>

//#include <pcl/io/vtk_io.h>

#include <pcl/io/pcd_io.h>
#include <pcl/visualization/cloud_viewer.h>
//#include <pcl/visualization/pcl_visualizer.h>
#include <pcl/visualization/point_cloud_handlers.h>
//#include <pcl/io/ply_io.h>

//#include <pcl/sample_consensus/ransac.h>
//#include <pcl/sample_consensus/sac_model_cylinder.h>
#include <pcl/features/normal_3d.h>

//#include <pcl/registration/ia_ransac.h>
#include <pcl/sample_consensus/method_types.h>
#include <pcl/sample_consensus/model_types.h>
#include <pcl/segmentation/sac_segmentation.h>
#include <pcl/ModelCoefficients.h>
#include <pcl/common/common.h>
#include <pcl/common/distances.h>
#include <pcl/common/centroid.h>


typedef pcl::PointCloud<pcl::PointXYZ> Pxyz;

//float pdist(pcl::PointXYZ pt, Eigen::Vector3f v, float norm_v);
double pdist(pcl::PointXYZ pt, Eigen::Vector3f v, double d);

int main(int argc, char** argv)
{
```

```
std::ifstream csvpoints;
if (argc > 0) csvpoints.open(argv[1]);
else csvpoints.open("trisides.csv");

Pxyz::Ptr plane1(new Pxyz);
Pxyz::Ptr plane2(new Pxyz);
Pxyz::Ptr plane3(new Pxyz);

int posn(0);
float Xc(0), Yc(0), Zc(0);
while(csvpoints.good())
{
   pcl::PointXYZ temp;
   char dump;
   csvpoints >> temp.x >> dump >> temp.y >> dump >> temp.z;
   if (posn < 100) plane1->push_back(temp);
   else if (posn < 200) plane2-> push_back(temp);
   else if (posn < 300) plane3-> push_back(temp);
   //if (posn < 300) {Xc += temp.x; Yc += temp.y; Zc += temp.z;}
   posn++;
}

Pxyz CentCloud;
CentCloud +=*plane1;
CentCloud +=*plane2;
CentCloud +=*plane3;
Eigen::Vector4f C;
pcl::compute3DCentroid(CentCloud, C);
//std::cout << "\nCentroud: " << C << std::endl;

//Calculate centroid
pcl::PointXYZ PC(C[0],C[1],C[2]);

//To calculate normals from the pointcloud
pcl::NormalEstimation<pcl::PointXYZ, pcl::Normal> ne;
pcl::search::KdTree<pcl::PointXYZ>::Ptr tree (new pcl::search::KdTree<pcl::PointXYZ> ());

pcl::PointCloud<pcl::Normal>::Ptr Nplane1 (new pcl::PointCloud<pcl::Normal>);
pcl::PointCloud<pcl::Normal>::Ptr Nplane2 (new pcl::PointCloud<pcl::Normal>);
pcl::PointCloud<pcl::Normal>::Ptr Nplane3 (new pcl::PointCloud<pcl::Normal>);

ne.setSearchMethod (tree);
ne.setKSearch (10);

ne.setInputCloud (plane1);
ne.compute (*Nplane1);
ne.setInputCloud (plane2);
ne.compute (*Nplane2);


ne.setInputCloud (plane3);
ne.compute (*Nplane3);

/*pcl::RandomSampleConsensus<pcl::PointXYZ> ransac (model_c);
ransac.setDistanceThreshold (.01);
ransac.computeModel();
ransac.getInliers(inliers);*/

//The sacmodel makes sure all the points are good and gives us the cylinder coeffs
pcl::SACSegmentationFromNormals<pcl::PointXYZ, pcl::Normal> seg;//Create the sac function

pcl::ModelCoefficients Pcoeffs1;
pcl::ModelCoefficients Pcoeffs2;
pcl::ModelCoefficients Pcoeffs3;

pcl::PointIndices Iplane1;
pcl::PointIndices Iplane2;
pcl::PointIndices Iplane3;

seg.setOptimizeCoefficients (true);//Set up the sac model
seg.setModelType (pcl::SACMODEL_PLANE);
seg.setMethodType (pcl::SAC_RANSAC); //Consider using different types of sac

seg.setNormalDistanceWeight (0.2); //Parameters to be tweaked
seg.setMaxIterations (1000);
seg.setDistanceThreshold (0.02);

seg.setInputCloud (plane1);
seg.setInputNormals (Nplane1);
seg.segment (Iplane1, Pcoeffs1);

seg.setInputCloud (plane2);
seg.setInputNormals (Nplane2);
seg.segment (Iplane2, Pcoeffs2);

seg.setInputCloud (plane3);
seg.setInputNormals (Nplane3);
seg.segment (Iplane3, Pcoeffs3);

//Spit out all coefficients (point, direction, radius) and index of inliers.
//All the points should be inliers
std::cout << "\nnum inliers1:" << (Iplane1.indices).size();
std::cout << "\nnum inliers2:" << (Iplane2.indices).size();
std::cout << "\nnum inliers3:" << (Iplane3.indices).size();
```

```
/*
std::cerr  << "\nCoefficients1: " << Pcoeffs1;
std::cerr  << "\nCoefficients2: " << Pcoeffs2;
std::cerr  << "\nCoefficients3: " << Pcoeffs3 << std::endl;

*/

Eigen::Vector3f v1,v2,v3;
double d1,d2,d3;

v1[0] = Pcoeffs1.values.at(0);
v1[1] = Pcoeffs1.values.at(1);
v1[2] = Pcoeffs1.values.at(2);
d1 = Pcoeffs1.values.at(3);

v2[0] = Pcoeffs2.values.at(0);
v2[1] = Pcoeffs2.values.at(1);
v2[2] = Pcoeffs2.values.at(2);
d2 = Pcoeffs2.values.at(3);

v3[0] = Pcoeffs3.values.at(0);
v3[1] = Pcoeffs3.values.at(1);
v3[2] = Pcoeffs3.values.at(2);
d3 = Pcoeffs3.values.at(3);

v1 = v1.normalized();
v2 = v2.normalized();
v3 = v3.normalized();

//Creating the proper orientation
if (pdist(PC,v1,d1) > 0) {v1 = -1*v1; d1 = -1*d1;}
if (pdist(PC,v2,d2) > 0) {v2 = -1*v2; d2 = -1*d2;}
if (pdist(PC,v3,d3) > 0) {v3 = -1*v3; d3 = -1*d3;}

double Cd1 = -1*pdist(PC,v1,d1);
double Cd2 = -1*pdist(PC,v2,d2);
double Cd3 = -1*pdist(PC,v3,d3);

/*
std::cout << "\nV1:" << v1
   << "\nV2:" << v2
   << "\nV3:" << v3 << std::endl;
*/

//Calculate distances to the respective planes
std::vector<double> distances1;
for(Pxyz::iterator i = plane1->begin(); i != plane1->end(); i++)
```

```
 {
      distances1.push_back(pdist(*i,v1,d1));
   }

   std::vector<double> distances2;
   for(Pxyz::iterator i = plane2->begin(); i != plane2->end(); i++)
   {

      distances2.push_back(pdist(*i,v2,d2));
   }

   std::vector<double> distances3;
   for(Pxyz::iterator i = plane3->begin(); i != plane3->end(); i++)
   {
      distances3.push_back(pdist(*i,v3,d3));
   }

   //Extract peak and valley points
   double peak1 = *(std::max_element(distances1.begin(),distances1.end()));
   double valley1 = *(std::min_element(distances1.begin(),distances1.end()));
   pcl::PointXYZ P1 = plane1->at(std::max_element(distances1.begin(),distances1.end()) -
distances1.begin());
   pcl::PointXYZ V1 = plane1->at(std::min_element(distances1.begin(),distances1.end()) -
distances1.begin());

   double peak2 = *(std::max_element(distances2.begin(),distances2.end()));
   double valley2 = *(std::min_element(distances2.begin(),distances2.end()));
   pcl::PointXYZ P2 = plane2->at(std::max_element(distances2.begin(),distances2.end()) -
distances2.begin());
   pcl::PointXYZ V2 = plane2->at(std::min_element(distances2.begin(),distances2.end()) -
distances2.begin());

   double peak3 = *(std::max_element(distances3.begin(),distances3.end()));
   double valley3 = *(std::min_element(distances3.begin(),distances3.end()));
   pcl::PointXYZ P3 = plane3->at(std::max_element(distances3.begin(),distances3.end()) -
distances3.begin());
   pcl::PointXYZ V3 = plane3->at(std::min_element(distances3.begin(),distances3.end()) -
distances3.begin());

   std::cout << "\n\nFile: " << argv[1]
      << "\n\nPlane1:\nV1:\n" << v1  << "\nD1:" << d1 << "\nCentroid to plane: " << Cd1 <<
"\nPeak1 Point: " << P1
      << "\nPeak1 height:" << peak1 << "\nValley1 Point: " << V1 << "\nValley1 height:" << valley1
      << "\n\nPlane2:\nV2:\n" << v2  << "\nD2:" << d2 << "\nCentroid to plane: " << Cd2 <<
"\nPeak2 Point: " << P2
      << "\nPeak2 height:" << peak2 << "\nValley2 Point: " << V2 << "\nValley2 height:" << valley2
      << "\n\nPlane3:\nV3:\n" << v3  << "\nD3:" << d3 << "\nCentroid to plane: " << Cd3 <<
"\nPeak3 Point: " << P3
```

```
  << "\nPeak3 height:" << peak3 << "\nValley3 Point: " << V3 << "\nValley3 height:" << valley3 <<
std::endl;

   //Open file for writing - use argv for name
   if (argc > 1)
   {
      for (int i = 2; i < argc; i++)
      {
         if ((strcmp(argv[i],"-f") == 0) && (i < (argc - 1)))

        {
            ofstream planes;
            planes.open(argv[i + 1], ios::out | ios::app);
            planes << "\n\nFile: " << argv[1]
               << "\n\nPlane1:\nV1:\n" << v1  << "\nD1:" << d1 << "\nCentroid to plane: " << Cd1 <<
"\nPeak1 Point: " << P1
               << "\nPeak1 height:" << peak1 << "\nValley1 Point: " << V1 << "\nValley1 height:" <<
valley1
               << "\n\nPlane2:\nV2:\n" << v2  << "\nD2:" << d2 << "\nCentroid to plane: " << Cd2 <<
"\nPeak2 Point: " << P2
               << "\nPeak2 height:" << peak2 << "\nValley2 Point: " << V2 << "\nValley2 height:" <<
valley2
               << "\n\nPlane3:\nV3:\n" << v3  << "\nD3:" << d3 << "\nCentroid to plane: " << Cd3 <<
"\nPeak3 Point: " << P3
               << "\nPeak3 height:" << peak3 << "\nValley3 Point: " << V3 << "\nValley3 height:" <<
valley3 << std::endl;


            planes.close();
            break;
        }
      }
   }

   bool isView(false);
   if (argc > 1)
   {
      for (int i = 2; i < argc; i++)
      {
         if (strcmp(argv[i],"-v") == 0) isView = true;
      }
   }

   if(isView)
   {
      pcl::visualization::CloudViewer viewer("Simple Cloud Viewer");
      Pxyz::Ptr forviewer (new Pxyz);
      *forviewer += *plane1;
*forviewer += *plane2;
        *forviewer += *plane3;
        viewer.showCloud(forviewer);

        while(!viewer.wasStopped())
        {
        }
    }
}



double pdist(pcl::PointXYZ pt, Eigen::Vector3f v, double d)
{
    Eigen::Vector3f ept(pt.x,pt.y,pt.z);
    return ((v.dot(ept) + d));
}
```